NBSIR 81-2191 (DoE)

The Use of the Slow Strain Rate Technique for the Evaluation of Structural Materials for Application in High-Temperature Gaseous Environments

C. E. Johnson and G. M. Ugiansky

Corrosion and Electrodeposition Group
Chemical Stability and Corrosion Division
Center for Materials Science
U.S. Department of Commerce
National Bureau of Standards
Washington, DC 20234

January 1981

Final Report

Prepared for
United States Department of Energy
Under Contract No. EA-77-A-01-6010

NBSIR 81-2191 (DoE)

THE USE OF THE SLOW STRAIN RATE TECHNIQUE FOR THE EVALUATION OF STRUCTURAL MATERIALS FOR APPLICATION IN HIGH-TEMPERATURE GASEOUS ENVIRONMENTS

C. E. Johnson and G. M. Ugiansky

Corrosion and Electrodeposition Group
Chemical Stability and Corrosion Division
Center for Materials Science
U.S. Department of Commerce
National Bureau of Standards
Washington, DC 20234

January 1981

DISTRIBUTION OF THIS DOCUMENT IS UNLIMITED

Final Report

Prepared for
United States Department of Energy
Under Contract No. EA-77-A-01-6010

U.S. DEPARTMENT OF COMMERCE, Malcolm Baldrige, *Secretary*
NATIONAL BUREAU OF STANDARDS, Ernest Ambler, *Director*

FOREWARD

Since 1974, the National Bureau of Standards has been engaged in research designed to address succinct materials problems and needs pertinent to coal conversion and utilization technologies. This work, sponsored in part, at first by the Office of Coal Research, then ERDA and currently the DOE, focuses on test method development, particularly accelerated procedures for materials behavior and durability; on the determination of the mechanisms of materials degradation; and on the development and operation of materials data centers to provide evaluated information on properties and performance including failures occurring in operating plants.

During the FY 77-79 period the NBS program, entitled "Materials Research for the Clean Utilization of Coal", consisted of a number of interrelated tasks including:

1. Metal Corrosion

    a. Slow Strain Rate Test
    b. Pre-cracked Fracture Test

2. Ceramic Deformation, Fracture and Erosion

3. Chemical Degradation of Ceramics

    a. Reactions and Transformations
    b. Slag Characterization (viscosity)
    c. Vaporization and Chemical Transport

4. Failure Prevention

    a. Failure Information Center
    b. Materials Properties Data Center

The results of the research have been disseminated through quarterly reports of progress (available from NTIS; report designation EA-6010; Dist. Category (UC-90C) as well as numerous scientific publications in technical journals. Further, as individual tasks are completed, an overall report is prepared detailing the results and accomplishments of the project. This present publication is the final report for the project on Metal Corrosion-Slow Strain Rate Test Technique.

SAMUEL J. SCHNEIDNER
Program Manager
Center for Materials Science
National Bureau of Standards

ABSTRACT

The slow strain rate technique has been evaluated as an accelerated test for determining the performance of structural materials in simulated coal gasification environments. Seven alloys, namely Types 309, 310, 310S, 347 and 446 stainless steels; Incoloy 800; and Inconel 671, were tested at temperatures from 370°C to 1040 C(700°F to 1900°F) at strain rates from 10^{-4} to 10^{-7}/s in H_2S plus water, gaseous mixtures of CO, CO_2, H_2, CH_4, H_2S, and H_2O, and in nominally inert environments of He and Ar. Type 310 steel, the most extensively studied material, showed a marked reduction in mechanical properties at low strain rates ($<10^{-5}$/s) in H_2S/H_2O at 540°C(1000°F), and this was associated with the occurrence of a large degree of secondary intergranular cracking in addition to the main ductile fracture mode. The occurrence of the secondary cracking was taken as the primary indication of embrittlement in subsequent tests. Of particular significance, it occurred to some degree in all alloys tested in the simulated coal-gasification environments at 600°C(1100°F). Comparison of the results for the nonstabilized austenitic steels with those for the stabilized grade, Type 347, indicated that sensitization had a detrimental effect with respect to intergranular cracking, although it was not clear that it is a necessary condition for this type of failure. The secondary cracking was surface-initiated in all alloys except the Inconel 671, which failed by the formation of internal cracks associated with the temperature and strain-induced α-chromium phase. While there was clearly an effect of environment on the behavior of the former alloys, interpretation was hindered by the absence of base-line data for an inert environment, since the nominally inert media caused limited oxidation. Consequently, the mechanism(s) of the embrittlement phenomena remain uncertain; a number of possible causes including creep and several environmentally-induced fracture processes are outlined. it is shown that the overall results of the test program are in good agreement with in-plant experience. it is concluded that the slow strain rate technique is an effective method for evaluating the performance of structural materials in the elevated-temperature gaseous environments.

INTRODUCTION

This study of the mechanical behavior of structural alloys in gaseous environments at elevated temperatures was initiated primarily to support current efforts in the development of the technology to convert the Nation's abundant coal reserves to gases of both high and low BTU values. The behavior of materials under such conditions was largely unexplored at the start of this investigation. The thrust of the program was not to test specific alloys, but to evaluate an accelerated test method for materials selection for this demanding application. Specifically, the slow strain rate technique (SSRT) was investigated.

Previous work utilizing this technique had been confined largely to the study of stress-corrosion cracking (SCC) and hydrogen embrittlement in aqueous media.* The test involves the application of a slow strain rate to smooth, i.e., un-notched, tensile specimens which are simultaneously exposed to the environment being investigated, and yields data of the type shown in Fig. 1. Region A, where strain rates are too slow to lead to SCC, the rate of repassivation is thought to be rapid enough to prevent any damaging interaction between the environment and the bare metal exposed during straining. At the opposite extreme, Region C, the strain rate is so rapid that failure occurs by the normal ductile mode, the time being insufficient for environmental interaction to have a significant effect. It is only in the intermediate range of strain rates, Region B, where the rate of production of bare metal is sufficiently high so that the rate of repassivation does not effectively stifle environmental reaction and the strain rate is sufficiently slow so that ductile fracture does not predominate. Under these conditions, SCC takes place. If SCC is not possible for the system studied, the reduction in ductility shown in Region B does not occur; the presence or absence of this reduction of mechanical properties is the essence of the SSRT.

The SSRT has become widely used in the study of SCC, both for mechanistic investigations and as a routine method for materials/environment evaluation. The advantages of the method are the relatively short testing times required, and the severe nature of the test -- it will promote SCC where other tests will not, unless inordinately long times are used. While it is extremely useful for ranking materials, it should be noted that the detailed interpretation of the results is not clear. The reduction in area, strain to fracture, and maximum tensile stress are commonly used as measures of susceptibility, but it is not established whether the reduction in these parameters relates to crack initiation, propagation or a combination of these processes. Moreover, no clear relationship exists between the results of the SSRT and those of other test methods.

*A monograph has recently been published, describing the SSRT in considerable detail [1].

The environmental conditions encountered in coal gasification, i.e., high-temperature gases, are basically different from those in the aqueous SCC systems which have been studied by the SSRT. The present studies were carried out to determine whether the method can be used to evaluate materials for the gaseous case. The tests were carried out on several candidate materials for use in proposed coal-gasification systems, namely several austenitic stainless steels (Types 309, 310, 310S and 347), a ferritic stainless steel (Type 446), and two nickel-base alloys (Inconel 671 and Incoloy 800). These materials were also being included in a DOE-sponsored study of high-temperature corrosion-erosion [2]. The main test environments used were the gases He and Ar; H_2S plus steam, and H_2S saturated with water vapor at 23°C; and mixtures of CO, CO_2, H_2, CH_4, H_2S and H_2O. He and Ar were used to provide baseline data. The wet H_2S environments were employed because of the high probability of embrittlement in those environments, based on the known susceptibility of austenitic alloys to SCC in sulfide environments in oil refineries. The gaseous mixtures of CO, CO_2, H_2, CH_4, H_2S, and H_2O simulated possible coal gasification environments.

EXPERIMENTAL PROCEDURES

Materials and Specimen Preparation

The compositions and heat treatments of the alloys used are given in Table 1. Note that two different batches of Type 310 steel were used. All the alloys were received in the form of 9.5 mm(0.375 in) diameter rods. The heat treatments were performed by the suppliers and no further heat treatment was carried out. The microstructures of the alloys are shown in Fig. 2.

The specimens were 58 cm(23 in) long by 9.5 mm(0.375 in) in diameter, and threaded on both ends for attachment to universal couplings outside the test cell. A central gauge section of effective length 2.5 cm(1.0 in) and diameter 4 mm(0.16 in) was produced by machining. The gauge section was subsequently polished using 320, 400, and 600 grit silicon carbide papers, respectively, followed by a final polish using CROCUS cloth. The surface was finally rinsed with acetone and alcohol, and air dried.

Test Facility

The SSRT facility is capable of testing four specimens simultaneously and is equipped with automatic digital data acquistion and storage. The facility is illustrated schematically in Fig. 3. A range of strain rates from 10^{-3}/s to 10^{-7}/s (over the 2.5 cm(1.0 in) gauge length) was achieved through the use of different gear ratios, reduction gear boxes, and variable speed motors. The tensile load was measured by a load cell with a maximum capacity of 900 kg(2000 lb) and an output of 39.6 μV/kg(18 μV/lb). The strain was measured by means of a LVDT attached across the shoulders of the specimen, at points outside the furnace, Fig. 3; the LVDT was calibrated to

give an output of 13.33 V/m(0.34/in). The elongation was determined after fracture from gauge marks on the reduced section of the specimen. Reduction in area measurements were made by measuring the diameter of the reduced section before and after testing using a stage micrometer. The load cells and LVDTs were sequentially scanned and their outputs were read on a digital multimeter and stored in a programmable calculator. These data were transferred to magnetic tape or flexible magnetic disc memory for later use in constructing stress-strain curves or other curves of tensile strength, elongation, or reduction in area versus strain rate.

The test cells were Type 304 stainless steel tubes (38 cm(15 in) long by 5 cm(2.0 in) diameter sealed at both ends with Type 304 plates using Viton-A gaskets. The cells were mounted in furnaces capable of producing test temperatures up to 1100 C(200°F). Ports for entrant and exit gases, thermocouples, and specimens were available on the end plates, Fig. 3. Sliding seals of Teflon or high vacuum O-ring couplings provided freedom of movement for specimen extension while testing. These seals are limited in use to below 300 C(570°F) and therefore were located outside of the furnace and cooled with fresh air.

The specimens were positioned in the test cell so that the reduced section was in the center of the cell and furnace, Fig. 3. The cells were purged with either N, Ar, or He. The test gas then was introduced into the cells and the furnaces brought up to test temperature. The specimens were pre-loaded to 100 kg(220 lb) to produce a positive output from the load cell. Data were taken at predetermined load intervals (approximated by dividing the expected maximum load by the number of data registers available), usually 0.3 mV or 0.4 mV [corresponding to 7.5 kg(16.5 lb) or 10 kg(22 lb).

Test Environments

The main environments were He, Ar, H_2S plus steam, and H_2S saturated at 23°C(73°F) with H_2O vapor (wet H_2S), and gaseous mixtures of CO, CO_2, H_2, CH_4, H_2S, and H_2O; limited tests were conducted in air, H_2, and in vacuum. The inlet gas compositions and the calculated equilibrium compositions of the simulated coal gasification environments are given in Table 2.

RESULTS AND DISCUSSION

Austenitic Stainless Steels

Type 310: Specimens were initially tested at 540°C(1000°F) in the H_2S environments. Typical stress-strain curves are shown in Fig. 4, and the various fracture parameters are presented in Fig. 5 and Table 3. It can be seen that the UTS, elongation and % reduction in area (RA) are markedly reduced at strain rates of 7.2×10^{-6}/s and slower. SEM examination indicated that the reduction in the tensile parameters was associated with the appearance of large numbers of surface cracks, Fig. 6. These formed throughout the gauge section and were approximately perpendicular to the stress axis, e.g., Fig. 6(d). In the case

of specimens showing reduced tensile properties, the central region of the primary fracture surface was ductile with a flat outer rim corresponding to the surface cracks. These cracks, seen below to be intergranular, are considered to be responsible for the degradation of the tensile properties at the slower strain rates. It can be seen in Fig. 6(a) and (b) that failure at the higher strain rates occurred by ductile shear; it should be noted that secondary shear cracks formed near the primary fracture, Figs. 6(a) and (b), are readily distinguished from the intergranular cracks, cf. Fig. 6(d). A thick scale was formed on the specimens and quantitative analysis indicated that it consisted of a duplex oxide-sulfide layer, Appendix A.

For comparison purposes, specimens were also tested in He at 540°C(1000°F). The results, Fig. 5, indicated that the RA was again decreased at the lower strain rates, and SEM examination revealed the presence of intergranular cracks. A visible oxide film was observed, raising the possibility that this was responsible for the reduced RA. The supplier's analysis of the He gave a value of O_2 content of 0.1 to 0.5% while H_2O was listed at 2-250 ppm. Accordingly, further testing was carried out at a strain rate of 10^{-6}/s in He which was first passed through heated Ti filings, phosphorus pentoxide, and a liquid-nitrogen trap; tests were also carried out in Ar and vacuum (2×10^{-2} Torr). Intergranular cracking occurred in each case, Fig. 7. However, a visible oxide film was detectable in each case, so that the environments cannot be regarded as inert. A hard vacuum test cell probably would have prevented the oxide on the specimens, but equipment and time were not available to test this idea.

Subsequent testing in a reducing environment of H_2 also produced a thin interference oxide film on the surface of the specimens. Cracking was also detected in these specimens in tests at 540°C(1000°F) at a strain rate of 10^{-6}/s. Figure 8 shows the intergranular cracking on the surfaces of the gauge section, and the intergranular facets on the primary fracture surface. The rim of intergranular cracking extended 250-400 μm from the free surface, and the remaining fracture surface corresponded to ductile shear.

It is probable that sensitization, detected from a chemical etch test, occurred during testing at 540°F(1000°F), and that carbide precipitation at grain boundaries and the associated chromium depletion played a role in the intergranular failures. To pursue this possibility, tests were run at a strain rate of 10^{-6}/s at 815°C(1500°F) and 1040°C(1900°F). The former was designed to give information near the top of the sensitization range, while the latter would give results above the temperature range for sensitization. These tests were run in air because the seals of the test chambers were not designed for these high temperatures. At 815°C(1500°F), the UTS was only 173 MPa(25 KSI) versus 414 MPa(60 KSI) when tested in He at 540°C(1000°F) at the same rate; the RA was 14.5% which was a lower value than obtained for that parameter for any test at 540°C(1000°F). Many secondary intergranular cracks were observed in this specimen, Fig. 9(a) and (b), and the primary fracture consisted largely of intergranular facets, in contrast to the shallow rim of

intergranular cracking observed at 540°C(1000°F). The intergranular nature of the secondary cracks is evident from Fig. 9(c). Intergranular cracking also occurred in the test at 1040°C(1900°F), thus ruling out the possibility that sensitization is necessary for this form of failure. The RA was 21%, UTS 76 MPa(11 KSI) in this case, and the elongation 41%. The latter was probably due to the more uniform yielding over the entire reduced section at the higher temperature.

To further investigate the role of sensitization, specimens were tested at a strain rate of 10^{-6}/s in dry He and H_2 at 370°C(700°F) and 450°C(840°F), both below the nominal temperature range for sensization. Examination of fractured specimens suggested that partial sensitization had in fact occurred, Figs. 10(b) and 11(b). However, the primary fracture was entirely ductile and no secondary intergranular cracks were detected, Figs. 10(a) and 11(a). The tensile properties were higher than in comparable tests at 540°C(1000°F), e.g., Fig. 12. In a further attempt to separate the effect of sensitization from that of combined thermo-mechanical processes, a test was made by heat-treating the unstressed specimen at 540°C(1000°F) for a time equivalent to the time required for specimen failure when tested at a strain rate of 10-6/s (approximately 60h). The Type 310 specimen failed in a ductile manner when subsequently tested at 540°C(1000°F) at a higher strain rate of 10^{-4}/s. These tests showed the need for simultaneous application of the slow strain rate (10^{-6}/s) and the sensitization temperature (>450°C) for the occurence of intergranular cracking.

Testing in simulated coal gasification environments, Table 2, was carried out at two test temperatures, one below the nominal sensitization range (450°C) and one within this range (600°C). A strain rate of 10^{-6}/s was chosen, based on the preceding tests. The tensile data are shown in Fig. 13. None of the specimens failed by intergranular cracking when tested at 450°C(840°F) in any of the three environments (ultra-pure helium, oxidizing/sulfidizing, or oxidizing/sulfidizing/carburizing). Photomicrographs of the fractured specimens, scanning electron micrographs of the fracture surfaces, and photomicrographs of the sectioned specimens tested in the three environments are shown in Figs. 14-16. These photographs show the ductile fracture and the partially sensitized grain boundaries. The variation in the measurements of the mechanical properties in each case are within measurement error. When tested at 600°C(1100°F), a large amount of intergranular cracking occurred in the three environments as revealed in Figs. 17-19. The oxidizing/sulfidizing environment seemed to produce the largest reductions in mechanical properties, Fig. 13.

As a precaution against the possibility that the Type 310 material may be from a bad lot, or harbored some pecularities, another lot of Type 310 Steel (RA 310) was tested in ultra-pure He at 600°C(1100°F) at a strain rate of 10^{-6}/s. The composition of RA 310 is shown in Table 1. The RA 310 failed in the same manner as the Type 310 SS, that is, with considerable amounts of intergranular cracking. The UTS, elongation, and RA for both lots tested in ultra-pure-He at 600°C(1100°F) are as follows:

	Type 310	RA310
UTS	368 MPa(53,400psi)	337 MPa(48,800psi)
Elongation	19.9%	19.2%
RA	28.8%	23.6%

Type 310S: The C content of this alloy was slightly lower than in Type 310, Table 1, and, if sensitization were important, this alloy should therefore be less susceptibile to intergranular cracking. Initial tests were conducted in wet H_2S at 540°C(1000°F). In contrast to Type 310, no intergranular cracking was observed over the range of strain rates from 10^{-4} to 10^{-7}/s. There was a reduction in the magnitude of elongation and RA at the strain rates of 10^{-6}/s and 10^{-7}/s, but these did not reach the low levels found in the Type 310, Table 4, Fig. 20.

Type 310S specimens tested in He and "house" vacuum (726mm Hg) at 540°C(1000°F) at a strain rate of 10^{-6}/s exhibited elongation and RA values twice as great as were seen for Type 310 tested under the same conditions, see Fig. 20. However, numerous intergranular cracks were present in the Type 310S specimens. Clearly, the lower C content does not eliminate intergranular cracks. The reason for the absence of such cracks in the wet H_2S is not known, though it may be speculated that the scale formed in this environment protects the specimens from damaging environmental interaction. It should also be noted that creep resistance of materials has been reported to be greater in air than in He and vacuum [3,4]; this will be discussed further below.

Further testing was done in the simulated coal gasification environments. Test tempeatures of 450(840°F) and 600°C(1100°F), and a strain rate of 10^{-6}/s were used for direct comparision with Type 310. The stress-strain data are shown in Fig. 21. The higher values of the tensile parameters at 450°C(840°F) are presumably due to the fact that no significant intergranular cracking occurred at 450°C(840°F), Figs. 22-24, whereas this form of cracking was prevalent at 600°C(1100°F), Figs. 25-27. It can be concluded that the lower C content in Type 310S does not impart significantly greater resistance to intergranular cracking in coal-gasification environments.

Type 347: This alloy was tested because it is stabilized with Nb and Ta, Table 1, to resist sensitization. Specimens were initially tested in wet H_2S at 540°C(1000°F) over a range of strain rates from 10^{-4} to 10^{-7}/s. The results are tabulated in Table 5 and shown graphically in Fig. 28. The elongation was low compared with those for Type 310 and Type 310S, cf. Tables 3-5, but the UTS and RA were comparable to the other alloys. More importantly, the tensile properties of Type 347 specimens were not strongly sensitive to strain rate, Fig. 28, and this was consistent with the finding that no intergranular cracking occurred at any of the strain rates. Further specimens were tested at 540°C(1000°F) in He, and house vacuum (723 mm Hg). No intergranular cracking was detected over the range of strain rates of 5×10^{-5} to 8.4×10^{-7}/s, and the mechanical properties were not significantly different from those in wet H_2S, see Fig.

28 for He.

Tests were carried out at 450°C(840°F) and 600°C(1100°F) in ultra-pure He and in the simulated coal gasification atmospheres, i.e., oxidizing/sulfidizing and oxidizing/sulfidizing/carburizing, using a strain rate of 10^{-6}/s. The resulting stress-strain curves are shown in Fig. 29. No intergranular cracking was observed at 450°C(840°F) in either environment, Figs. 30-32. The UTS values were higher at 450°C(840°C) than at 540°C(1000°F). Elongation was still relatively low (17-19%), while RA was high (60-66%) due to necking. In some of the first tested specimens, tool marks were present on the reduced area, but these did not seem to act as stress-raisers. Subsequent specimens were polished to remove the tool marks. At 600°C(1100°F), the tensile properties were lower than at 450°C(840°C) in all of the test environments, Fig. 29. Small surface cracks were detected in the necked regions next to the fracture surface in specimens tested in He, Fig. 33, and in the oxidizing/sulfidizing/carburizing environment, Fig. 34, but no cracks were visible in the case of the oxidizing/sulfidizing case, Fig. 35. The cracks were shallow and were confined to the necked region, and there was no significant difference in mechanical properties for the three environments, Figs. 29 and 33-35. It is not clear whether the cracks shown in Figs. 33 and 34 are the same type as the intergranular cracks in the other alloys. However, it is clear that the stabilized alloy is far less susceptibile to this form of cracking. Thus the absence of sensitization may be beneficial with respect to intergranular cracking.

Type 309: Limited tests were carried out on this alloy, which is similar in composition to Type 310 except for its lower Ni and Cr contents and higher Si content, Table 1. The Type 309 specimens were tested at 600°C(1100°F), in various environments and at several strain rates and the results were compared to those for Type 310 tested under similar conditions. Stress-strain curves for both alloys tested at a strain rate of 10^{-6}/s in He are shown in Fig. 36. The ductility of Type 309 is far greater, see also Table 6, and this correlates with the small amount of surface cracking observed in this alloy, Fig. 37, compared to that in Type 310, Fig. 17. The cracking in Type 309 is shallow and is confined to the necked region; no well defined rim of intergranular fracture could be detected at the main fracture, in contrast to the case of Type 310. Similar shallow secondary cracking was observed in tests on Type 309 specimens at 600°C(1100°F) in Ar and the oxidizing/sulfidizing/ carburizing atmosphere; the tensile parameters for these atmospheres are given in Table 6.

The microstructure of the Type 309 steel was found to contain ferrite, in which carbides were precipitated during testing at 600°C(1100°F), Fig. 38. There was no evidence for the formation of sigma phase, which is known to be formed from ferrite during long times at high temperatures. The presence of the ferrite may account for the greater resistance of Type 309 to intergranular cracking in our tests, but its specific role was not determined.

Ferritic Stainless Steel

Tests were carried out on Type 446 steel, selected because of its resistance to corrosion and oxidation at high temperatures. Tests were carried out at 450°C(840°F) and 600°C(1100°F) in ultra-pure tank He and in the simulated coal gasification environments, i.e., oxidizing/sulfidizing and oxidizing/sulfidizing/carburizing, using a strain rate of 10^{-6}/s. The resulting stress-strain curves are shown in Fig. 39. The data for 450°C(840°F) were not significantly different for the three environments, despite the fact that shallow surface cracks were visible within the necked region of specimens tested in the coal gasification environments, Figs. 41 and 42, but not in the He test, Fig. 40. The nature of the shallow cracks, i.e., inter- or transgranular, was not determined. At 600°C(1100°F), UTS values were significantly lower than at 450°C(840°F) in all test environments, and the elongation and RA were higher, Figs. 39 and 43-45. The mechanical properties can be seen to be significantly lower for the coal gasification environments compared to the specimen tested in He. Surface cracking was visible in the necked region in the three environments, Figs. 43-45, but the morphology was different in the coal gasification cases, the cracks adopting a mosaic pattern. Despite the apparent environmental effect, the overall failure was ductile in each case, as evidenced by the large values of elongation and RA. Moreover, the question of whether environmental reactions occur at this temperature is academic, since it is clear from a comparison of the UTS values at 450°C(840°F) and 600°C(1100°F) that the latter is above the temperature at which this alloy should be used under stress.

Nickel Base Alloys

Incoloy 800: Specimens were initially tested at 540°C(1000°F) in the wet H_2S environment over a range of strain rates from 10^{-4} to 10^{-7}/s. However, severe scaling occurred in this environment, drastically reducing the cross-section, Fig. 46, so that the tensile data had no meaning. It is clear that the alloy cannot be used in this environment at elevated temperatures.

Further testing was carried out in the simulated coal gasification environments and in ultra-pure He at 450°C(840°F) and 600°C(1100°F) at a strain rate of 10^{-6}/s. The stress-strain curves, Fig. 47, indicate that the properties were markedly affected by both the oxidizing/sulfidizing and oxidizing/sulfidizing/carburizing atmospheres. However, no secondary cracking was observed at 450°C(1100°F) in any of the three environments, and the values of RA were essentially the same, Figs. 48-50. At 600°C(1100°F), secondary cracks were found in the regions of the fracture in each environment, but were more shallow in the case of He, Figs. 51-53.

Inconel 617: This alloy was tested since it has found some use as a weld overlay in coal gasification pilot plants. Tests were confined to 450°C(840°F) and 600°C(1100°F) in the simulated coal gasification environments and ultra-pure He, using a strain rate of 10^{-6}/s. The stress-strain curves were almost coincident for all three environments at each temperature, Fig. 54. However, shallow secondary cracks were visible near the primary fractures in both coal gasification atmospheres at 450°C(840°F), but not in the case of He, Figs. 55-57. The primary fractures were ductile in character in each case, but involved less necking than in other alloys tested; this is evident from the relatively low values of RA, Figs. 55-57. At 600°C(1100°F), the strengths and ductilities were considerably reduced, Fig. 54, and this was associated with the presence of α-chromium in each case, Figs. 58(c), 59(c) and 60(c). Studies of sections of the fractured specimens indicated that numerous secondary cracks, many of which were internal, occurred within the α-chromium or at the interface between this phase and the matrix. The amount of α-chromium was found to decrease with increasing distance from the primary fracture, Fig. 61, and thus it seems that the formation of this phase is assisted by strain. It is concluded that the poor mechanical properties of the alloy at 600°C(1100°F) are due to the presence of the α-chromium phase, which was both temperature- and strain-induced. Because of the internal nature of the cracking in many instances, it appears unlikely that the presence of the environments had any influence on the formation or fracture of this embrittling phase.

COMPARISON OF RESULTS OBTAINED FROM THE SSRT WITH IN-PLANT EXPERIENCE*

The present results for the main environment/temperature combinations are summarized in Table 7. Embrittlement is identified by the occurrence of secondary cracking (SC); this was intergranular in the case of Type 310 specimens but was not characterized in some of the other materials. The results indicate that Type 310 steels undergo embrittlement at 540°C(1000°F) and 600°C in various gaseous media. Several in-plant failures are consistent with these findings. A Type 310 gasifier probe in the Consol plant was reported to fail by stress-enhanced intergranular corrosion [5]. Tests showed the sensitization of the steel when operated between 425 - 875°C (800 - 1600°F), which was thought to significantly reduce the corrosion resistance of the grain boundaries. A Type 310 N_2 purge line from the Hygas plant failed by brittle fracture due to grain boundary embrittlement and S corrosion when operated at 760 - 875°C (1400 - 1600°F)[6]. A Type 310 welded tube (inlet line to regeneration) in the CO_2 Acceptor plant failed [7].

*Information on our plant performance was obtained from the NBS Failure Prevention Information Center. The identification number of each report is given in the References so that they may be obtained from the Center.

Corrosion due to S was the fundamental cause of failure but was accentuated by the stress and strains from the fluidized bed and thermal cycling which was the immediate cause of failure . A cracking failure was reported in a Type 310 nozzle plate in the Westinghouse multi-stage coal gasification system [8]. Cracking was due to high thermal stresses set up during thermal cycling. The cracking progressed along massive carbide precipitates along grain broundaries. The synthesis gas environment could have been oxidizing or reducing at 980 - 1300°C(1800 - 2400°F). Failure of a Type 310 air distributor plate from an atmospheric fluidized bed combustor resulted from embrittlement due to sigma phase formation along with intergranular carbide precipitates [9]. Plant exposure of the plates resulted in a decrease in ductility at elevated temperatures, especially at 840°C(1550°F). Other plant reports have indicated that no failures have occurred with Type 310 when used at temperatures of 350 - 470°C(660 - 875°F) even at pressures up to 17 MPa(2500 psi).

Type 347 steel was seen to perform significantly better than Type 310 in the SSRT, and again this is consistent with pilot-plant experience. Thus, no evidence of cracking was found in the initial examination of Type 347 top closure flanges or inlet nozzles to the dissolver vessel in the Solvent Refined Coal plant operated at 525°C(975°F) at a pressure of 21 MPa(3000 psi) [10]. However, subsequent examination of the Type 347 cover plate on the SRC dissolver vessel revealed cracks that were very shallow and exhibited a pattern suggestive of a partially intergranular failure mode [11]. Thermal cycling during welding and residual stresses were expected in the cracked regions, and it was speculated that these effects contributed to this cracking. Four cracked ares were detected on the top surface of the Type 347 flange between the gasket grove and inner wall of the dissolver vessel. All appeared to be relatively shallow. From the location and appearance of the cracks, it was speculated that these occurred at regions that were mechanically damaged or perhaps repair welded.

Some secondary cracking was observed in our tests of the ferritic steel at both 450°C(840°F) and 600°C(1100°F), but it was clear that the latter is above the normal operating range for this material. An in-plant failure report also revealed the same results [12]. Two Type 446 thermowells failed in the Battelle's Agglomerating-Burner Process Development Unit and it was recommended that lower temperatures be used.

Incoloy 800 was seen to undergo embrittlement in the 600°C(1100°F) tests. There have been numerous in-plant service failures in this material. Fourteen cracking failures of schedule 40 Incoloy 800 pipe have occurred in the Westinghouse gasification PDU at temperatures of 315°C(600°F) [13]. These failures were closed to welds, but not necessarily in the weld metal or HAZ. Evidence indicates that the failures resulted from intergranular SCC. The material was heavily sensitized. The corroding agent was not identified. An Incoloy 800 nozzle reducer cracked and failed in the Synthane plant [14]. The operating environment was aqueous condensate at 205°C(400°F) and pressure of 4 MPa(600 psi). The crack appeared to have occurred

in the HAZ. Failure was due to intergranular SCC of the sensitized material, and caused a 5-week shutdown of the plant. An Incoloy 800 pipe union developed a 360° circumferential crack in the central pipe weld on the cyclone (C119) of the Westinghouse system [15]. Environmental conditions were product gas at 925 - 1035°C(1700-1900°F) at a pressure of 1.5 MPa(200 psi). Cracking was reported to be due to SCC. Cracking was observed in a schedule 40 Incoloy 800 pipe which was part of a line in the second stage gasifier reactor in the Hygas pilot plant [16]. The pipe transported char and gas at 815°C(750°F). Fracture occurred immediately adjacent to a welded flange. It was noted that the cracking mode changed with increasing depth from intergranular at the surface to transgranular at the crack tip. It was speculated that the change in crack mode might be due to an increase in the effective stress as crack depth increases, chemical effects at the surface, or chemical changes at the crack tip. The laboratory tests suggested that Incoloy 800 is an useful material at 400°C. An in-plant service report bears this out. An Incoloy 800 preheater coil in the Hygas plant has operated for 3820 h of coal processing at a maximum temperature of 400°C(750°F) at a pressure of 17 MPa(2500 psi) [17].

The tests on Inconel 671 indicated that degradation of mechanical properties resulted from the formation of the α-chromium phase at 600°C. This is in essential agreement with the recommmendation that in-plant use be restricted to cladding material and not for structural purposes. The alloy has been found to be a good material for high temperature corrosion resistance, but the elevated temperature mechanical properties are poor and cannot be recommended for components subject to directional stresses [18].

GENERAL DISCUSSION AND CONCLUSIONS

The present results clearly demonstrate the usefulness of the SSRT as a method of evaluating the performance of materials in gaseous environments at elevated temperatures. This is seen in the strong correlation between the test data and in-plant experience, discussed in the preceding section. The results of Type 310 steel tested at 540°C(1000°F) in the H_2S/H_2O environment show a reduction in mechanical properties as the strain rate decreased from 10^{-4}/s to 10^{-5}/s and below, Table 3 and Fig. 5; it was seen in the Introduction that such a reduction is indicative of the operation of an embrittling process. The reduction in properties in the case of Type 310 specimens was seen to be associated with the occurrence of secondary intergranular cracking, and this was taken as an indication of embrittlement in subsequent tests on this and other alloys. It should be noted that, while the RA exhibited a decrease with decreasing strain rate, it did not show the increase at lower strain rates commonly observed in the case of SCC in aqueous media, Fig. 1. Thus, there does not appear to be an analogous effect to the repassivation which occurs in aqueous environments.

The mechanism of the intergranular fracture observed in Type 310 steel and in certain of the other alloys was not determined. In particular, it was not established whether the failure was due to creep or to some environmentally-induced fracture process. For the austenitic materials, temperatures of 540°C(1000°F) and above are in

the range where creep can occur [19]. To pursue this possibility, it would be necessary to carry out tests under constant load in inert environments (see below) as well as under the same environmental/temperature conditions used in the SSR tests. A number of environmentally-induced fracture processes could be proposed to account for the intergranular fractures. For example, it has been suggested that such failures can be produced by an oxide-rupture mechanism [20], similar to that advocated for certain aqueous stress-corrosion systems [21,22]. Alternatively, it could be speculated that embrittlement resulted from the penetration of grain boundaries by oxygen; or, in the S-bearing environment, by the formation of brittle sulfide compounds [23]. The present results do not permit us to distinguish between these possibilities, and it is clear that further work is necessary in this area.

A major uncertainity in the present work concerns the influence of the environments. This arises because of the absence of baseline data for inert environments -- it was seen that thin oxide layers were produced by each nominally inert medium such as He and Ar. As indicated in the text, it would be necessary to construct a test chamber capable of maintaining a hard vacuum ($\sim 10^{-9}$ torr) to resolve this question. Another parameter which was not evaluated is the influence of initial grain size. It was seen in Fig. 2 that significant variation existed between the different alloys, but no attempt was made to investigate the effect of this variation on mechanical behavior.

Comparison of the results for Type 310 and the stabilized austenitic steel, Type 347, indicates that sensitization has a detrimental effect on the high-temperature mechanical properties. Such an effect would be expected if the intergranular failures resulted from creep, since sensitization is known to adversely affect the creep resistance of austenitic stainless steels [19]. It could also be rationalized in terms of a stress-corrosion mechanism, since the chromium-depleted regions at the grain boundaries in sensitized material would be expected to be preferentially oxidized.

In summary, the SSRT has been shown to be a useful method for evaluating the performance of structural materials under conditions simulating those in coal-gasification plants. The mechanism(s) of the embrittlement phenomena encountered during the tests was not determined, and this serves to emphasize the need for further work in this important area.

ACKNOWLEDGEMENTS

The support of this work under the project "Materials Research for the Clean Utilization of Coal" for the U.S. Department of Energy (Contract No. EA-77-A-01-6010 is gratefully acknowledged. We thank J. Kruger for the many helpful discussions; E. N. Pugh for his assistance in the preparation of this report; C. H. Brady for the work on the optical and scanning electron micrographs; and W. A. Willard for the in-plant service failure reports. We also wish to thank I. G. Wright of Battelle Columbus Laboratories for information on the gas equilibrium compositions and phase equilibrium.

PULICATIONS

Ugiansky, G. M. and Johnson, C. E., "Slow Strain-Rate Stress Corrosion Testing of Metals in Gaseous Atmospheres at Elevated Temperatures", Stress Corrosion Cracking-The Slow Strain-Rate Technique, ASTM, STP 665, G. M. Ugiansky and J. H. Payer, Eds., American Society for Testing and Materials, pp. 113-131, (1979).

Ugiansky, G. M. and Johnson, C. E., "Stress Corrosion Testing at Elevated Temperatures in Simulated Coal Conversion Gases", Proceedings of 7th International Congress on Metallic Corrosion, Vol. II, ABRACO, Rio de Janiero, pp. 915-924, (1979).

TALKS

"Constant Strain-Rate Stress Corrosion Testing for Coal Gasification Systems", Workshop on Materials Technology for Coal Gasification (Gaithersburg, Maryland: National Bureau of Standards, September, 1975).

"Constant Strain-Rate Stress Corrosion Testing", ASM-AIME Joint National Meeting, 1975 Materials Science Seminar (Cincinnati, Ohio: November, 1975). (Invited).

"Constant Strain Rate Stress Corrosion Testing for Coal Gasification Systems", NACE Annual Meeting (Houston, Texas: March, 1976).

"Constant Strain Rate Stress Corrosion Testing of Metals at Elevated Temperatures", Mechanical Failures Prevention Group Symposium on Prevention of Failures in Coal Gasification Systems (Columbus, Ohio: April, 1976).

"Constant Strain Rate Stress Corrosion Testing at Elevated Temperatures", General Electric Co., Research and Development Center Staff Seminar (Schenectady, NY: February: 1977). (Invited).

"Constant Strain Rate Stress Corrosion Testing of Metals in Gaseous Environments at Elevated Temperatures", ASTM/NACE Symposium on Stress Corrosion Cracking - The Constant Strain Rate Technique (Toronto, Ontario: May 1977).

"Slow Strain Rate Stress Corrosion Testing in Coal Gasifier Environments", First International Conference on Materials for Coal Conversion and Utilization (NBS, Gaithersburg, Maryland: October, 1977).

"Stress Corrosion Testing at Elevated Temperatures in Simulated Coal Conversion Gases", 7th International Congress on Metallic Corrosion, (Rio de Janeiro, Brazil: October, 1978).

REFERENCES

[1] Stress Corrosion Cracking - The Slow Strain Rate Technique, Ugiansky, G. M., and Payer, J. H., editors, ASTM STP 665, 1979.

[2] Hill, V., Corrosion-Erosion Study of Materials for the Gasification of Coal, IITRI Reports to Metal Properties Council under DOE Contract Number EX-76-C-01-1784.

[3] Shepard, O. C., and Schalliol, W., Symposium on Corrosion of Materials at Elevated Temperatures, ASTM STP 108, April 1951.

[4] Hosoi, Y., and Abe, S., Met. Trans. A., 6A, 1975, p. 1171.

[5] Leterle, J. F., Continental Oil Co. Technical Service Report, No. 116-74-1301, May 13, 1974; National Bureau of Standards - Failure Prevention Information Center Identification Number 98.

[6] Danyluk, S., Argonne National Laboratory Service Failure Report, Dec. 22, 1976; NBS-Failure Prevention Information Center Identification Number 255.

[7] Schulz, C. A., Conoco Materials and Component Failure Report, No. 75-8, Aug. 8, 1975; NBS-Failure Prevention Information Center Identification Number 144.

[8] Albertin, L., et al., Westinghouse Technical Document Summary, No. 75-8D9-PDUOP-P1, Nov. 25, 1975; NBS-Failure Prevention Information Center Identification Number 191.

[9] King, R. T., et al., Oak Ridge National Laboratory Report ORNL/TM-6444, Feb. 1979; NBS-Failure Prevention Information Center Identification Number 609.

[10] King, R. T., et al., ORNL Intralaboratory Correspondence, May 4, 1977; NBS-Failure Prevention Information Center Identification Number 397.

[11] King, R. T., et al., ORNL Failure Analyses Reports, Oct-Nov. 1977; NBS-Failure Prevention Information Center Identification Numbers 471 and 491.

[12] Danyluk, S. and Dragel, G. M., Component Performance and Failure Analysis, Argonne National Laboratory, April-June, 1977, ANL-77-62.

[13] NBS-Failure Prevention Information Center Identification Number 409.

[14] Greene, B. N., C. E. Lummus Summary to DOE Newsletter on Materials and Components in Fossil Energy Applications, Dec. 5, 1977; NBS-Failure Prevention Informaion Center Identification Number 493.

[15] Vandergrift, E., Westinghouse Failure Report to DOE, July 6, 1977; NBS-Failure Prevention Information Center Identification Number 455.

[16] Danyluk, S. and Dragel, G. M., Argonne National Laboratory Report, ANL-78-6, July-Dec 1977.

[17] Barney, W. G., University of North Dakota, Letter to DOE Newsletter on Materials and Components in Fossil Energy Applications, May 31, 1978.

[18] MacNab, A., Letter to Institute of Gas Technology, April 2, 1975; NBS-Failure Prevention Information Center Identification Number 1.

[19] Metals handbook, Vol. 10, Failure Analysis and Prevention, p. 249, eighth edition, 1975.

[20] Bleakney, H. H., Can. Met. Quart., Vol. 4, p. 13, 1965.

[21] Forty, A. J. and Humble, P., Phil. Mag., Vol. 8, p. 247, 1963.

[22] McEvily, Jr., A. J. and Bond, A. P., J. Electrochem. Soc., Vol. 112, p. 131, 1965.

[23] Floreen, S. and Kane, R. H., Met Trans. A, Vol. 10A, p. 1745, Nov. 1979.

Appendix A

Qualitative microprobe analysis was made on the duplex corrosion products in the cracks on the profile of a Type 310 specimen that was tested in H_2S plus steam at 540°C(1000°F) at a strain rate of 10^{-6}/s. Figure A-1 shows the fracture surface and outside surface (a), the etched cross-section (b), and the cracks in the unetched profile (c). The corrosion products appear as two layers on the surface and in the cracks. The qualitative microprobe analysis was made on the largest crack seen in Fig. A-1c. The area of the crack was studied with a lithium-drifted silicon Si(Li), detector. This area is seen in the accompanying target current (TC) image (Fig. A-2a). The numbered regions in the TC image correspond to the numbers on the attached energy dispersive spectra (Figs. A-3 and A-4). Spectrum #1 (Fig. A-3) of the dark area in the crack shows mostly sulfur with some Cr, Mn, Fe, and Ni. These latter four elements are constituents of the matrix as seen in spectrum #2 (Fig. A-4). A small Si peak is usually expected in the energy spectra, and is an artifact of the Si(Li) detector. In this case, a Si peak is also expected from the matrix as 0.5 percent Si is present in the steel. The microprobe analysis was unable to determine whether the Si peak is the artifact or is, in fact, present in the matrix.

An x-ray scan of sulfur (Fig. A-2b) shows the distribution of this element throughout the crack and along the exterior edge of the sample. An x-ray scan of oxygen (Fig. A-2c) shows that this element is found mostly along the interior edge of the crack as well as along the surface of the sample.

The microprobe analysis has revealed that the duplex corrosion products on the surface of the specimen and in the cracks are mixed oxides and sulfides with the lighter colored corrosion product next to the bulk metal, rich in oxygen.

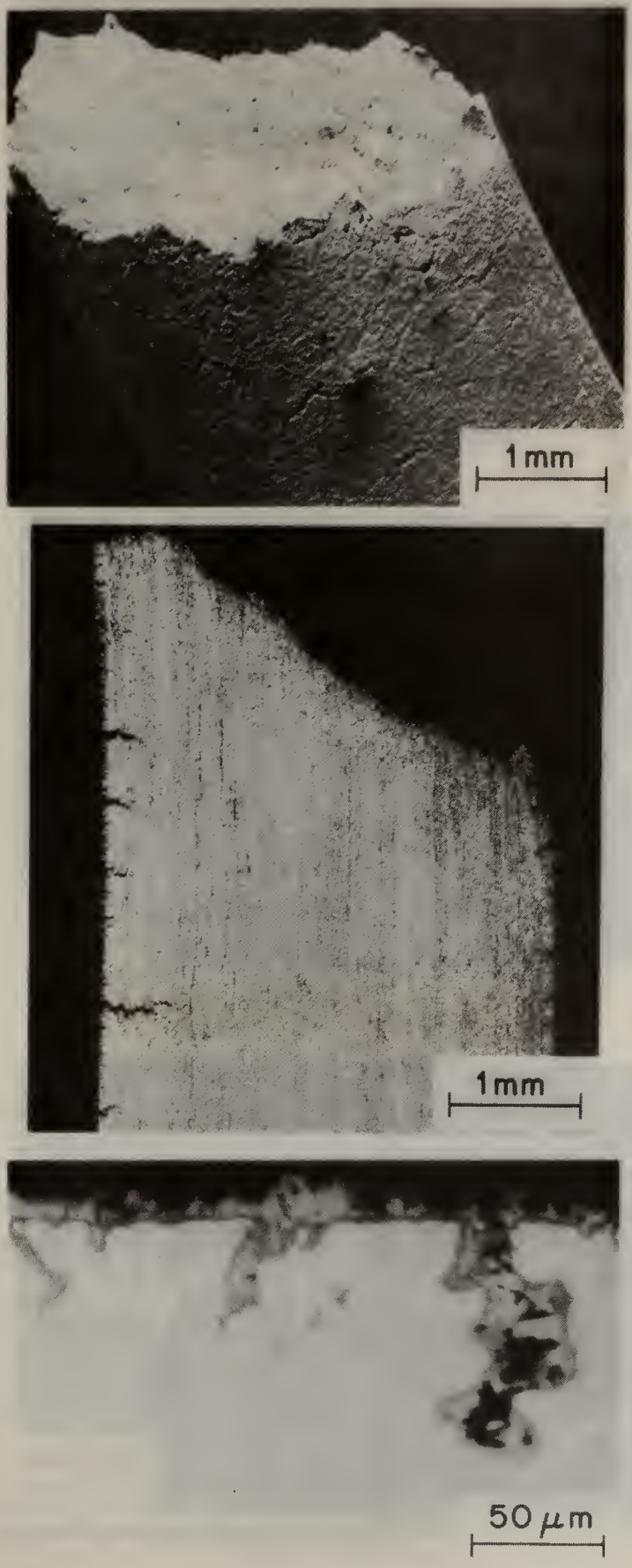

Fig. A-1. Type 310 specimen tested at 540 °C (1000 °F) at a strain rate of 10^{-6}/s in H_2S plus steam. (a) SEM of specimen at region of fracture. (b) Photomicrograph of etched cross-section near fracture. (c) Photomicrograph of cracks in the unetched profile.

(a)

(b)

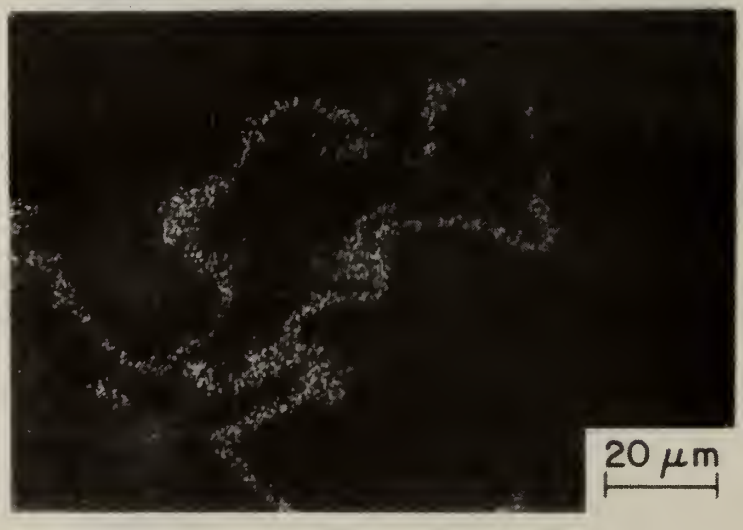

(c)

Fig. A-2. (a) Area of target current image for microprobe analysis.
(b) X-ray scan of crack showing sulfur distribution.
(c) X-ray scan of crack showing oxygen distribution.

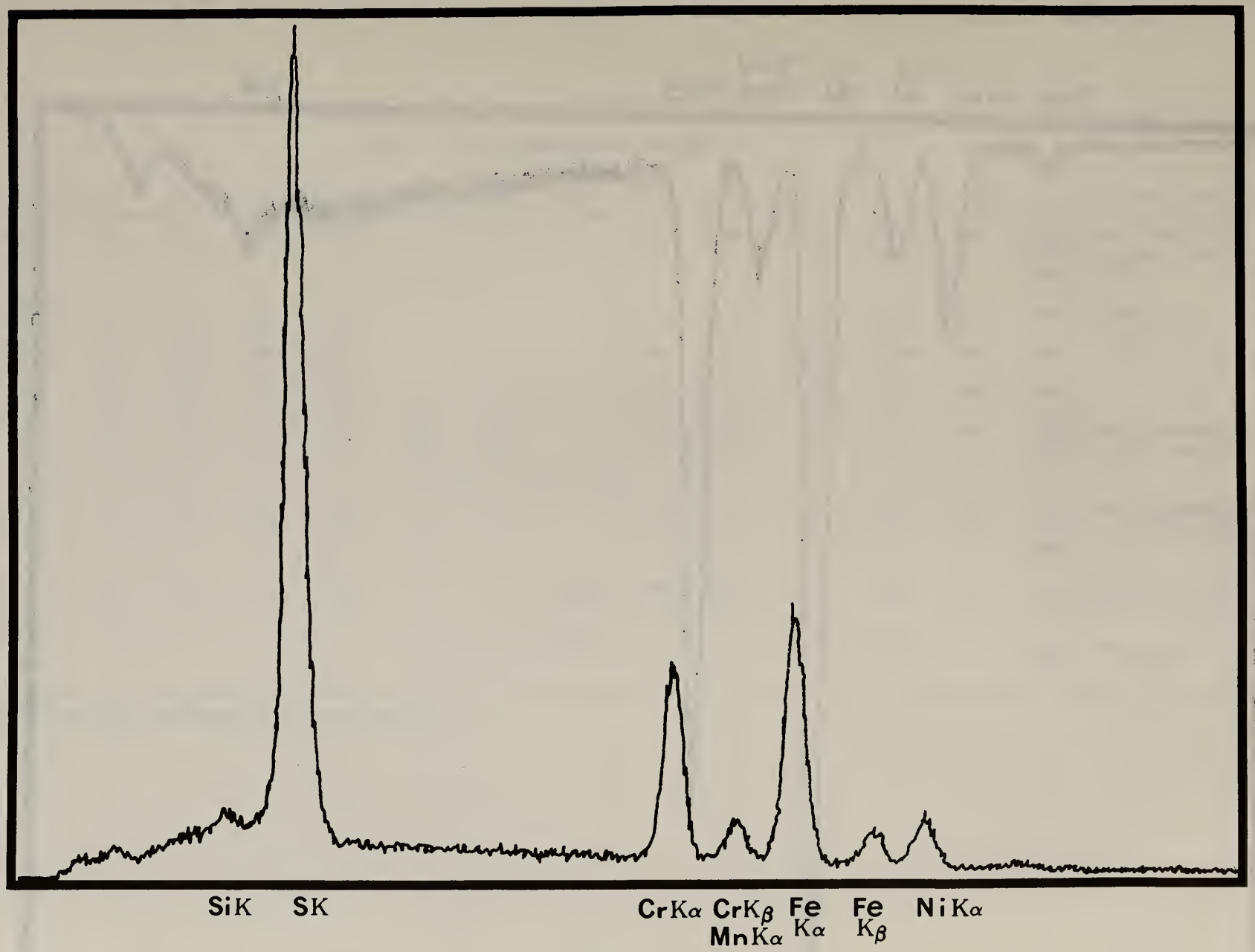

Fig. A-3. Microprobe analysis spectrum of the dark area within the crack. Area #1 from Fig. A-2a.

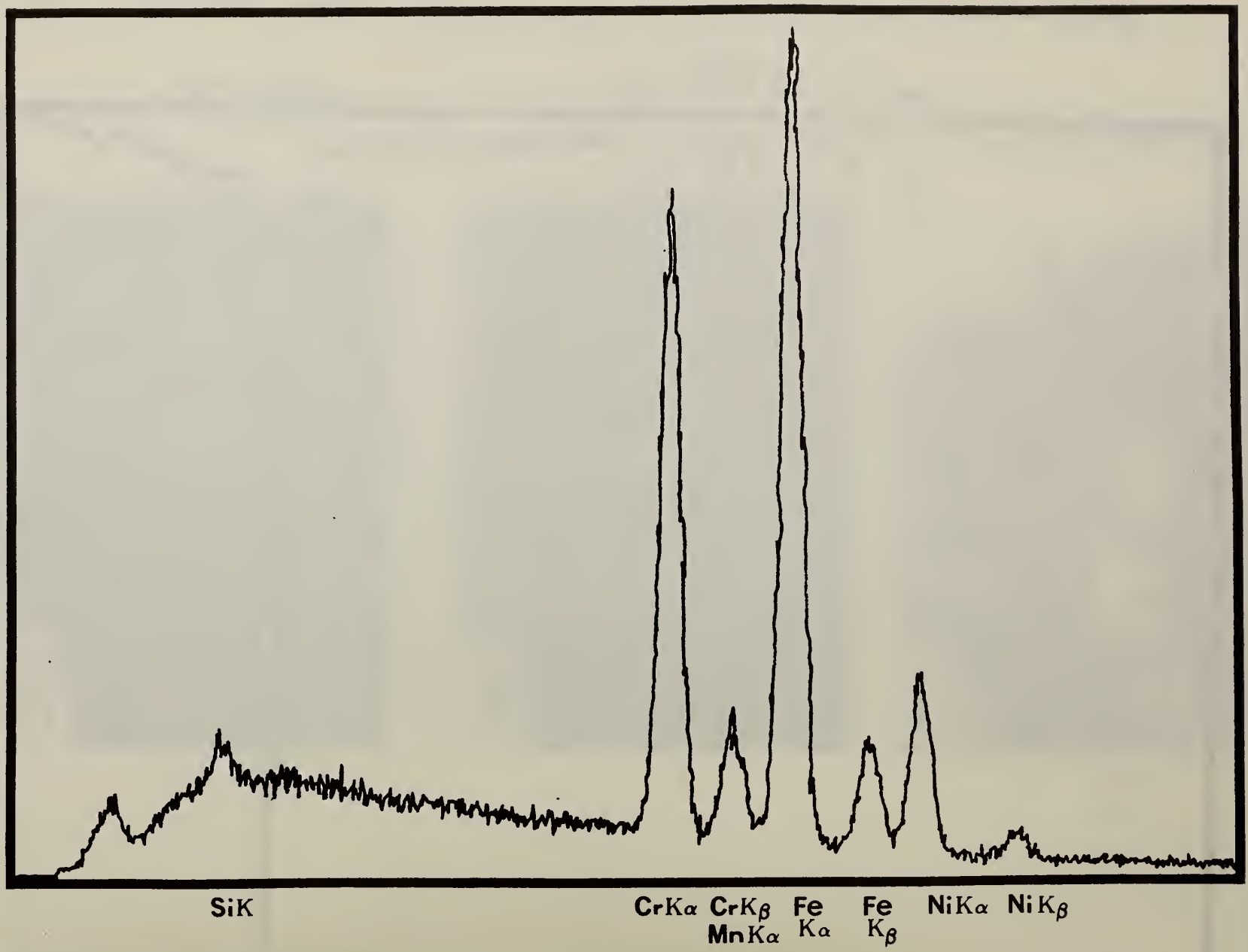

Fig. A-4. Microprobe analysis spectrum of the Type 310 specimen matrix. Area #2 from Fig. A-2a.

Table 1. Alloy Compositions, Weight %

Alloy	C	Mn	Si	S	P	Nb	Ta	Ti	Cu	Mo	Ni	Cr	Fe	Heat Treatment
Type 309	0.07	1.74	0.70	0.013	0.018				0.07	0.08	13.22	22.96	Bal	Cold drawn, Annealed 1040-1150 °C, water quench, pickled (HNO_3 - HF)
Type 310	0.08	1.78	0.48	0.02	0.028				0.17	0.10	19.59	24.84	Bal	Same as Type 309 SS
RA 310	0.05	1.81	0.62	0.009	0.010				0.06	0.02	20.02	24.62	Bal	Same as Type 309 SS
Type 310S	0.06	1.68	0.72	0.011	0.017				0.14	0.11	19.60	24.67	Bal	Same as Type 309 SS
Type 347	0.06	1.45	0.69	0.01	0.024	.64	.02		0.28	0.43	9.49	18.21	Bal	Cold drawn, Annealed 980-1090 °C, water quench, pickled (HNO_3 - HF)
Type 446	0.11	0.52	0.47	<0.005	0.035				0.03	0.13	0.59	25.77	Bal	Cold drawn, Annealed 790-870 °C, water quench, pickled (HNO_3 - HF)
Incoloy 800	0.04	0.93	0.29	0.01	0.005			0.38	0.54	0.08	32.51	20.02	Bal	Cold drawn, Solution annealed 980-1040 °C, pickled
Inconel 671	0.06							0.30			50.27	46.74		Cold drawn, Solution annealed 1150 °C, Pickled

(*) From quantitative analyses performed by Chicago Spectro.

Table 2. Gas Compositions[1]

	Oxidizing/Sulfidizing Gas[2]			Oxidizing/Sulfidizing/Carburizing Gas[3]		
	INPUT	EQUILIBRIUM		INPUT	EQUILIBRIUM	
	1atm, 25 °C	1atm, 450 °C	1atm, 600 °C	1atm, 25 °C	1atm, 450 °C	1atm, 600 °C
CO	11.6	1.2	9.2	26.0	1.1	12.5
CO_2	15.4	24.9	20.6	14.8	22.0	20.0
H_2	13.0	16.0	36.3	26.0	12.8	32.7
CH_4	10.0	12.5	2.9	10.0	11.2	5.5
H_2S	1.0	1.0	0.9	1.0	1.0	0.9
H_2O	49.0	44.4	30.3	22.2	34.3	19.4
C	--	--	--	--	17.6	9.0
$\log P_{O_2}$		-28.995	-23.919		-29.026	-24.216
$\log P_{S_2}$		-10.260	-8.878		-10.086	-8.751
$\log a_C$		-0.043	-0.288		+0.017	+0.038

(1) The above gas mixtures are two of twelve mixtures being used at Battelle Columbus Laboratories and Argonne National Laboratory.

(2) This mixture corresponds to Battelle's "Gas Mixture 1A".

(3) This mixture corresponds to Battelle's "Gas Mixture 3A".

Note: The major difference between the two mixtures is the deposition of carbon from the oxidizing/sulfidizing/carburizing gas at both temperatures, the oxidizing and sulfidizing potentials being similar at each temperature.

Table 3. Properties of 310 stainless steel tested in wet H_2S[1] and H_2O/H_2S[2] at 540 °C(1000 °F).

Strain Rate, s^{-1}		Gas	UTS, KSI,	MPa	Elongation, %	Reduction in Area, %
1.3	10^{-4}	2	82	566	33.8	63.2
7.8	10^{-5}	1	73	504	32.9	55.9
5.5	10^{-5}	2	76	524	33.4	62.8
7.2	10^{-6}	2	68.5	473	22.5	33.1
3.9	10^{-6}	1	70	483	22.9	25.4
3.6	10^{-6}	2	69	476	23.7	30.2
1.1	10^{-6}	1	68	469	17.2	18.4
8.4	10^{-7}	2	68	469	18.7	17.5
1.9	10^{-7}	1	--	--	9.0	14.4

[1]Wet H_2S = H_2S saturated with water vapor at room temperature.

[2]H_2O/H_2S = H_2S plus steam.

Table 4. Properties of 310 S stainless steel tested in wet H_2S at 540 °C(1000 °F).

Strain Rate, s^{-1}		UTS, KSI,	MPa	Elongation, %	Reduction in Area, %
1.3	10^{-4}	71.5	493	33.6	63.0
3.7	10^{-5}	71.6	494	34.5	62.6
7.3	10^{-6}	69.0	476	35.9	62.3
8.4	10^{-7}	63.1	435	34.8	50.1
1.2	10^{-7}	--	--	27.0	36.5

Table 5. Properties of 347 stainless steel tested in wet H_2S at 540 °C(1000 °F).

Strain Rate, s^{-1}		UTS, KSI,	MPa	Elongation, %	Reduction in Area, %
1.3	10^{-4}	78.8	544	17.4	62.0
3.7	10^{-5}	78.1	539	15.5	63.1
7.3	10^{-6}	71.6	494	15.1	64.3
8.4	10^{-7}	75.6	522	14.5	55.4
8.4	10^{-7}	75.4	520	17.1	61.4
1.2	10^{-7}	--	--	8.6	48.8

Table 6. Comparison of Type 310 SS and Type 309 SS in Various Gaseous Environments at 600 °C at a Strain Rate of 10^{-6}/s.

Specimen	Test Environment	Tensile Strength MPa	(psi)	Elongation %	Reduction in Area, %
310 SS	Argon[1]	411	(59,500)	18.7	24.2
310 SS	Helium	368	(53,400)	19.9	28.8
310 SS	O/S/C[2]	362	(52,500)	19.9	23.4
309 SS	Argon	323	(46,800)	31.2	57.1
309 SS	Helium	334	(48,400)	37.7	69.2
309 SS[3]	Helium	--	--	34.3	62.1
309 SS	O/S/C[2]	--	--	36.5	62.7

[1] Tested at 540 °C.

[2] O/S/C: oxidizing/sulfidizing/carburizing simulated coal gasification environment.

[3] Tested at a strain rate of 5×10^{-7}/s.

Table 7. Summary of the Fracture Modes for the Main Environment/Temperature Combinations for Specimens Tested at 10^{-6}/s.

	540 °C		450 °C			600 °C		
	He	H_2S/H_2O	He	O/S	O/S/C	He	O/S	O/S/C
Type 310	ISC[1]	ISC	D[2]	D	D	ISC	ISC	ISC
Type 310 S	ISC	D	D	D	D	ISC	ISC	ISC
Type 347	D	D	D	D	D	SC[3]	D	SC
Type 309	--	--	--	--	--	SC	--	SC
Type 446	--	--	D	SC	SC	SC	SC	SC
Inconel 800	--	--	D	D	D	SC	SC	SC
Incoloy 671	--	--	D	SC	SC	SC	SC	SC

[1] Intergranular secondary cracking.

[2] Ductile failure.

[3] Path of secondary cracking was not determined.

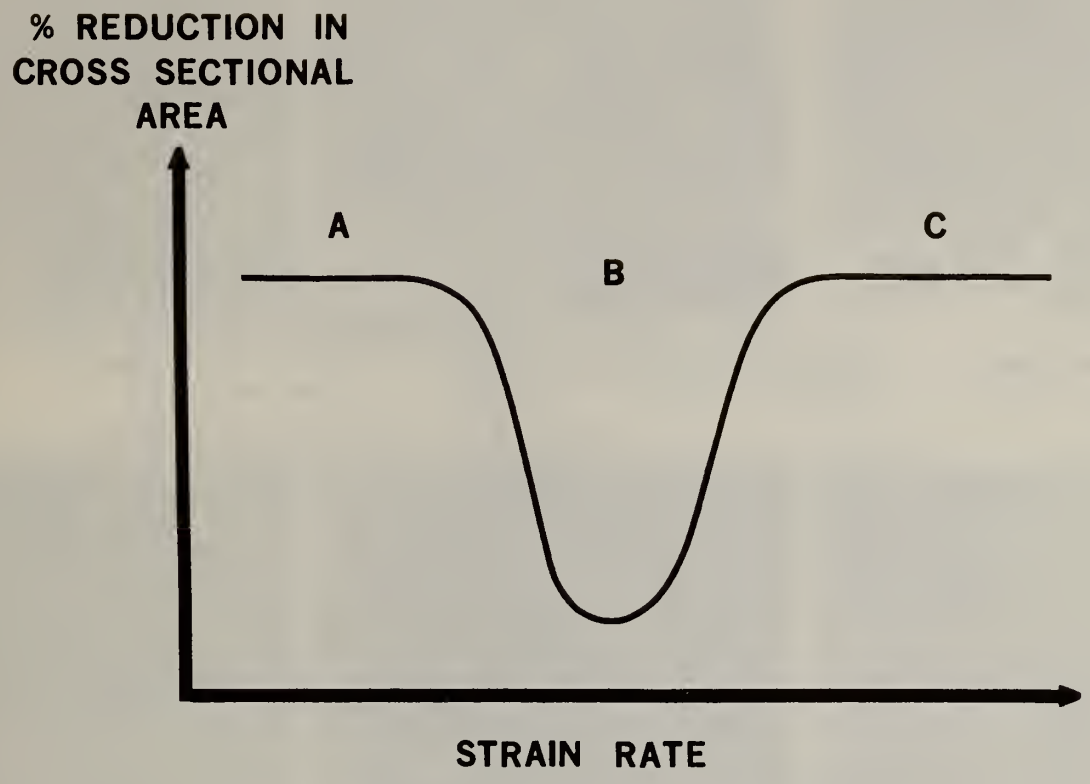

Fig. 1. Schematic representation of typical results obtained from the application of the SSRT to the study of SCC in aqueous media. The interpretation of Regions A, B and C is discussed in the text.

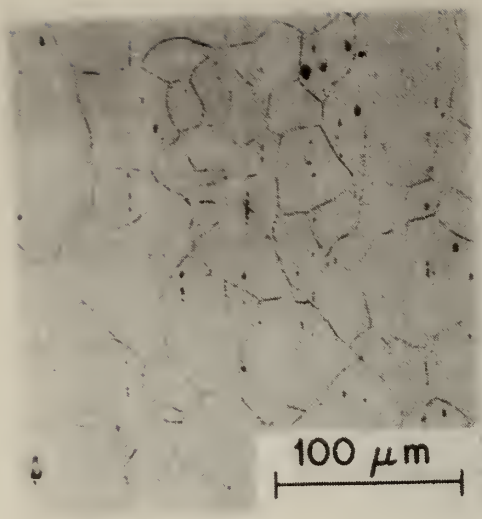

Type 309, 250 X

Type 310, 250 X

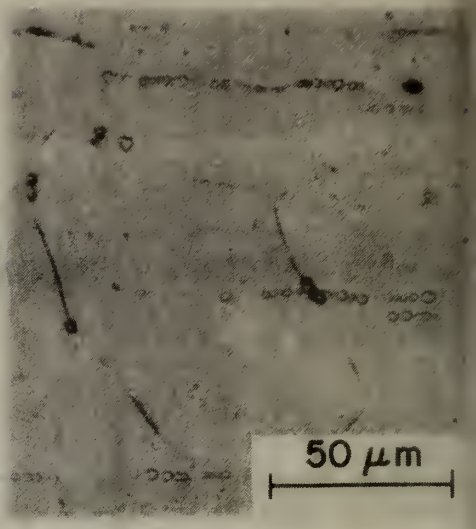

Type 310 S, 500 X

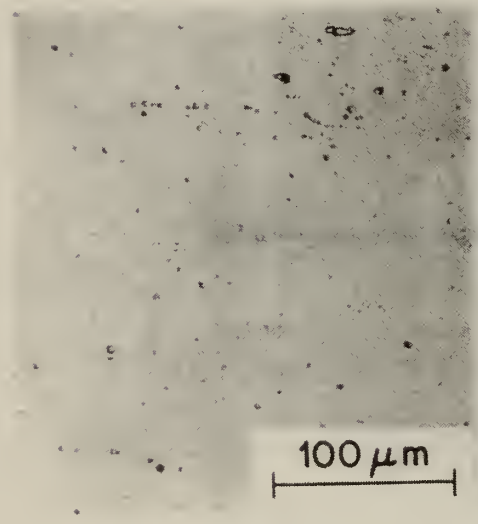

Type 347, 250 X

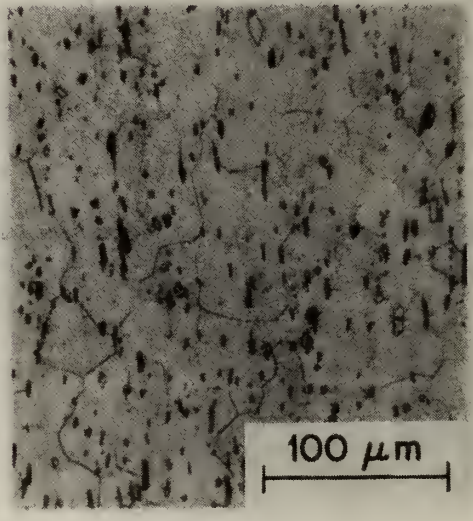

Type 446, 250 X

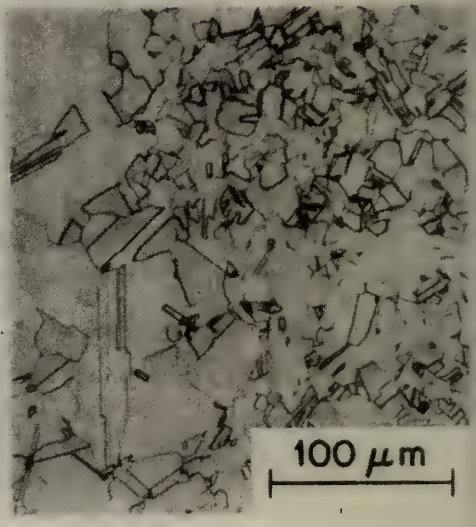

Incoloy 800, 250 X

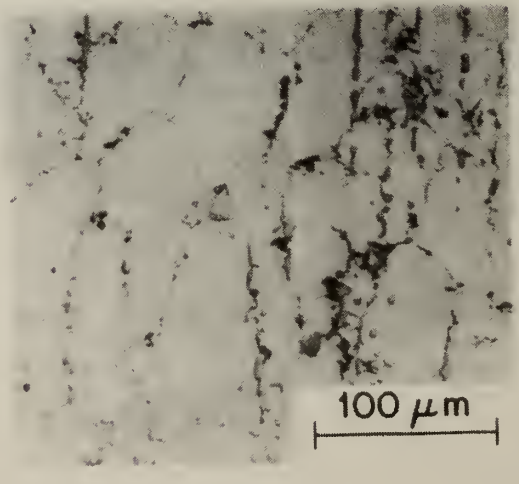

Inconel 671, 250 X

Fig. 2. Microstructures of test alloys in the as-received condition.

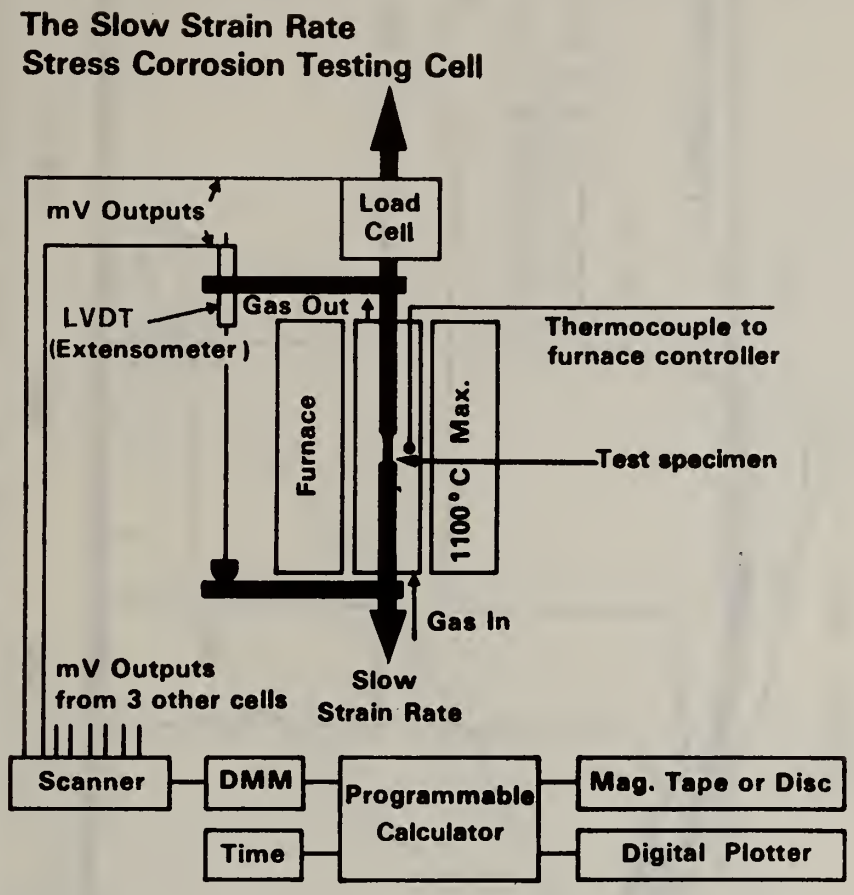

Fig. 3. A schematic representation of the slow strain rate testing facilities.

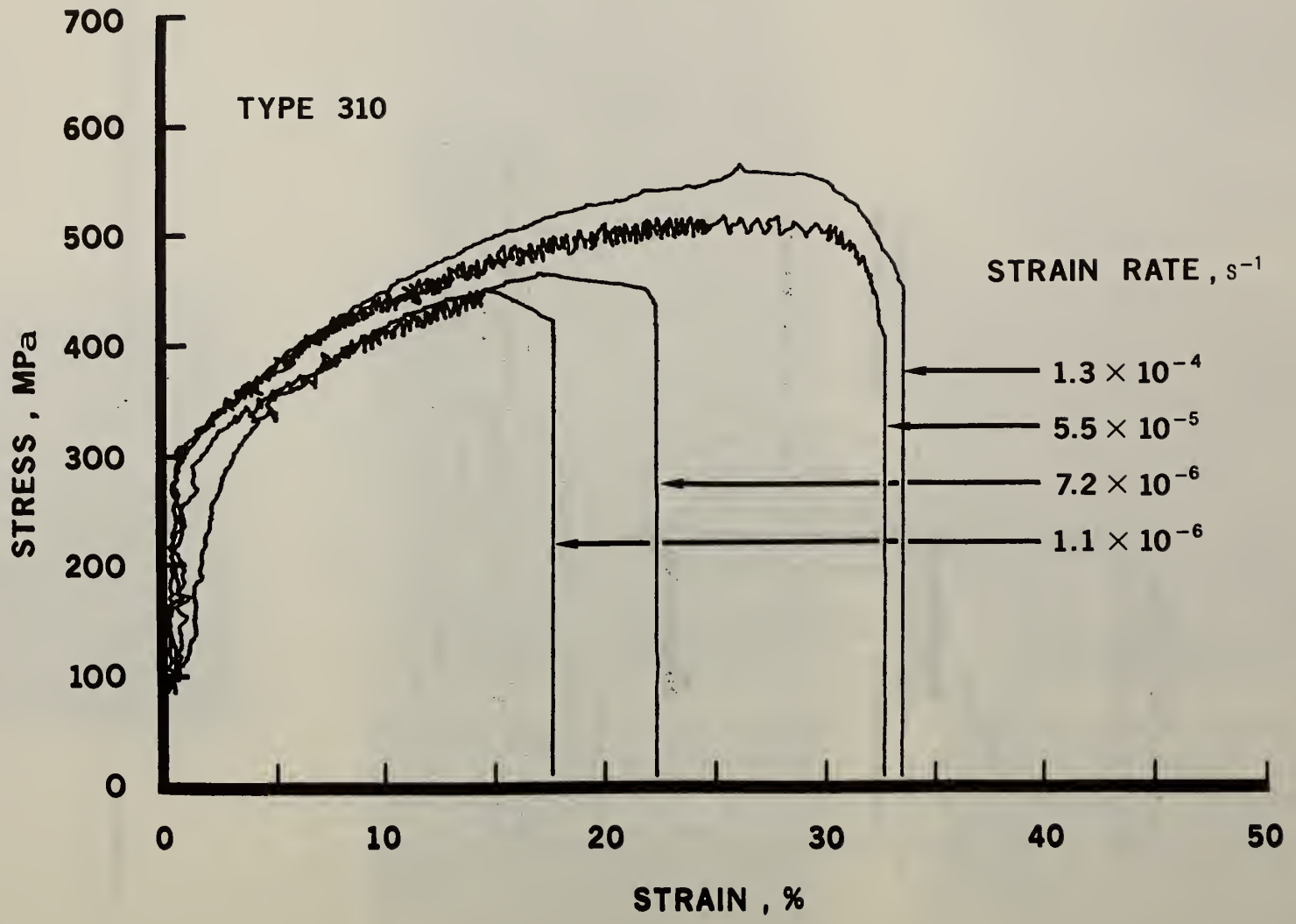

Fig. 4. Effect of strain rate on stress-strain curves of Type 310 specimens tested in H_2O/H_2S at 540 °C.

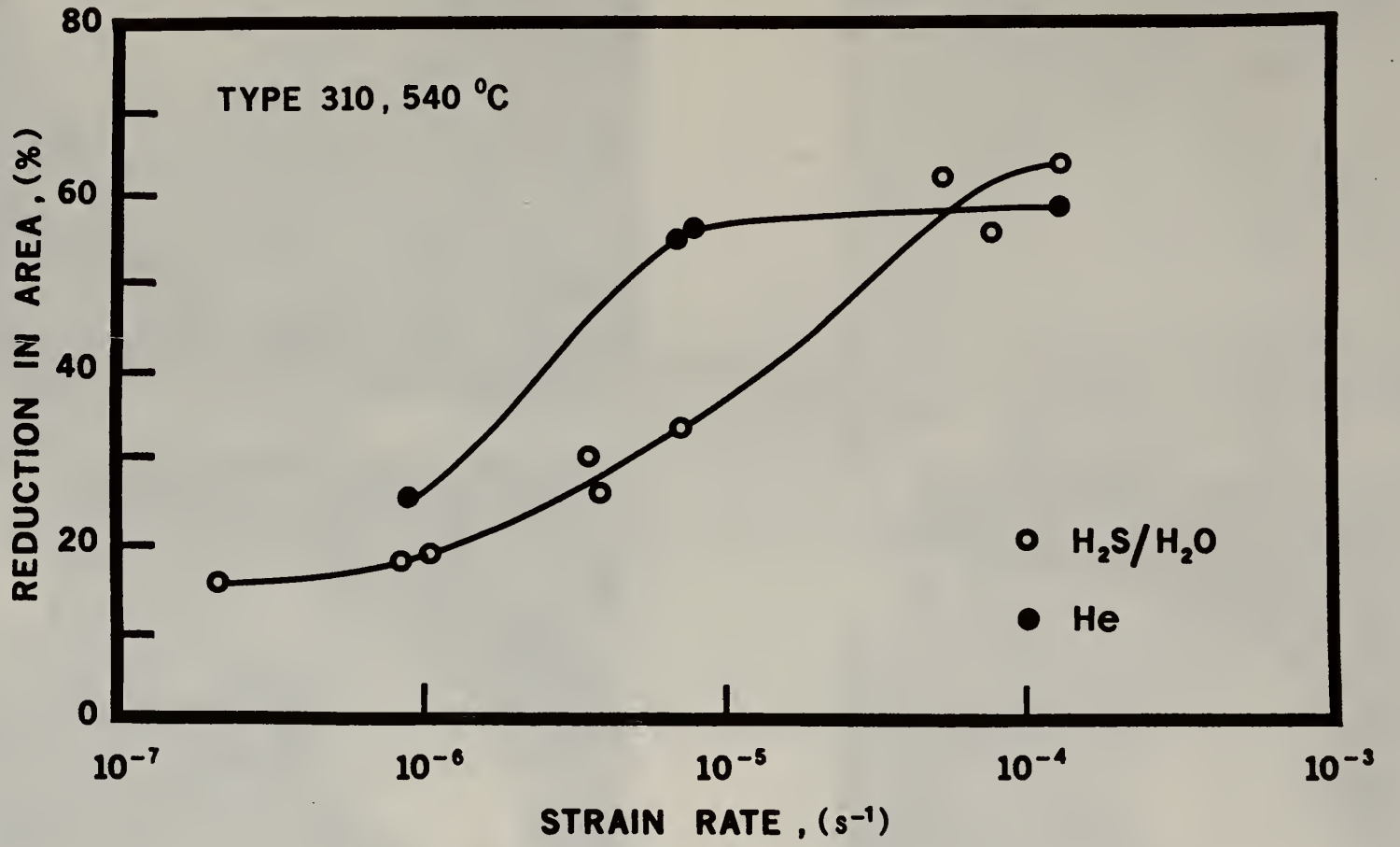

Fig. 5. Ductility as reduction in area versus strain rate for Type 310 specimens tested in gaseous H_2O/H_2S and He at 540 °C (1000 °F).

(a) $\dot{\varepsilon} = 1.3 \times 10^{-4}/s$

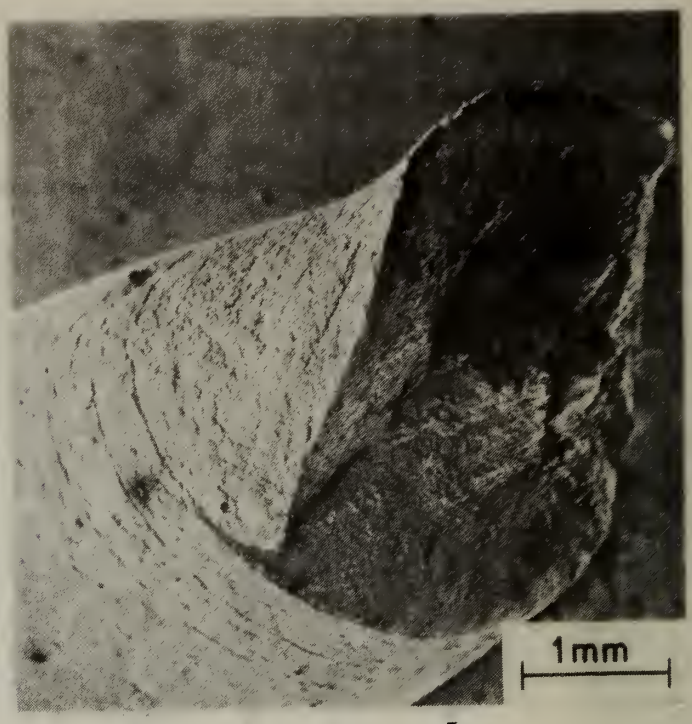

(b) $\dot{\varepsilon} = 5.5 \times 10^{-5}/s$

(c) $\dot{\varepsilon} = 7.2 \times 10^{-6}/s$

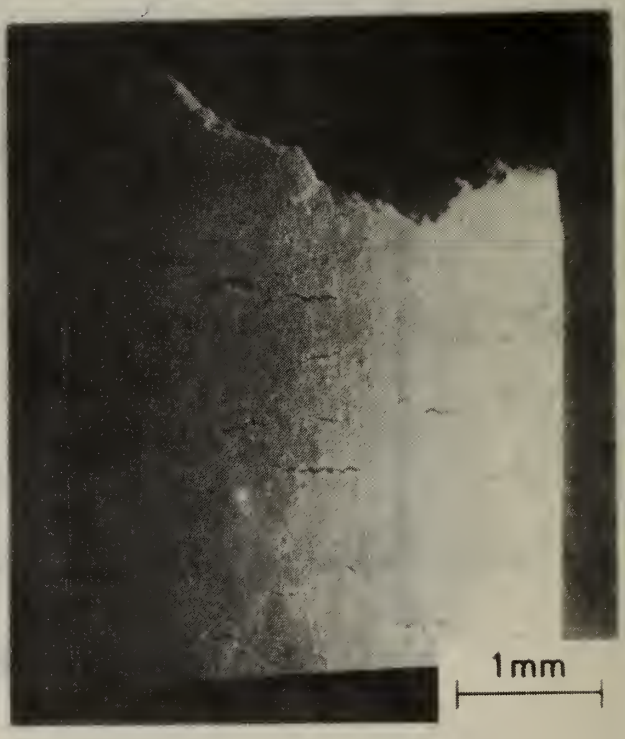

(d) $\dot{\varepsilon} = 1.1 \times 10^{-6}/s$

Fig. 6. Scanning electron micrographs indicating the effect of strain rate ($\dot{\varepsilon}$) on the fracture of Type 310 specimens when tested in H_2O/H_2S at 540 °C (1000 °F).

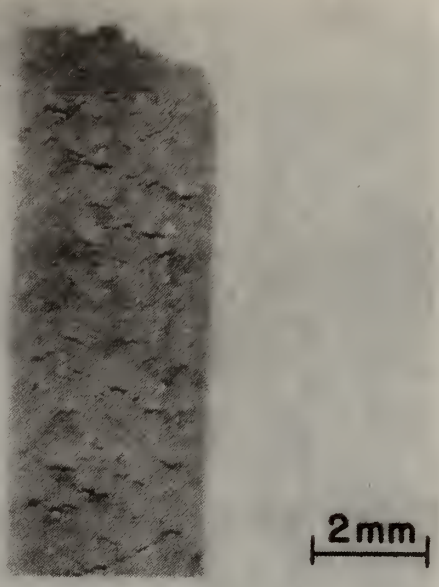

Dry Purified He

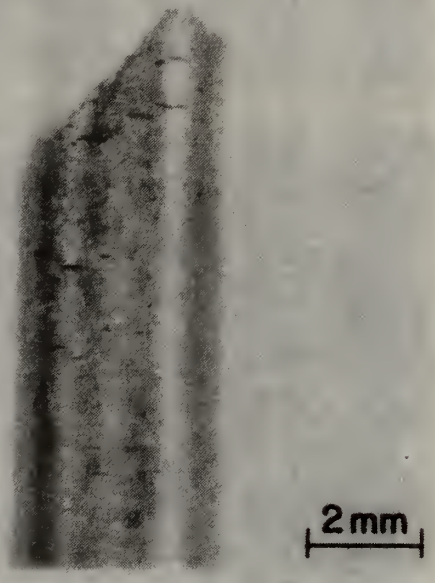

Ar

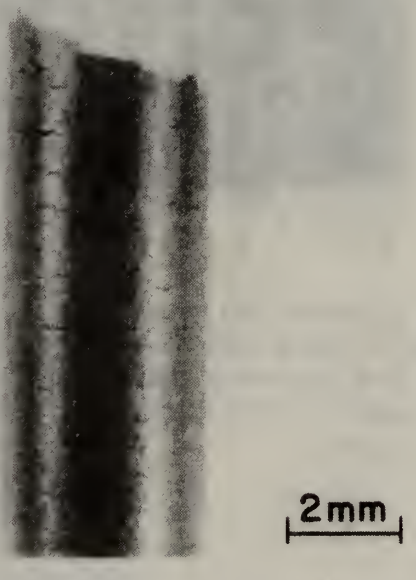

Vacuum, 2 x 10^{-2} Torr

Fig. 7. Cracking of Type 310 specimens in various "inert" environments when tested at 540 °C (1000 °F) at a strain rate of 10^{-6}/s. Original magnification 7 X.

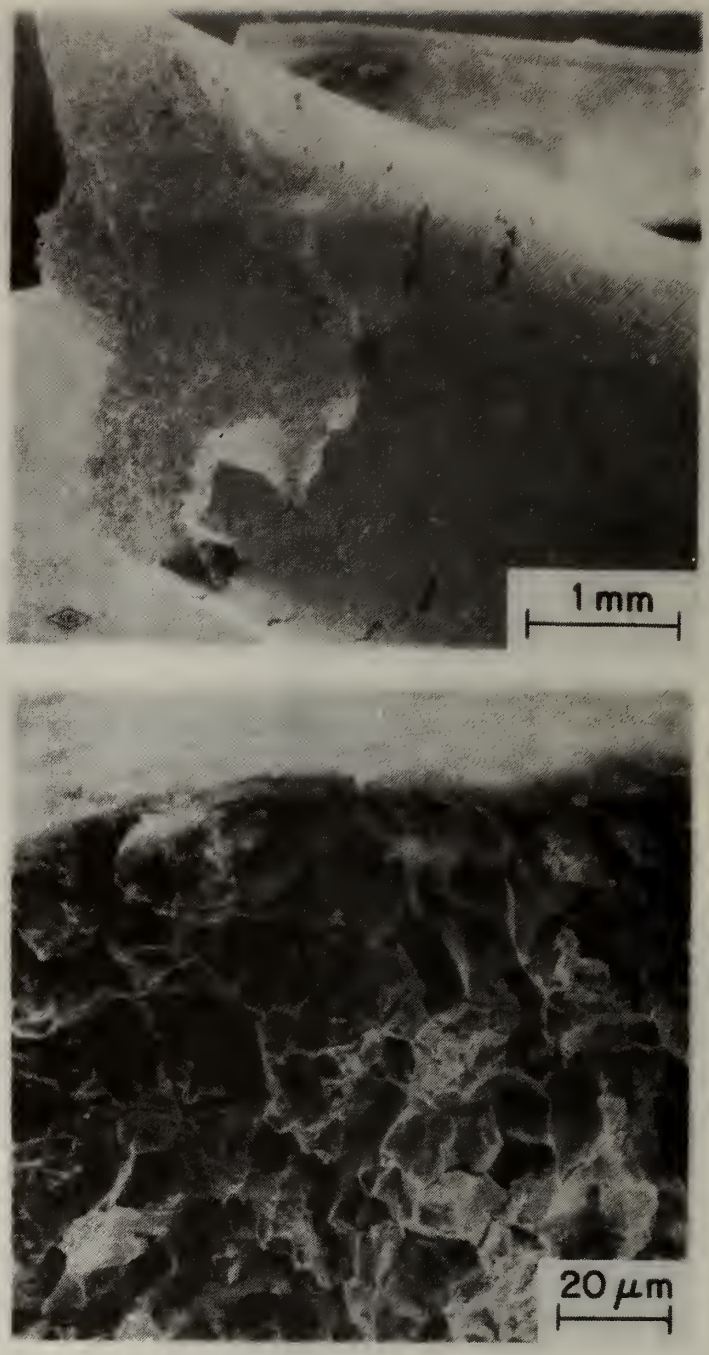

Fig. 8. Scanning electron micrographs of a Type 310 specimen tested in H_2 at 540 °C at a strain rate of 10^{-6}/s, showing the primary fracture and numerous secondary intergranular cracks (above), and the zone of intergranular failure on the primary fracture surface (below).

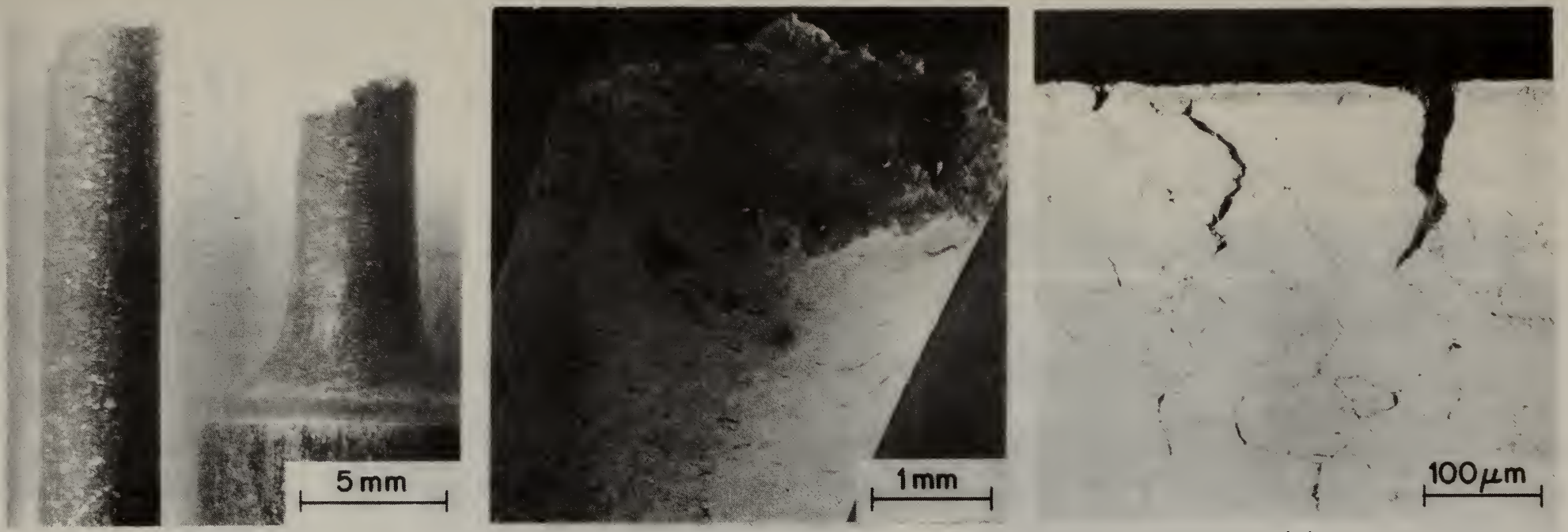

Fig. 9. Type 310 specimen tested in air at 815 °C (1500 °F) at a strain rate of 10^{-6}/s. (a) Photomicrograph of the fractured specimen. (b) Scanning electron micrograph at the region of fracture. (c) Photomicrograph of the sectioned specimen near the fracture.

(a)

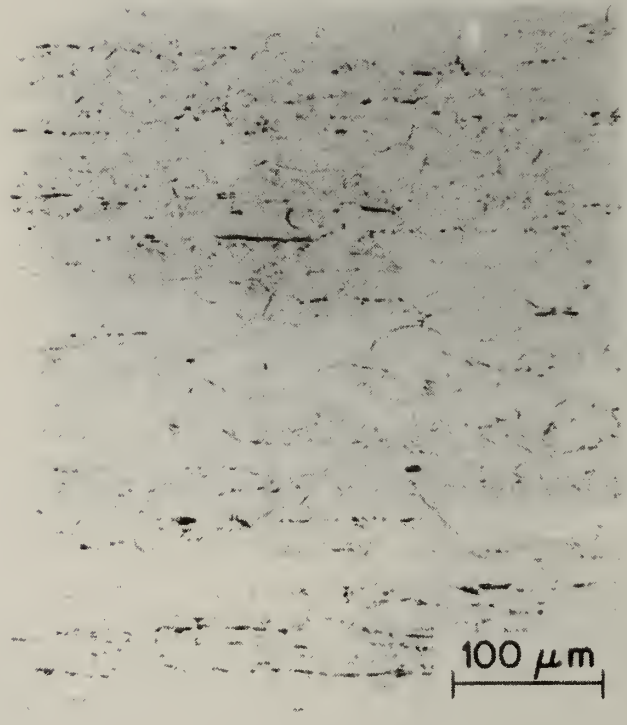

(b)

Fig. 10. Scanning electron micrograph and photomicrograph of Type 310 specimen showing the ductile fracture and partially sensitized grain boundaries after testing in He at 370 °C (700 °F) at a strain rate of 10^{-6}/s.

(a)

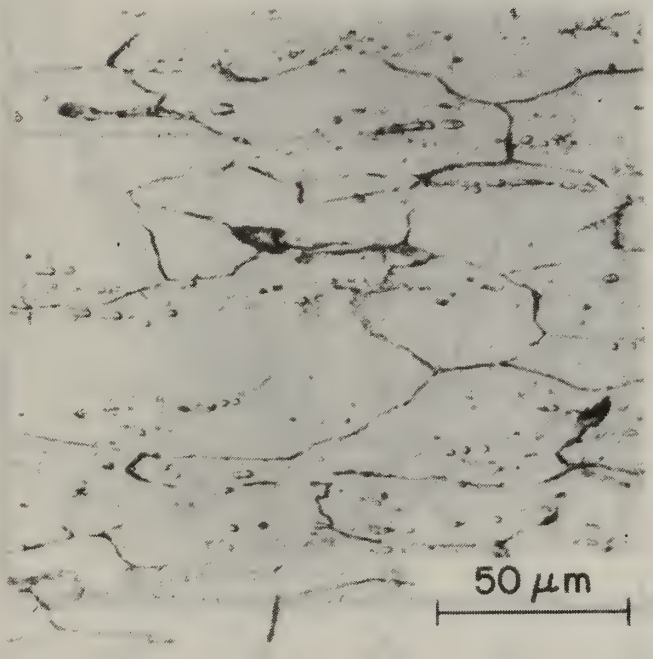

(b)

Fig. 11. Scanning electronmicrograph and photomicrograph of Type 310 specimen showing the ductile fracture and partially sensitized grain boundaries after testing in H_2 at 450 °C (840 °F) at a strain rate of 10^{-6}/s.

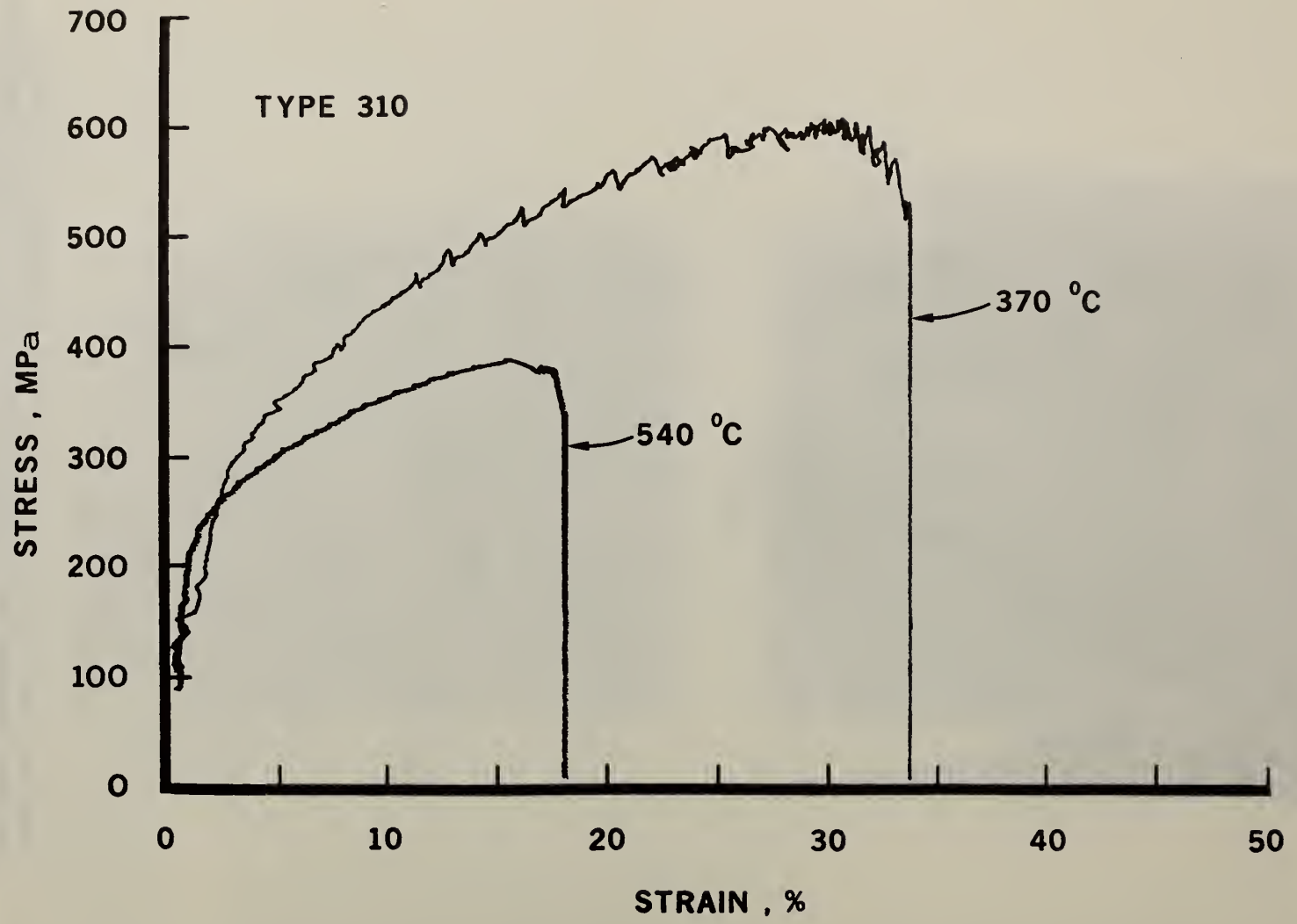

Fig. 12. Stress-strain curves for Type 310 specimens showing the effect of temperature when tested in dry He (passed through inert gas purifier) at a strain rate of 8.43×10^{-7}/s.

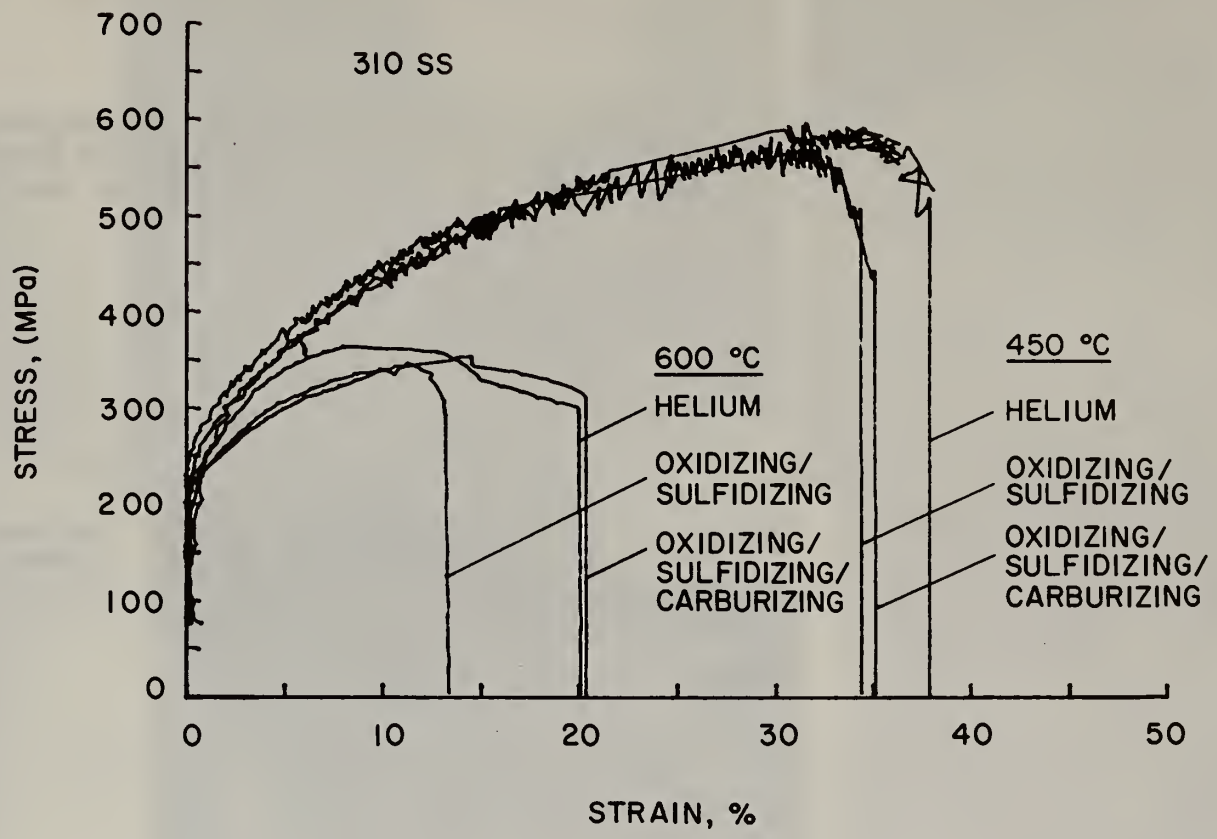

Fig. 13. Stress-strain curves for Type 310 specimens tested at 450 °C (840 °F) and 600 °C (1100 °F) in He and in oxidizing/sulfidizing and oxidizing/sulfidizing/carburizing coal gasification environments at a strain rate of 1 X 10^{-6}/s.

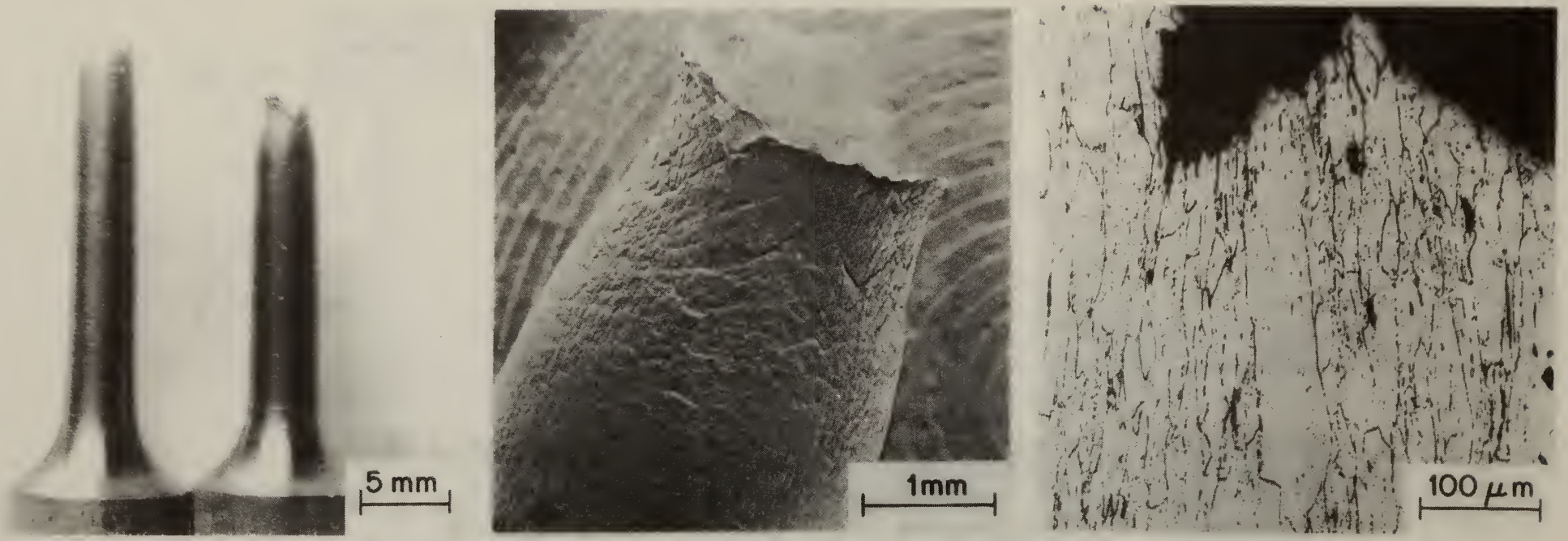

(a) (b) (c)

UTS — 602 MPa(87,300 psi)
Elongation — 37.9%
RA — 64.6%

Fig. 14. Type 310 specimen tested in He at 450 °C at a strain rate of 1 X 10^{-6}/s. (a) Photomicrograph of the fractured specimen. (b) Scanning electron micrograph at the region of fracture. (c) Photomicrograph of the sectioned specimen near the fracture.

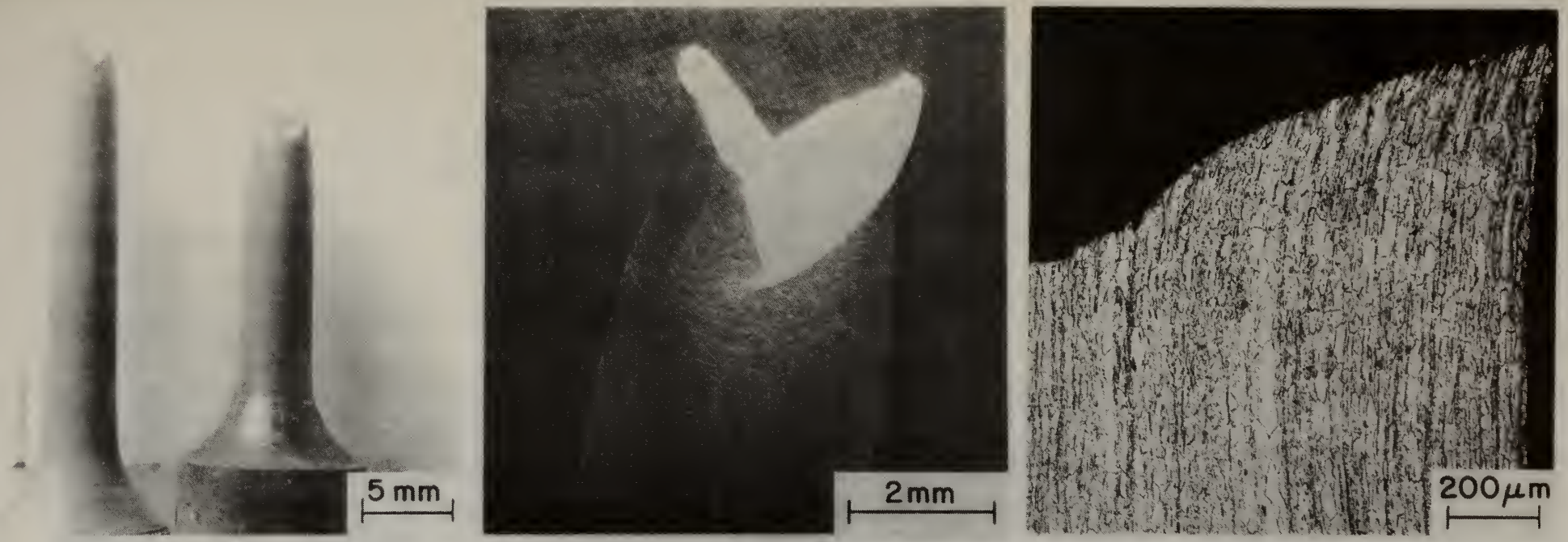

(a) (b) (c)

UTS — 581 MPa (84,200 psi)
Elongation — 35.4%
RA — 55.1%

Fig. 15. Type 310 specimen tested in the oxidizing-sulfidizing environment at 450 °C at a strain rate of 1×10^{-6}/s.
(a) Photomicrograph of the fractured specimen.
(b) Scanning electron micrograph at the region of fracture.
(c) Photomicrograph of the sectioned specimen near the fracture.

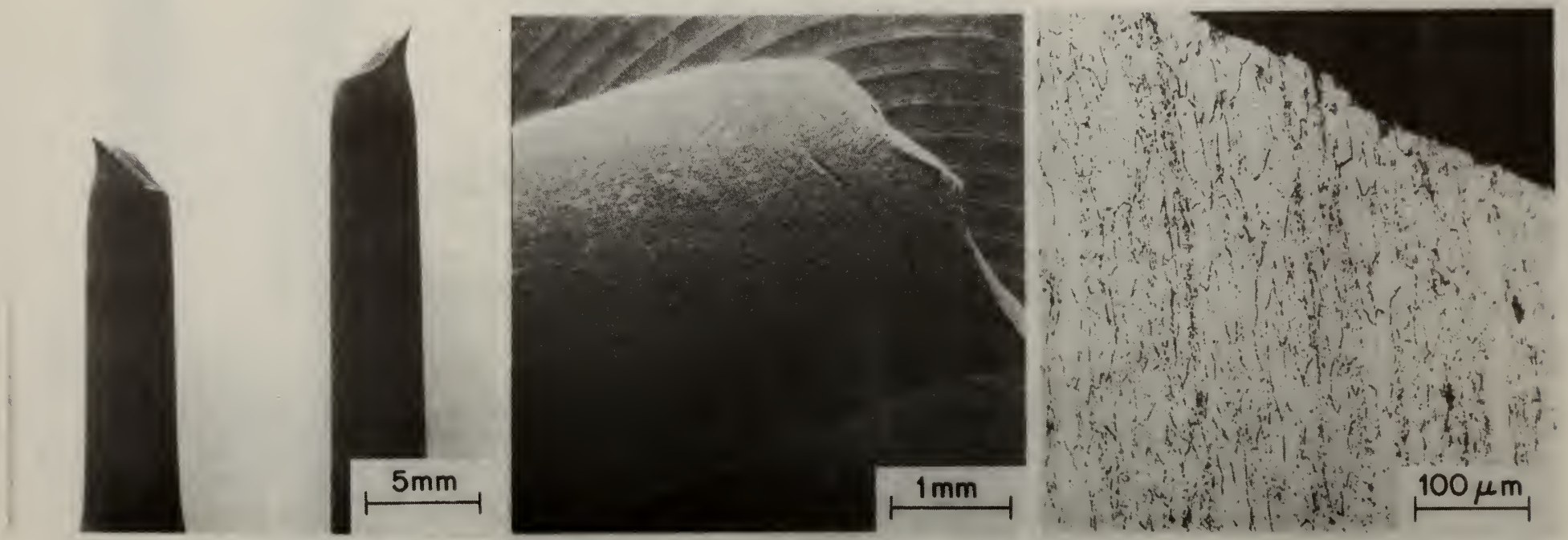

(a) (b) (c)

UTS — 598 MPa (86,700 psi)
Elongation — 35.6%
RA — 60.2%

Fig. 16. Type 310 specimen tested in the oxidizing-sulfidizing-carburizing environment at 450 °C at a strain rate of 1×10^{-6}/s.
(a) Photomicrograph of the fractured specimen.
(b) Scanning electron micrograph at the region of fracture.
(c) Photomicrograph of the sectioned specimen near the fracture.

(a)

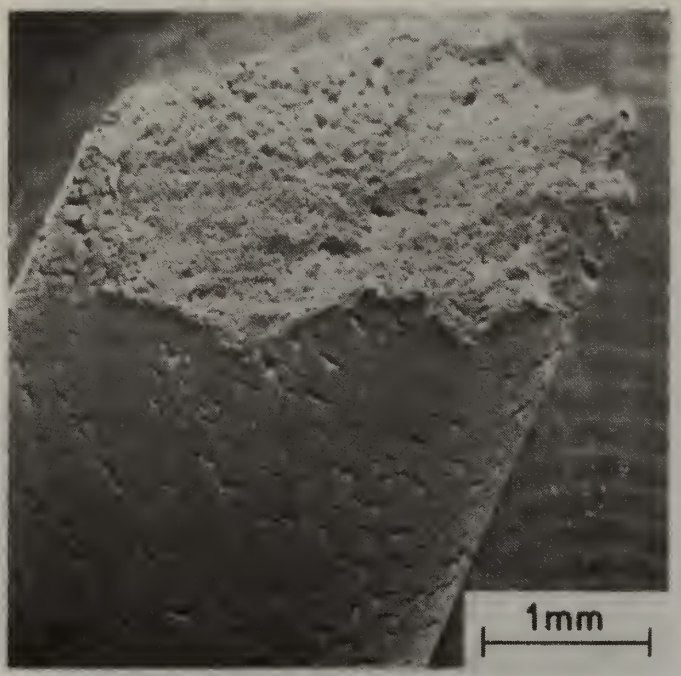

(b)

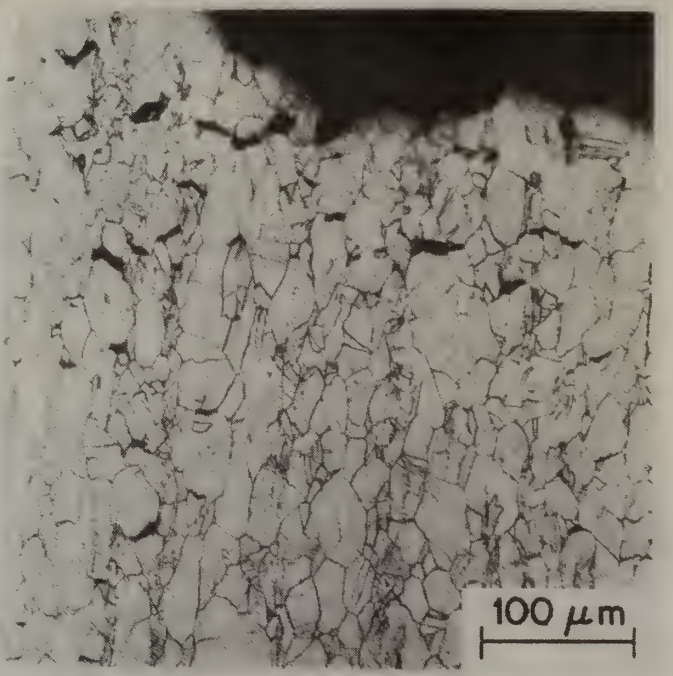

(c)

UTS — 368 MPa (53,400 psi)
Elongation — 19.9%
RA — 28.8%

Fig. 17. Type 310 specimen tested in dry He at 600 °C at a strain rate of 1×10^{-6}/s.
(a) Photomicrograph of fractured specimen.
(b) Scanning electron electron micrograph at the region of fracture.
(c) Photomicrograph of the sectioned specimen near the fracture.

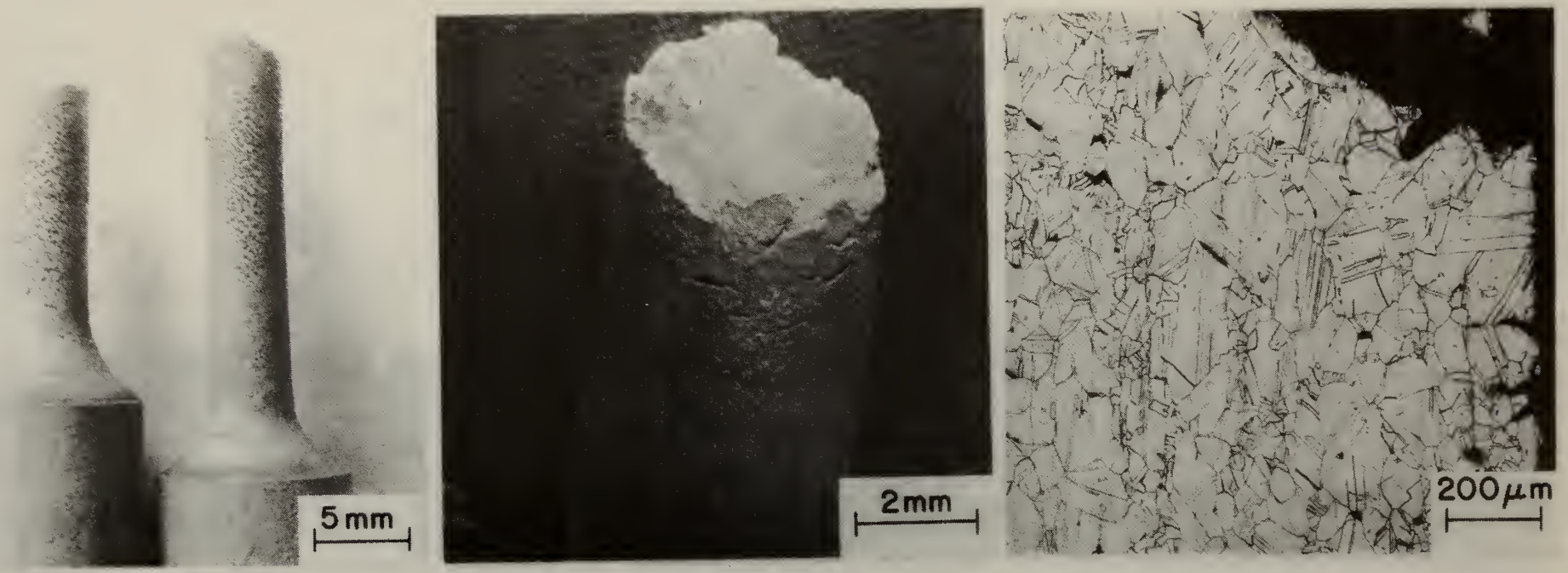

UTS — 347 MPa (50,300 psi)
Elongation — 14.0%
RA — 21.6%

Fig. 18. Type 310 specimen tested in the oxidizing-sulfidizing environment at 600 °C at a strain rate of 1 X 10^{-6}/s. (a) Photomicrograph of fractured specimen. (b) Scanning electron micrograph at the region of fracture. (c) Photograph of the sectioned specimen near the fracture.

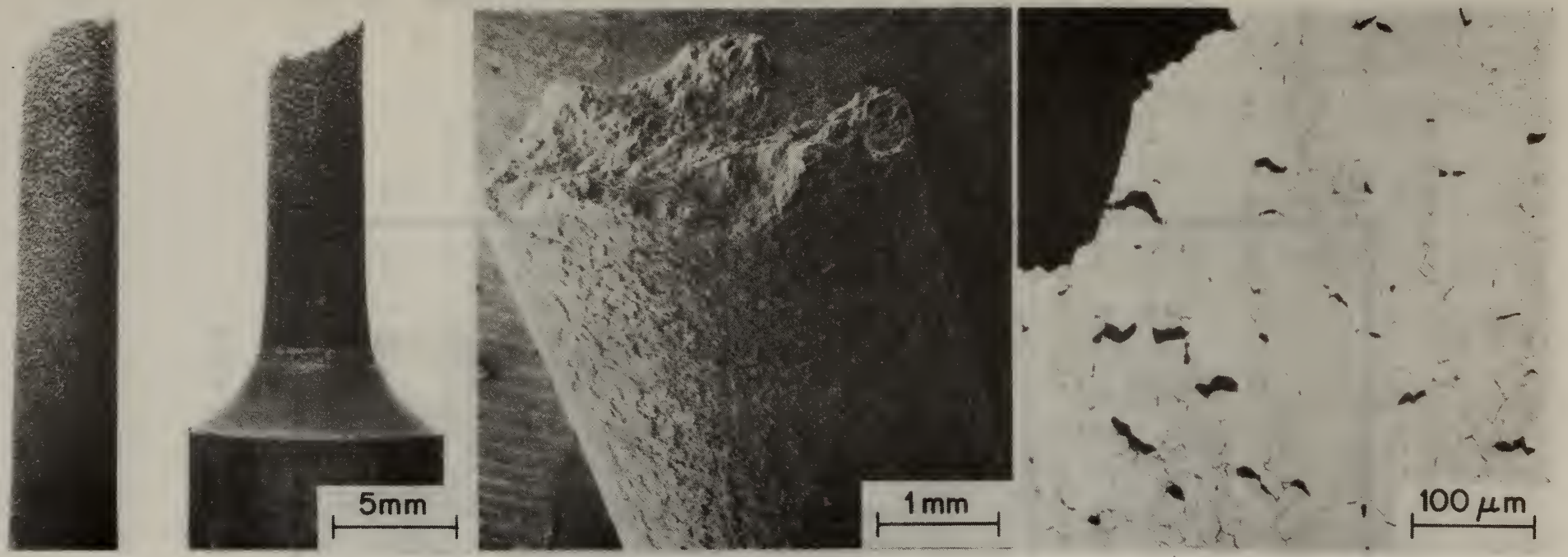

UTS — 362 MPa (52,500 psi)
Elongation — 19.9%
RA — 23.4%

Fig. 19. Type 310 specimen tested in the oxidizing-sulfidizing-carburizing environment at 600 °C at a strain rate of 1×10^{-6}/s.
(a) Photomicrograph of the fractured specimen.
(b) Scanning electron micrograph at the region of fracture.
(c) Photomicrograph of the sectioned specimen near the fracture.

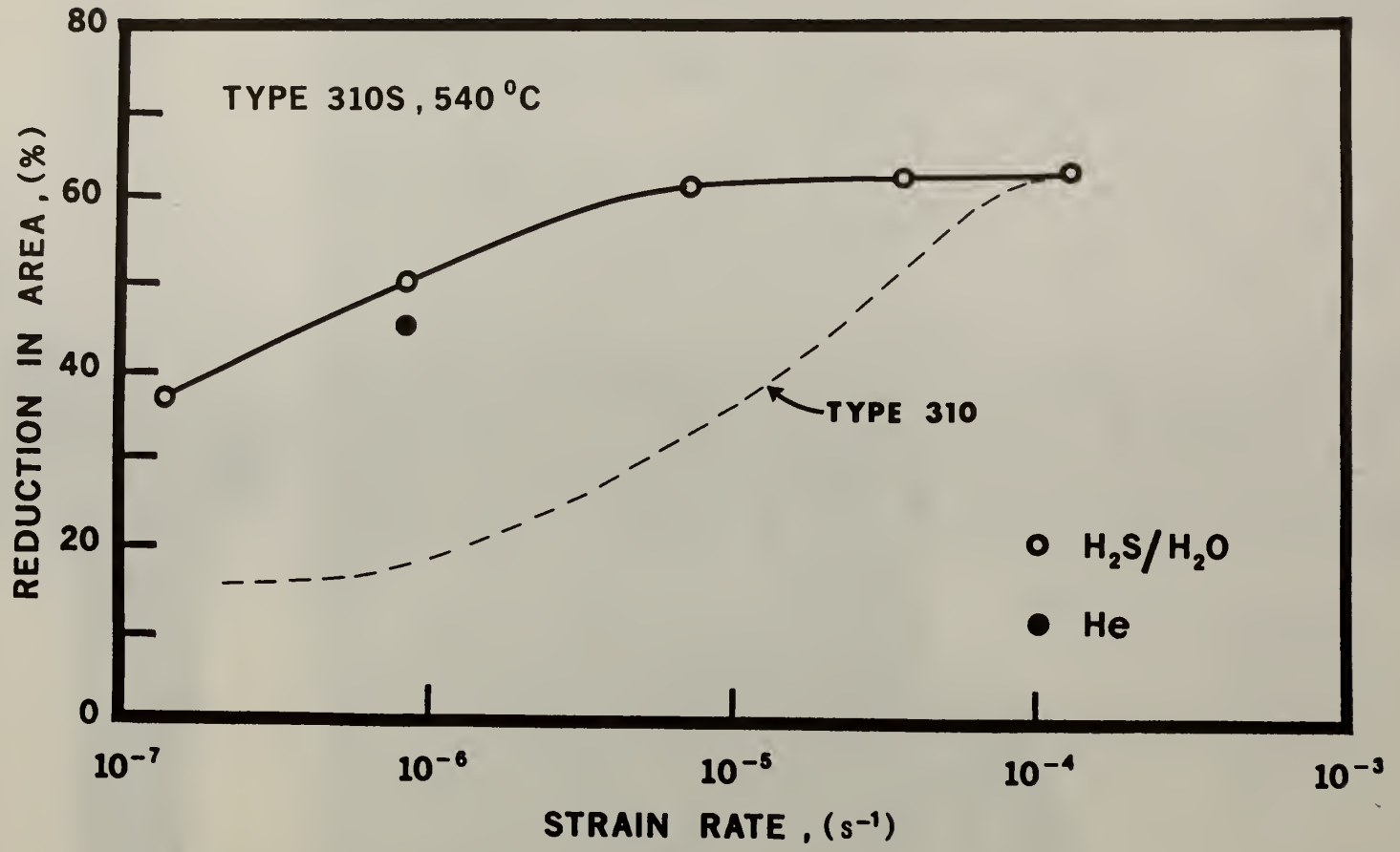

Fig. 20. Ductility as reduction in area versus strain rate for Type 310S specimens tested in gaseous H_2O/H_2S and He at 540 °C (1000 °F). Type 310 curve is shown for comparison.

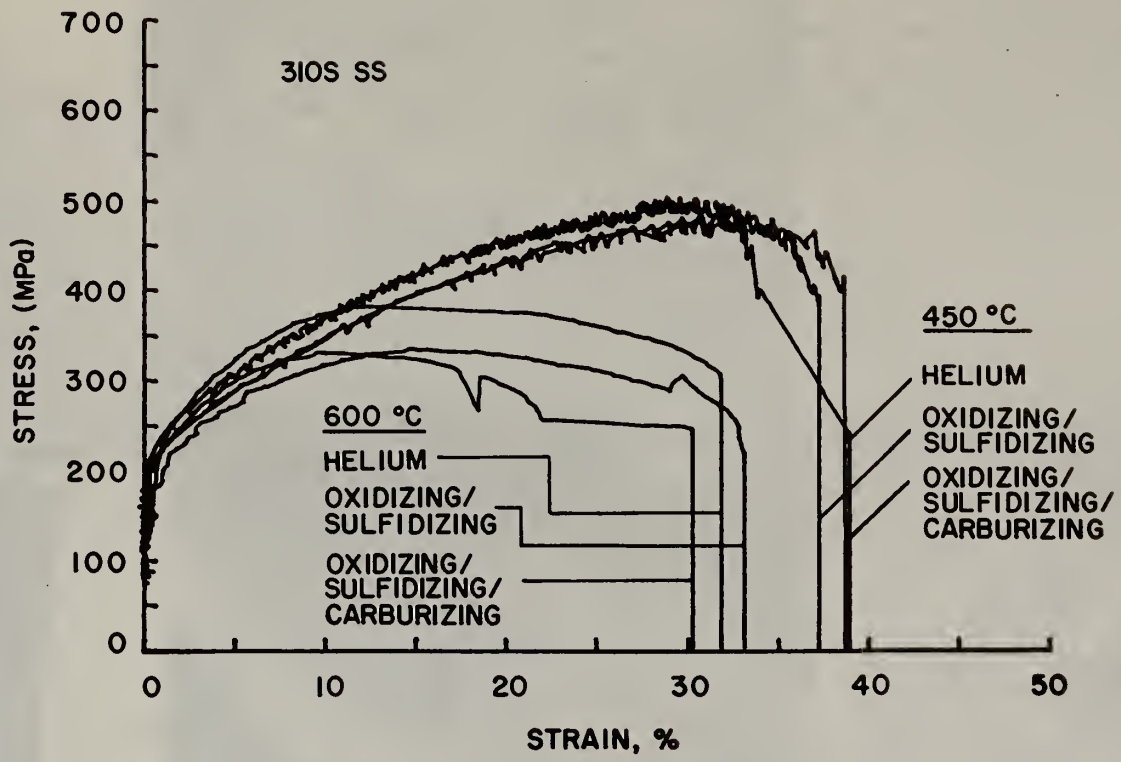

Fig. 21. Stress-strain curves for 310S steel tested at 450 °C (840 °F) and 600 °C (1100 °F) in He and in oxidizing/sulfidizing and oxidizing/sulfidizing/carburizing coal gasification environments at a strain rate of 1 X 10^{-6}/s.

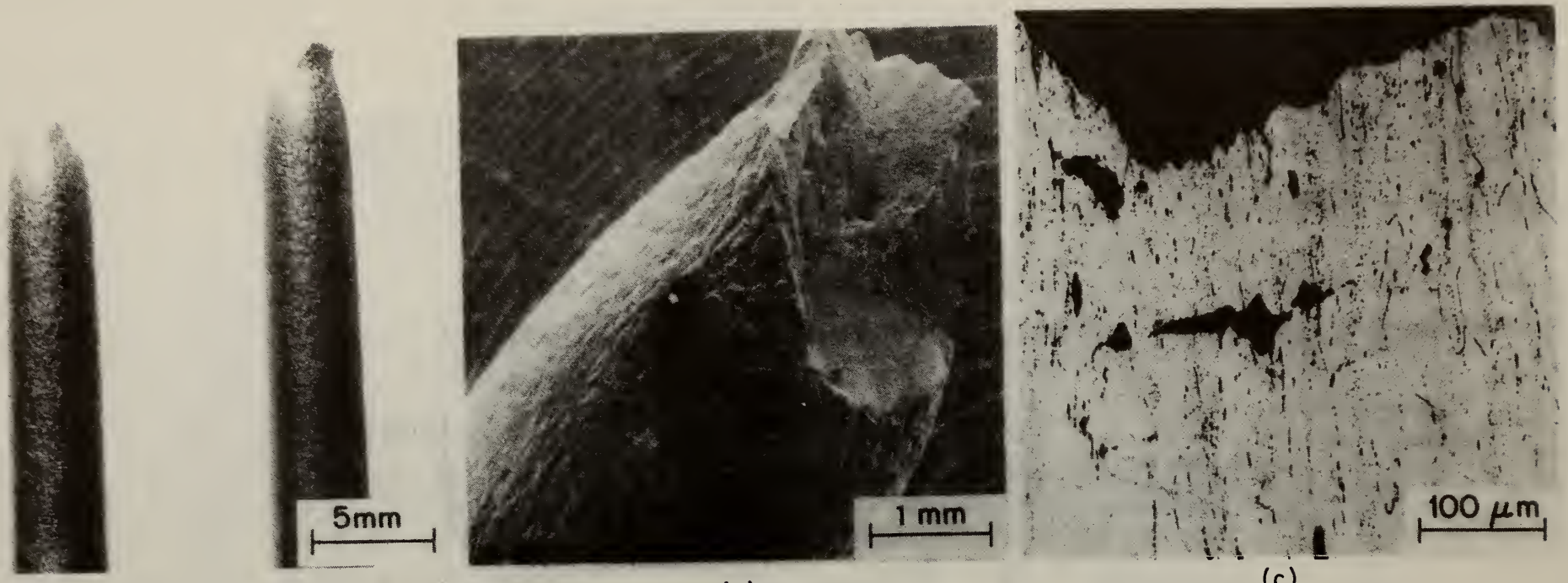

UTS — 518 MPa (75,100 psi)
Elongation — 38.9%
RA — 63.7%

Fig. 22. Type 310S stainless steel tested in He at 450 °C at a strain rate of 1 X 10^{-6}/s. (a) Photomicrograph of the fractured specimen. (b) Scanning electron micrograph at the region of fracture. (c) Photomicrograph of the sectioned specimen near the fracture.

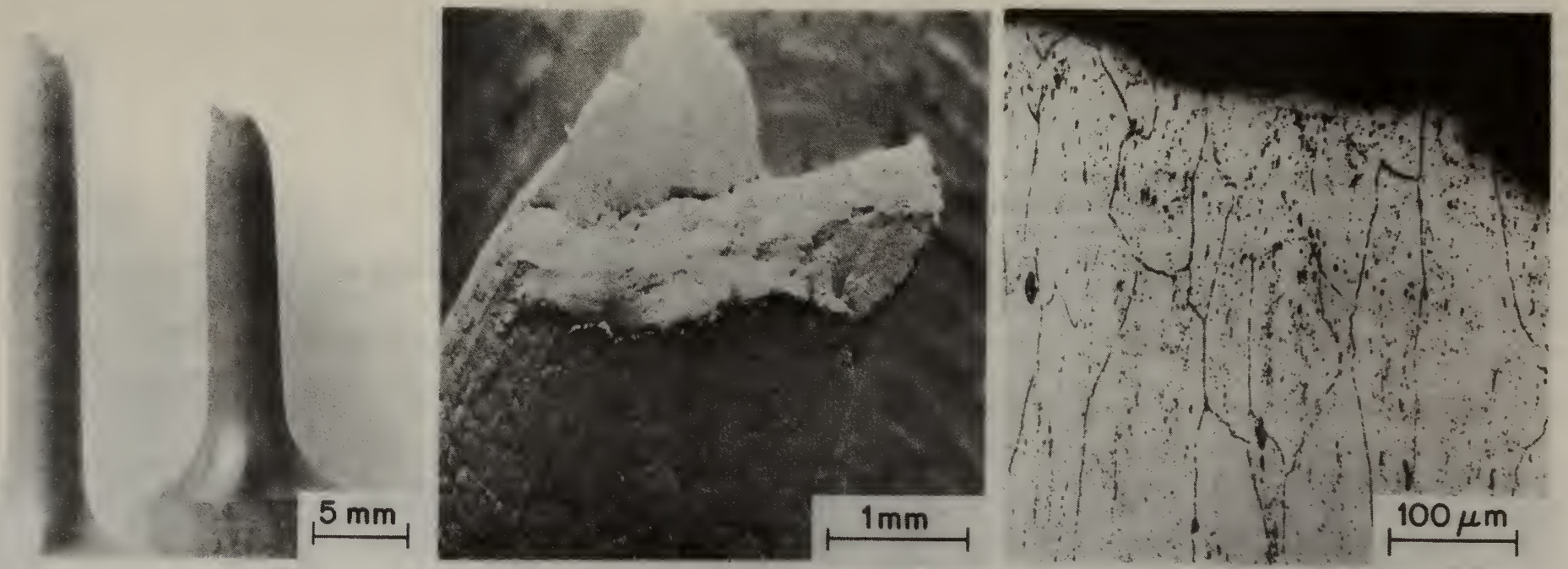

UTS — 519 MPa (75,200 psi)
Elongation — 38.6%
RA — 65.1%

Fig. 23. Type 310S stainless steel tested in the oxidizing-sulfidizing environment at 450 °C at a strain rate of 1×10^{-6}/s.
(a) Photomicrograph of the fractured specimen.
(b) Scanning electron micrograph at the region of fracture.
(c) Photomicrograph of the sectioned specimen near the fracture.

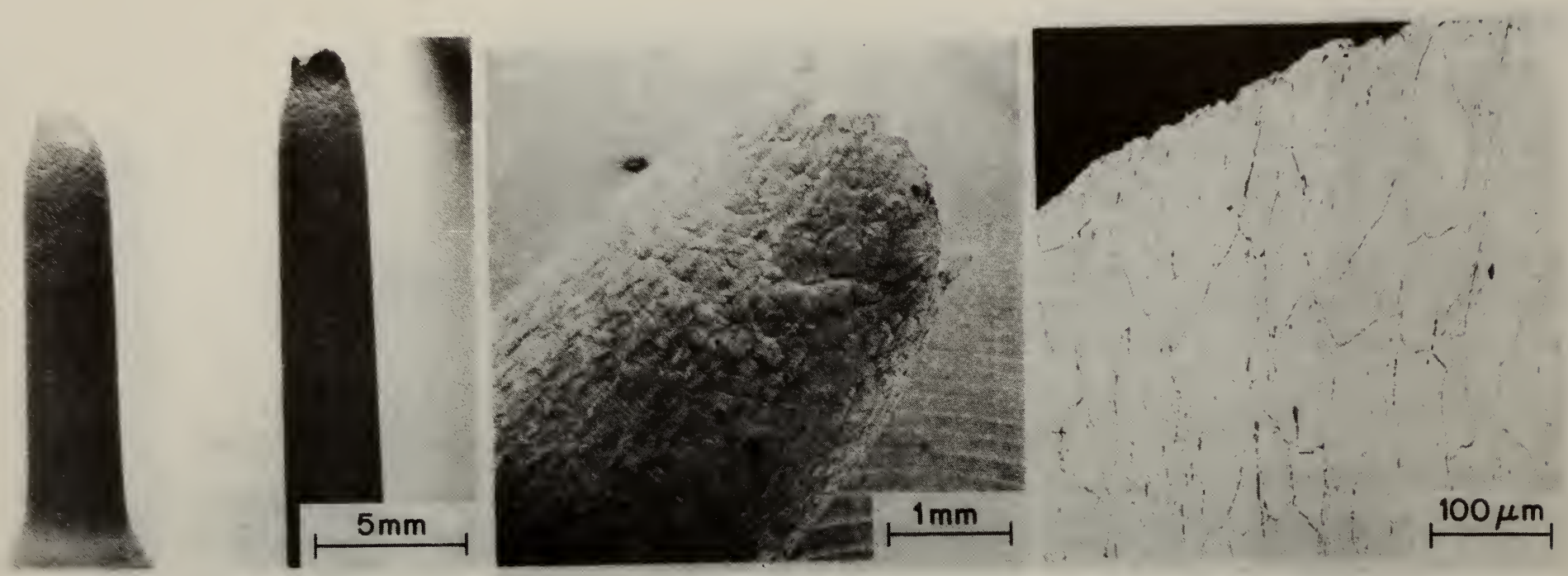

UTS — 513 MPa (74,400 psi)
Elongation — 38.8%
RA — 69.9%

Fig. 24. Type 310S stainless steel tested in the oxidizing-sulfidizing-carburizing environment at 450 °C at a strain rate of 1×10^{-6}/s.
(a) Photomicrograph of the fractured specimen.
(b) Scanning electron micrograph at the region of fracture.
(c) Photomicrograph of the sectioned specimen near the fracture.

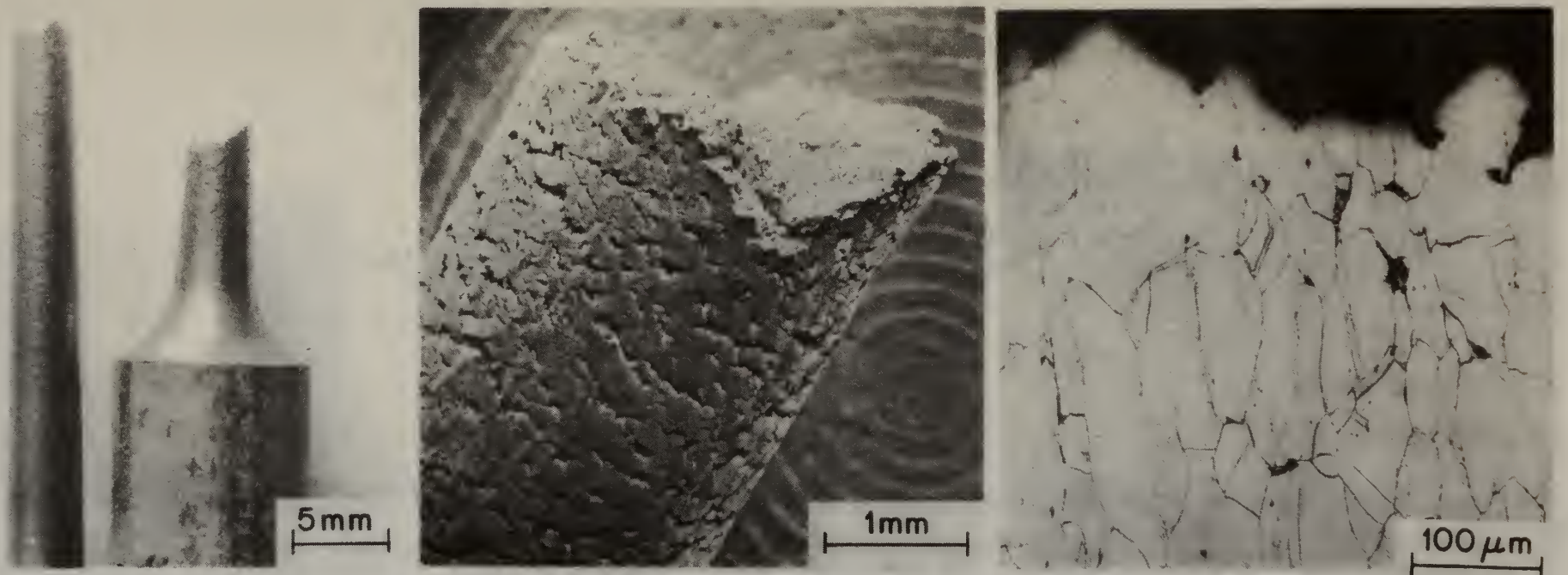

(a) (b) (c)

UTS — 437 MPa (63,400 psi)
Elongation — 31.9%
RA — 42.8%

Fig. 25. Type 310S stainless steel tested in dry He at 600 °C at a strain rate of 1×10^{-6}/s.
(a) Photomicrograph of the fractured specimen.
(b) Scanning electron micrograph at the region of fracture.
(c) Photomicrograph of the sectioned specimen near the fracture.

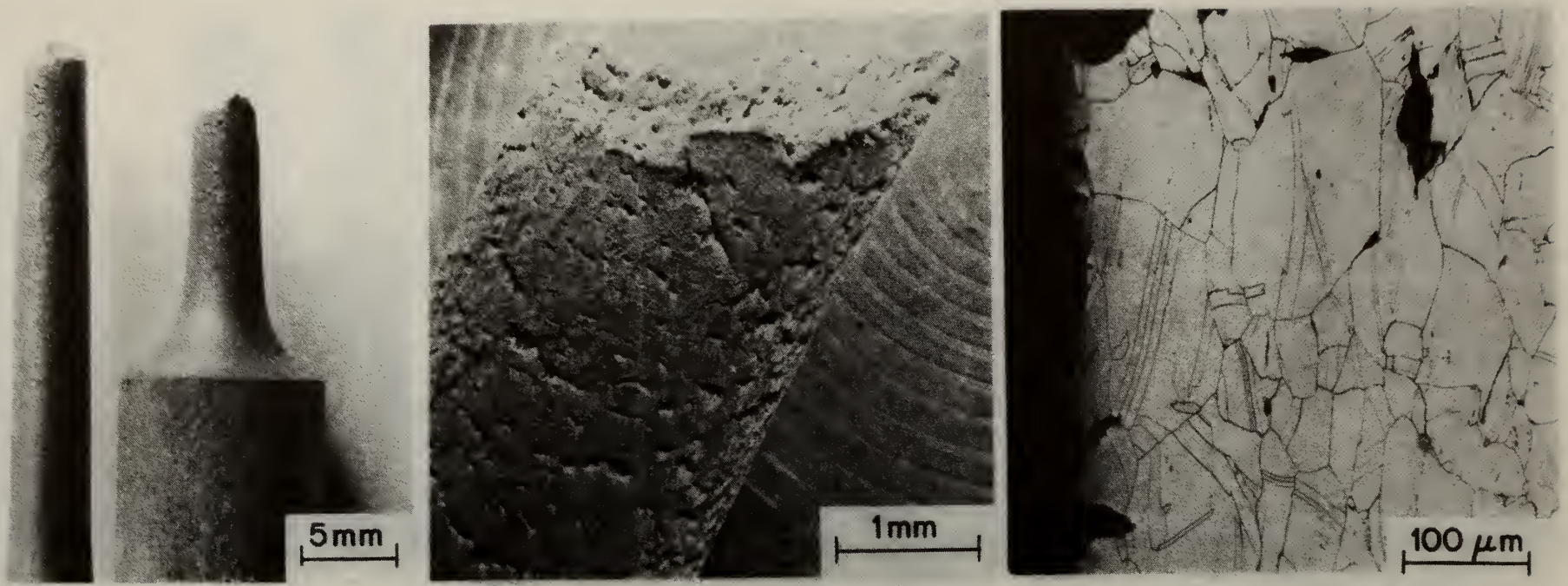

(a) (b) (c)

UTS — 376 MPa (54,500 psi)
Elongation — 32.8%
RA — 43.9%

Fig. 26. Type 310S stainless steel tested in the oxidizing-sulfidizing environment at 600 °C at a strain rate of 1×10^{-6}/s.
(a) Photomicrograph of the fractured specimen.
(b) Scanning electron micrograph at the region of fracture.
(c) Photomicrograph of the sectioned specimen near the fracture.

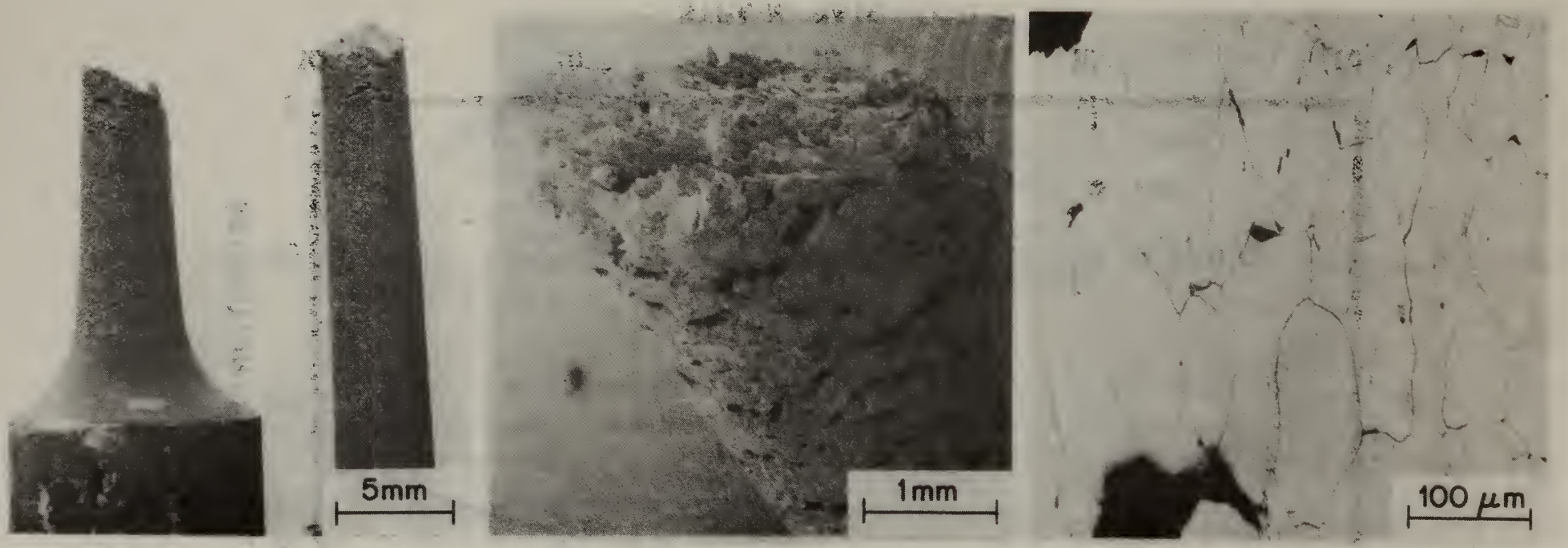

UTS — 336 MPa (48,700 psi)
Elongation — 30.3%
RA — 33.8%

Fig. 27. Type 310S stainless steel tested in the oxidizing-sulfidizing-carburizing environment at 600 °C at a strain rate of 1×10^{-6}/s.
(a) Photomicrograph of the fractured specimen.
(b) Scanning electron micrograph at the region of fracture.
(c) Photomicrograph of the sectioned specimen.

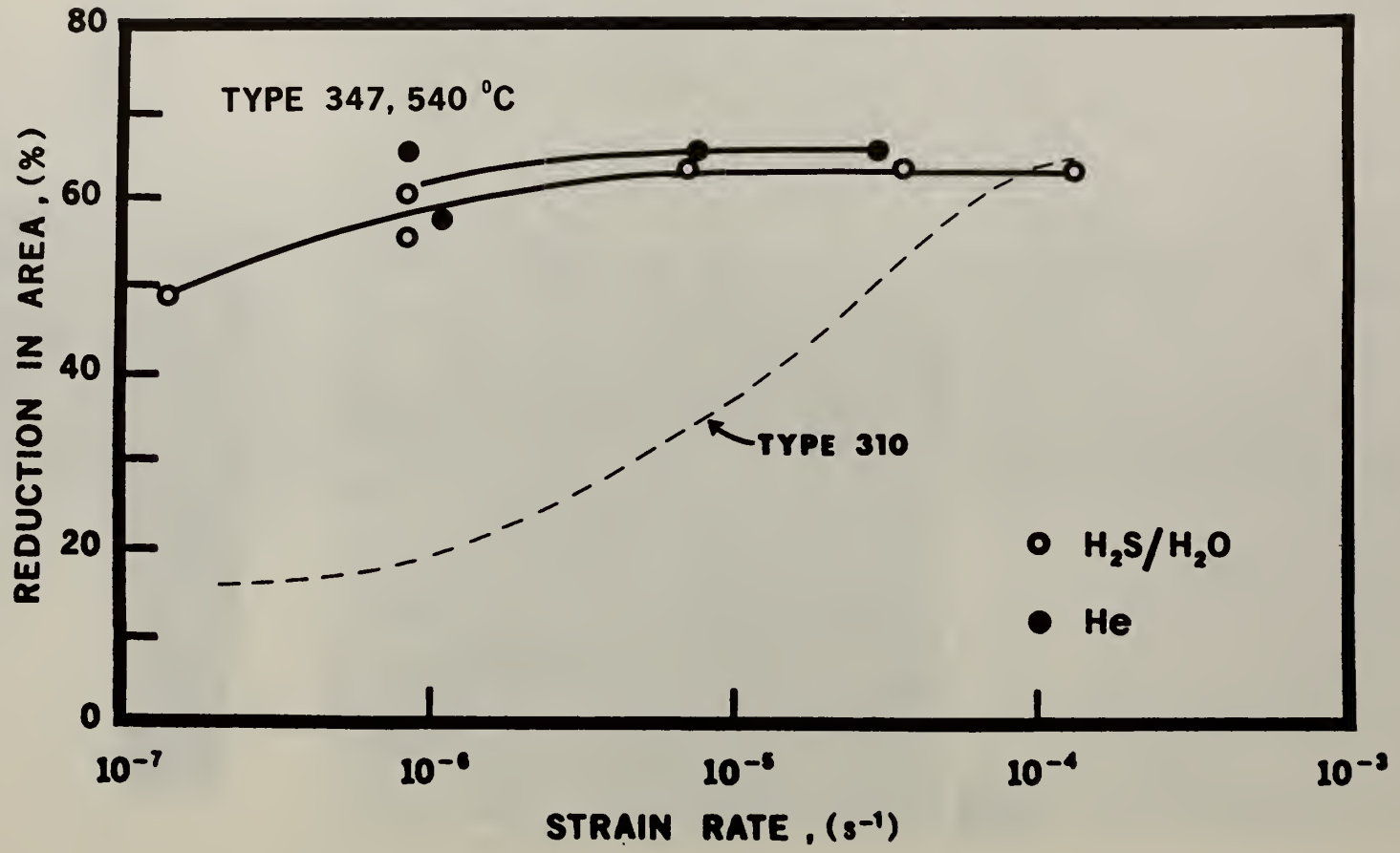

Fig. 28. Ductility as reduction in area versus strain rate for Type 347 specimens tested in gaseous H_2O/H_2S and He at 540 °C (1000 °F). Type 310 curve is shown for comparison.

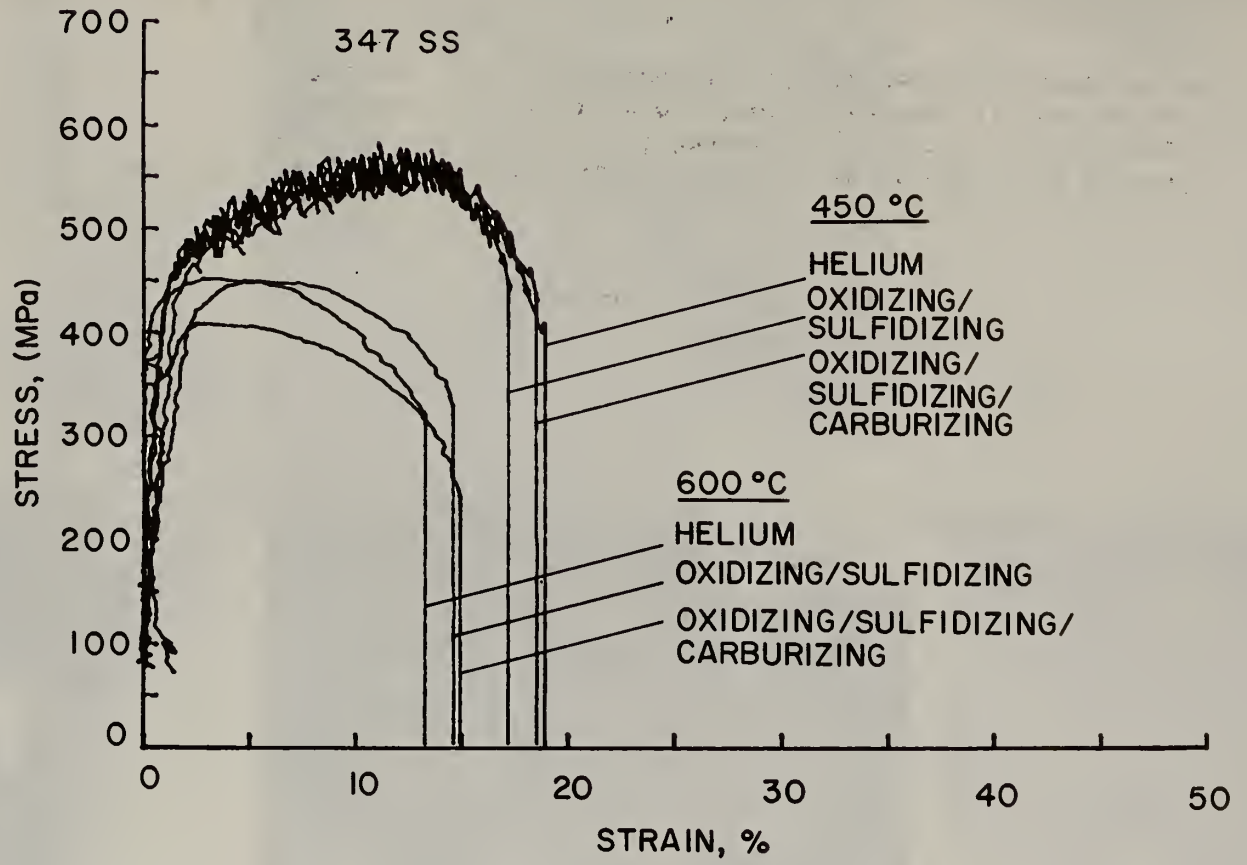

Fig. 29. Stress-strain curves for Type 347 specimens tested at 450 °C (840 °F) and 600 °C (1100 °F) in He and in oxidizing/sulfidizing and oxidizing/sulfidizing/carburizing coal gasification environments at a strain rate of 1 X 10^{-6}/s.

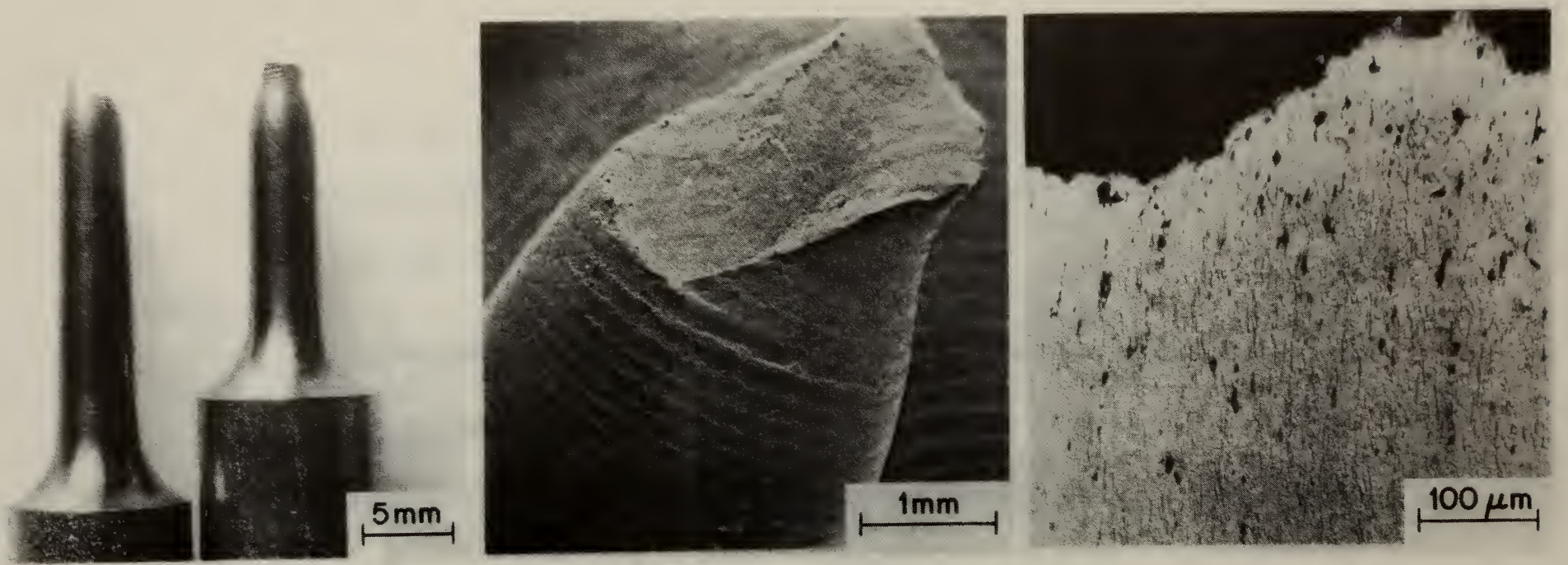

UTS — 568 MPa (82,300 psi)
Elongation — 18.8%
RA — 65.2%

Fig. 30. Type 347 stainless steel tested in He at 450 °C at a strain rate of 1 X 10^{-6}/s. (a) Photomicrograph of the fractured specimen. (b) Scanning electron micrograph at the region of fracture. (c) Photomicrograph of the sectioned specimen near the fracture.

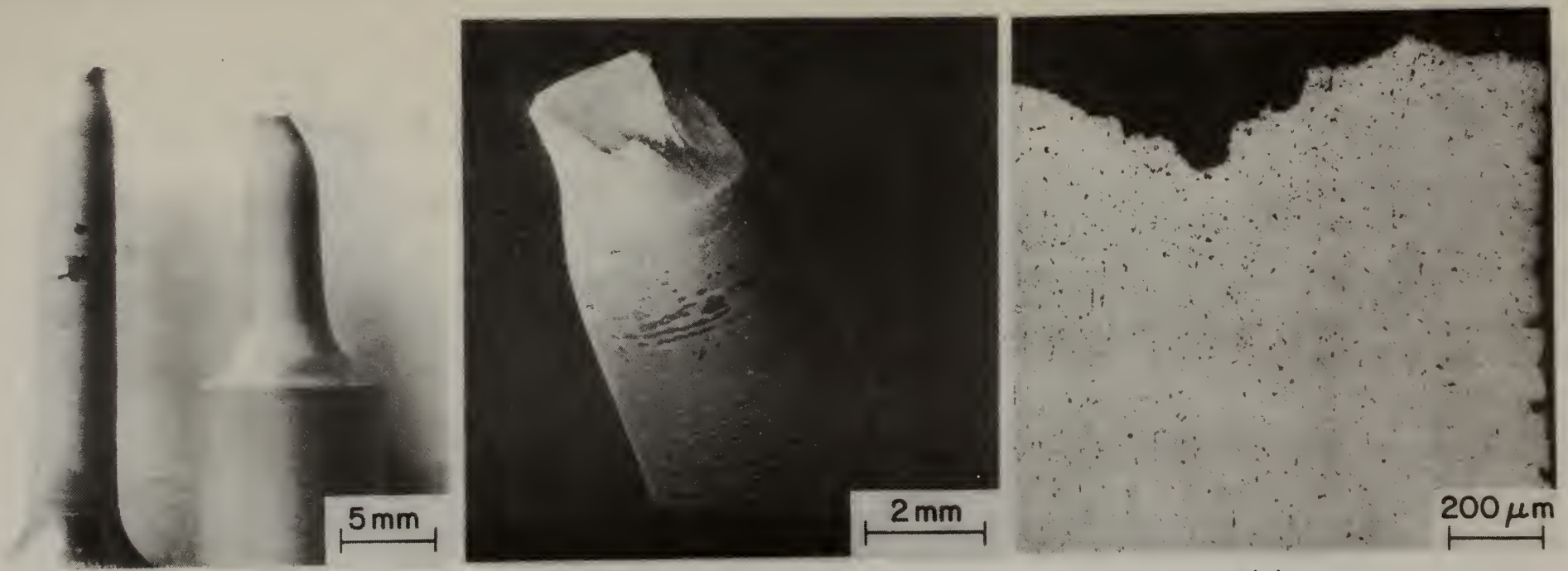

UTS	— 591 MPa (85,700 psi)
Elongation	— 17.0%
RA	— 60.2%

Fig. 31. Type 347 stainless steel tested in the oxidizing-sulfidizing environment at 450 °C at a strain rate of 1 X 10^{-6}/s. (a) Photomicrograph of the fractured specimen. (b) Scanning electron micrograph at the region of fracture. (c) Photomicrograph of the sectioned specimen near the fracture.

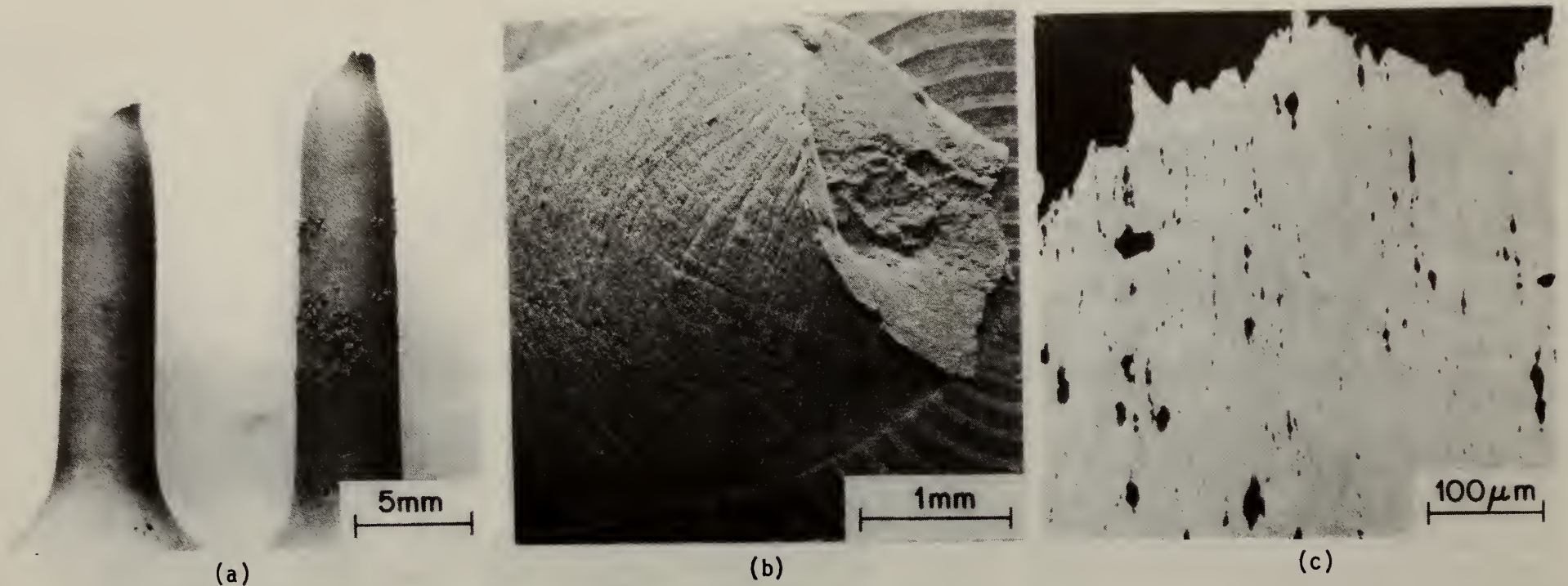

UTS — 590 MPa (85,500 psi)
Elongation — 18.4%
RA — 59.7%

Fig. 32. Type 347 stainless steel tested in the oxidizing-sulfidizing-carburizing environment at a strain rate of 1×10^{-6}/s.
(a) Photomicrograph of the fractured specimen.
(b) Scanning electron micrograph at the region of fracture.
(c) Photomicrograph of the sectioned specimen near the fracture.

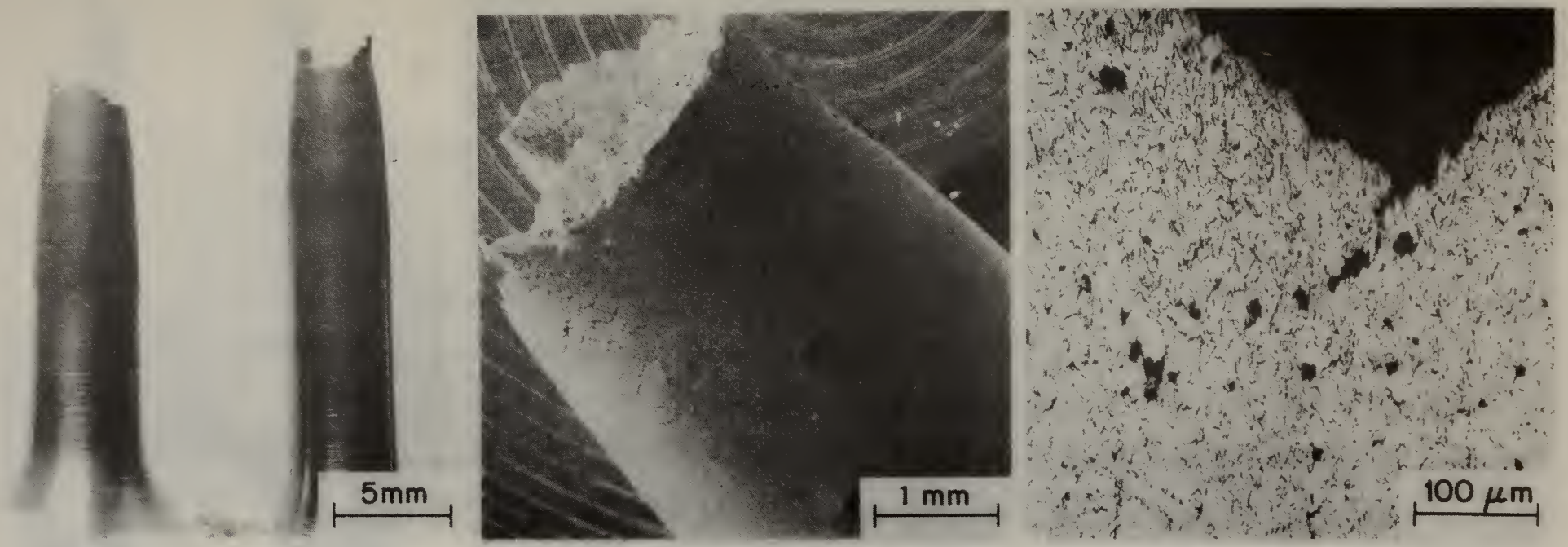

UTS — 451 MPa (65,300 psi)
Elongation — 13.4%
RA — 52.2%

Fig. 33. Type 347 stainless steel tested in He at 600 °C at a strain rate of 1 X 10^{-6}/s. (a) Photomicrograph of the fractured specimen. (b) Scanning electron micrograph at the region of fracture. (c) Photomicrograph of the sectioned specimen near the fracture.

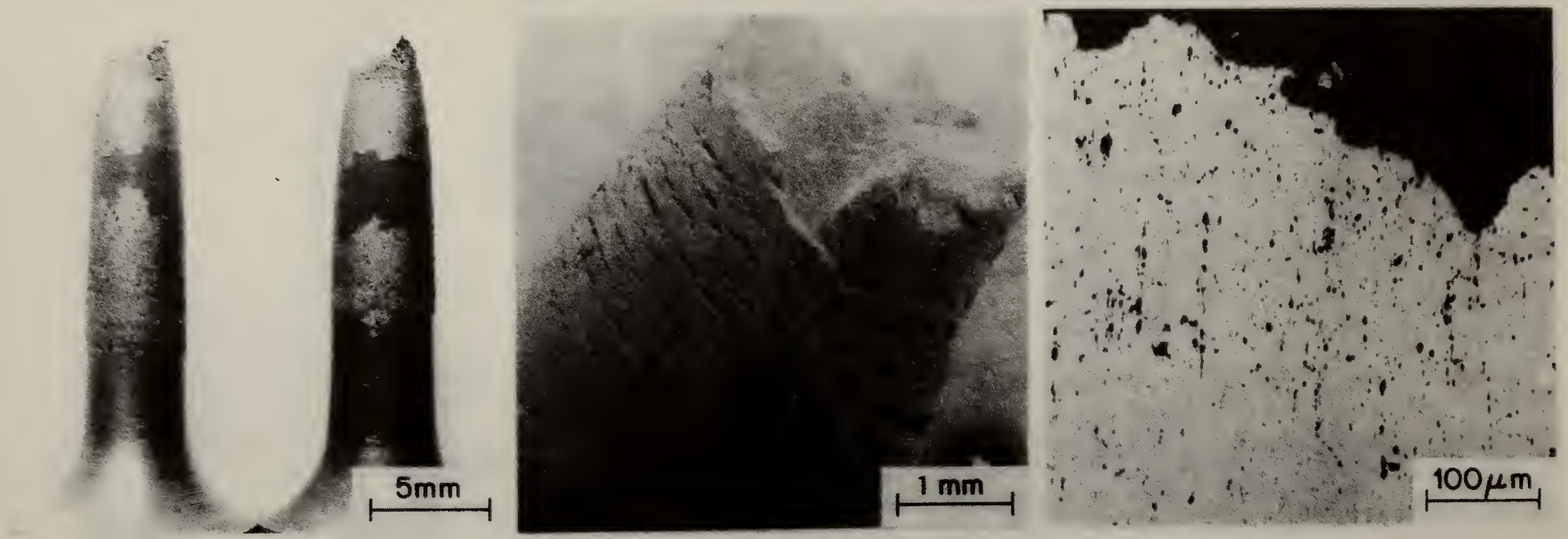

UTS — 426 MPa (61,700 psi)
Elongation — 14.8%
RA — 58.3%

Fig. 34. Type 347 stainless steel tested at 600 °C in the oxidizing-sulfidizing-carburizing environment at a strain rate of 1 X 10^{-6}/s. (a) Photomicrograph of the fractured specimen. (b) Scanning electron micrograph at the region of fracture. (c) Photomicrograph of the sectioned specimen near the fracture.

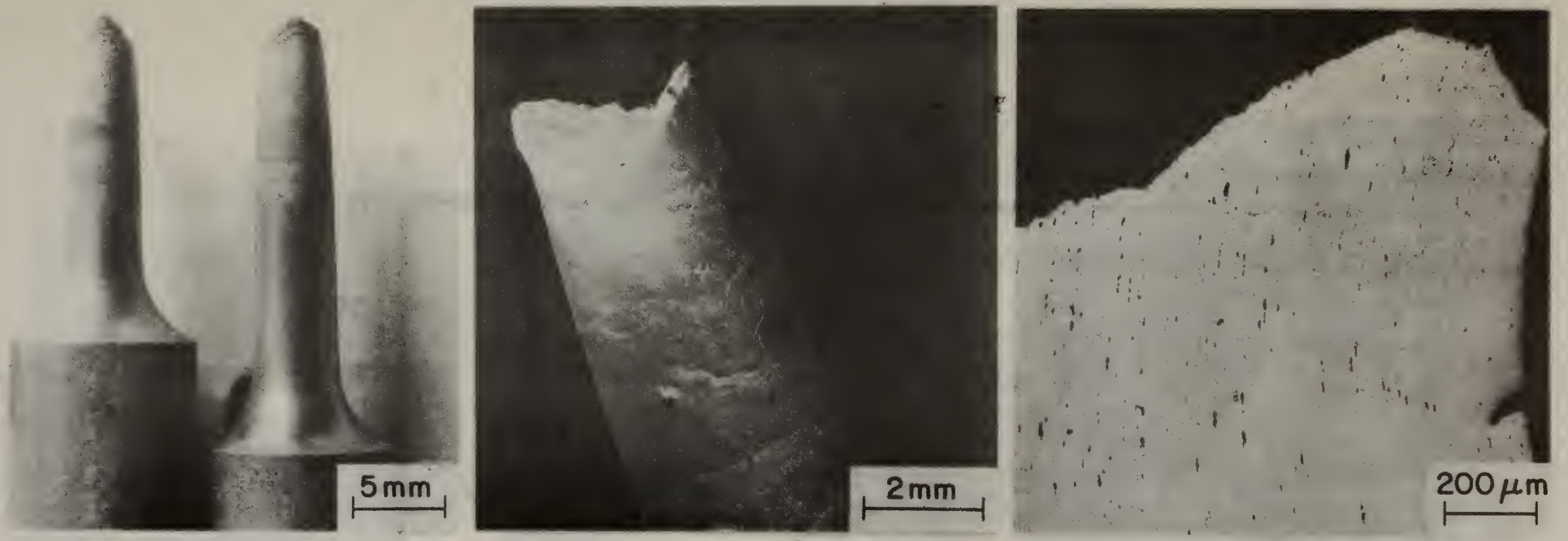

UTS — 460 MPa (66,600 psi)
Elongation — 14.5%
RA — 46.0%

Fig. 35. Type 347 stainless steel tested in the oxidizing-sulfidizing environment at 600 °C at a strain rate of 1 X 10^{-6}/s. (a) Photomicrograph of the fractured specimen. (b) Scanning electron micrograph at the region of fracture. (c) Photograph of the sectioned specimen near the fracture.

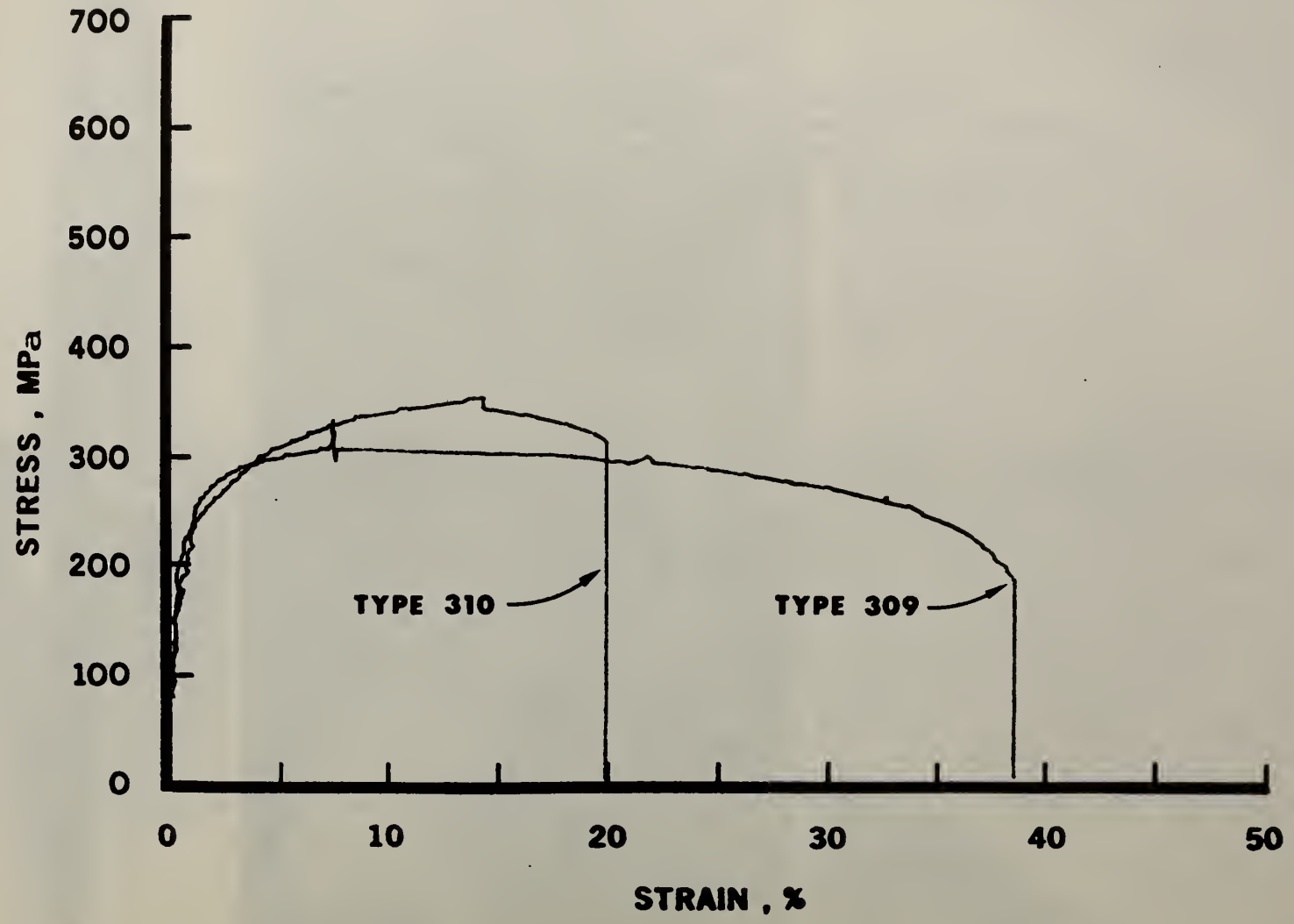

Fig. 36. Comparison stress-strain curves of Types 309 and 310 specimens tested at a strain rate of 10^{-6}/s in He at 600 °C.

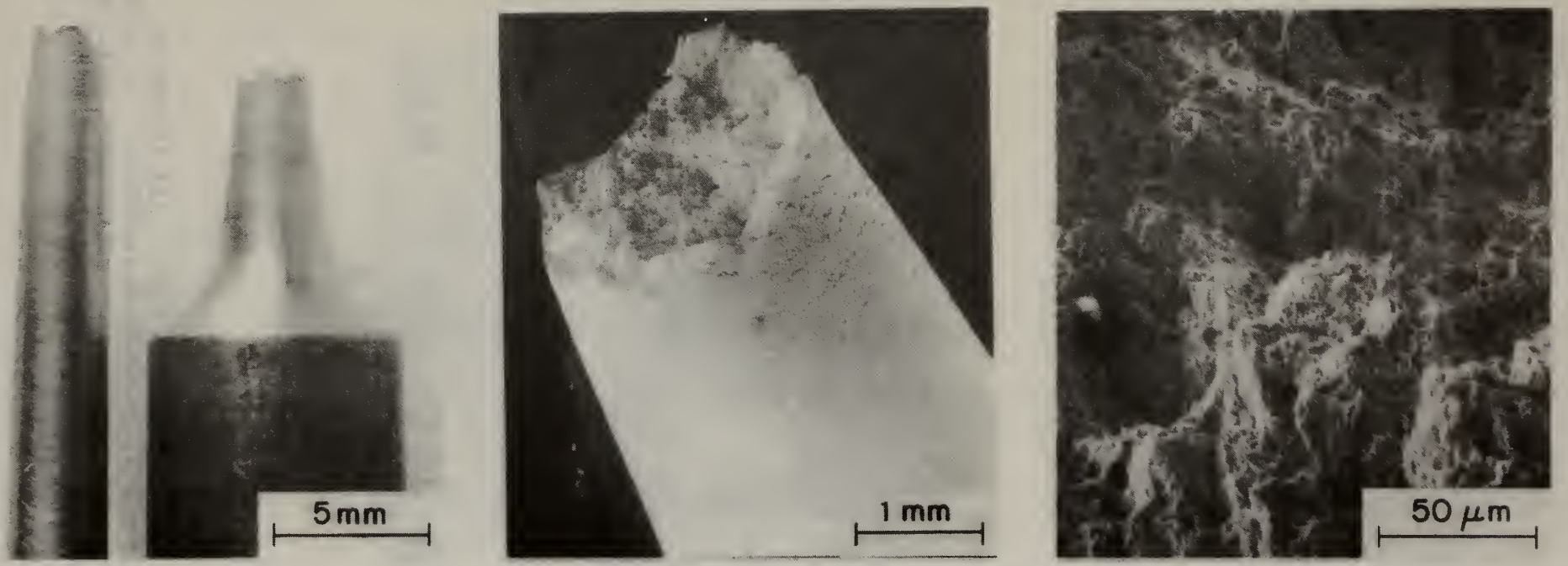

UTS — 334 MPa (48,400 psi)
Elongation — 37.7%
RA — 69.2%

Fig. 37. Type 309 specimen tested in He at 600 °C and strain rate of 1×10^{-6}/s. (a) Photomicrograph of fractured specimen (5 X). (b) SEM at the region of fracture (20 X). (c) SEM of fractured surface near edge (500 X).

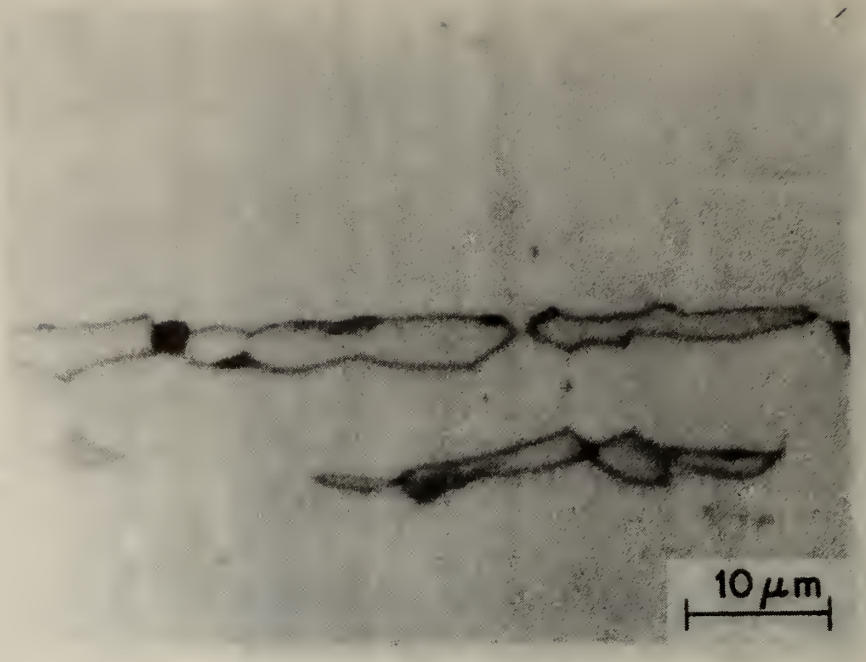

(a)

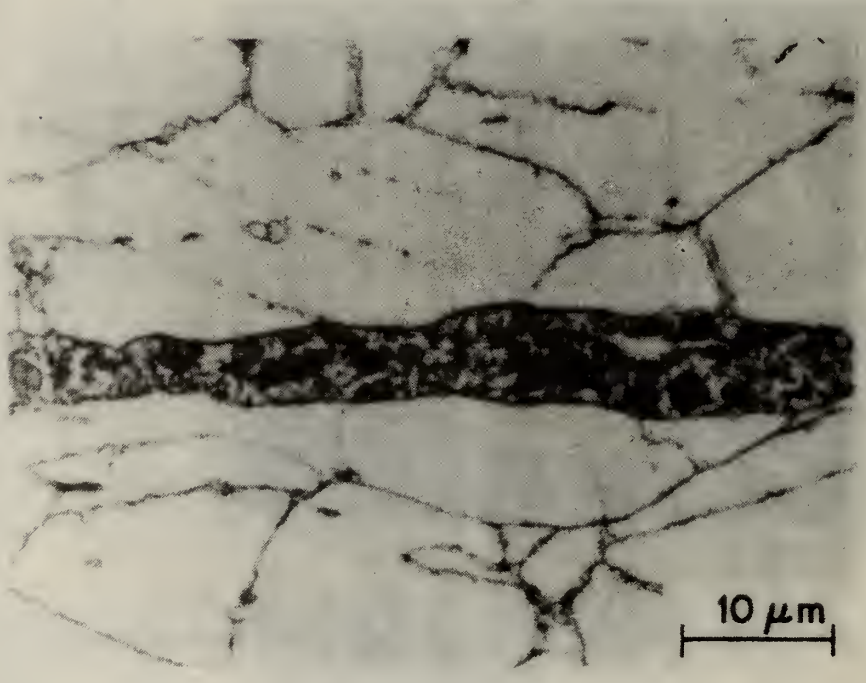

(b)

Fig. 38. Microstructure of Type 309 stainless steel. (a) Islands of ferrite in austenite matrix, as-received condition. (b) Islands of ferrite transformed to mixed ferrite and carbides, which were indentified by chemical etchants, after being tested at 600 °C in He at a strain rate of 10^{-6}/s.

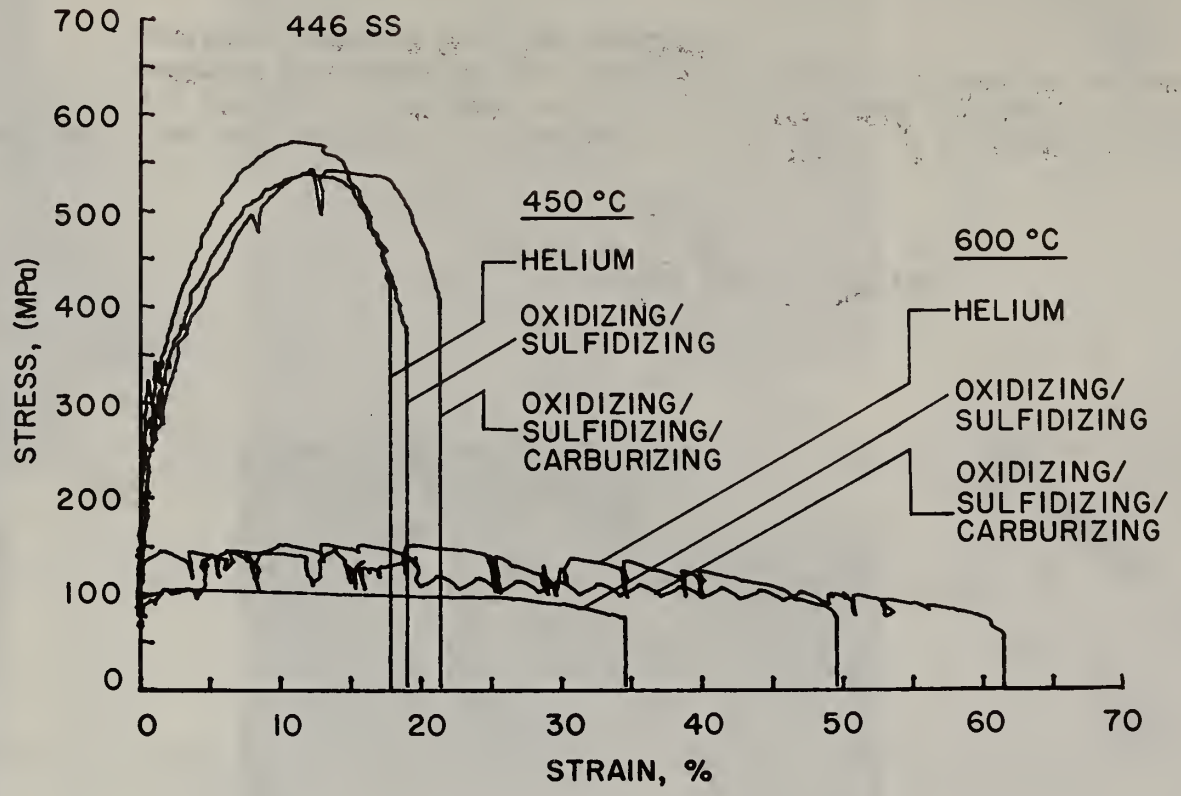

Fig. 39. Stress-strain curves for Type 446 specimens tested at 450 °C (840 °F) and 600 °C (1100 °F) in He and in oxidizing/sulfidizing and oxidizing/sulfidizing/carburizing coal gasification environments at a strain rate of 1 X 10^{-6}/s.

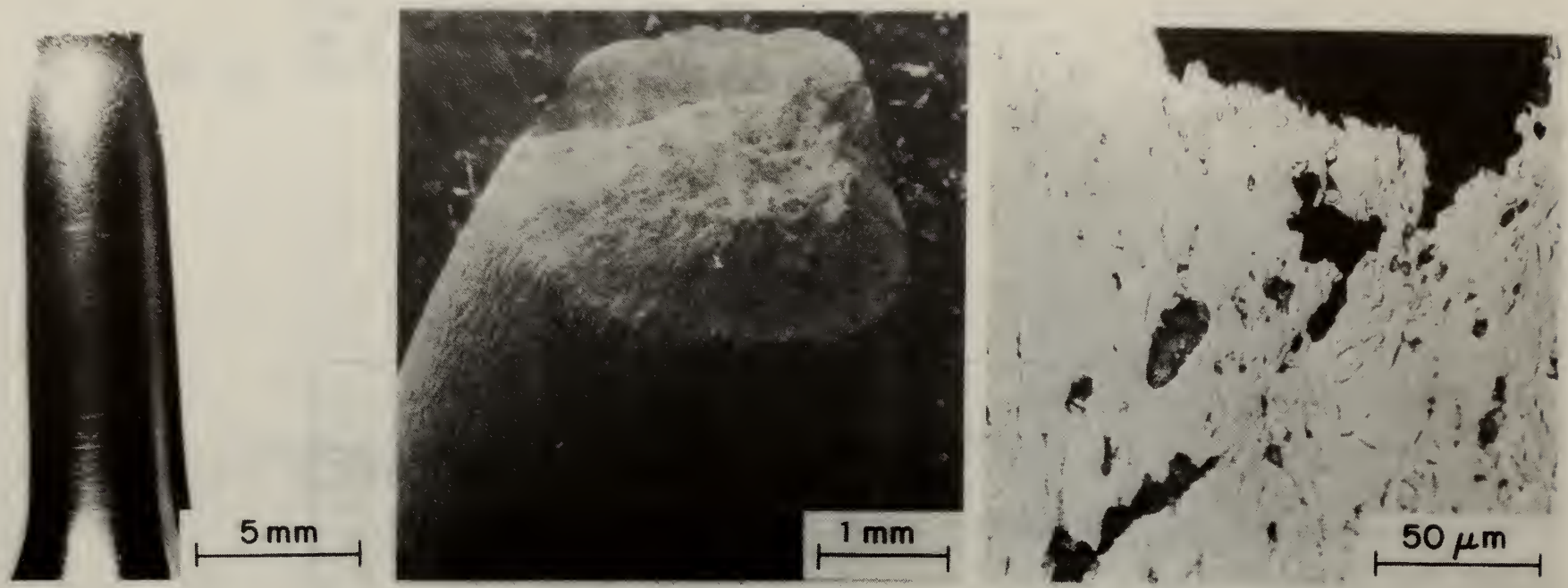

UTS — 586 MPa (85,000 psi)
Elongation — 17.3%
RA — 57.0%

Fig. 40. Type 446 stainless steel tested in He at 450 °C at a strain rate of 1×10^{-6}/s. (a) Photomicrograph of the fractured specimen. (b) Scanning electron micrograph at the region of fracture. (c) Photomicrograph of the sectioned specimen near the fracture.

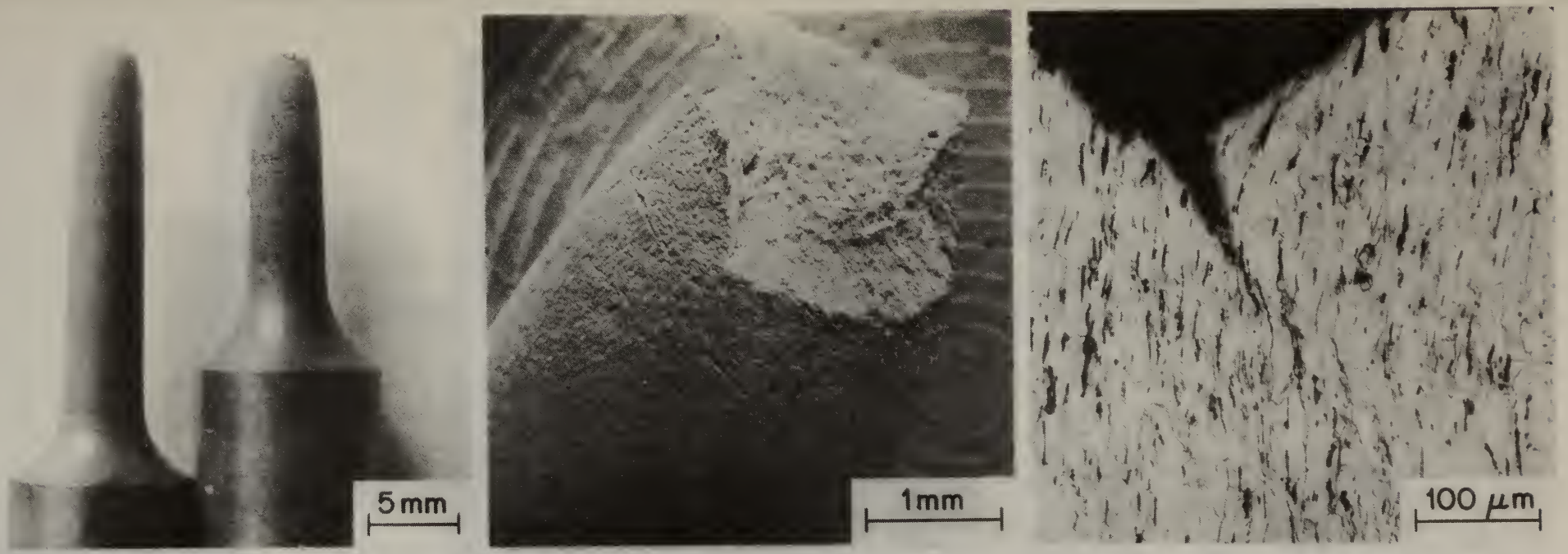

UTS — 552 MPa (80,000 psi)
Elongation — 19.3%
RA — 61.4%

Fig. 41. Type 446 stainless steel tested in the oxidizing/sulfidizing environment at 450 °C at a strain rate of 1 X 10^{-6}/s. (a) Photomicrograph of the fractured specimen. (b) Scanning electron micrograph at the region of fracture. (c) Photomicrograph of the sectioned specimen near the fracture.

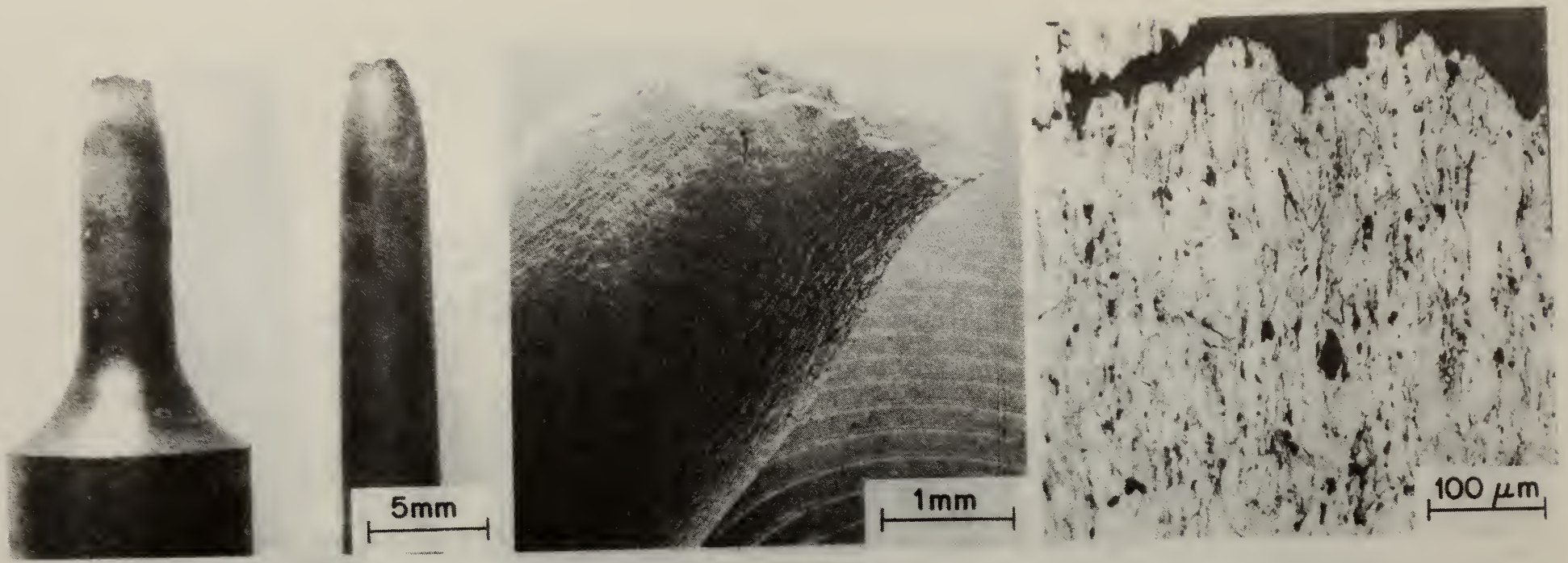

UTS — 574 MPa (83,200 psi)
Elongation — 21.0%
RA — 58.0%

Fig. 42. Type 446 stainless steel tested in the oxidizing/sulfidizing/carburizing environment at 450 °C at a strain rate of 1 X 10^{-6}/s. (a) Photomicrograph of the fractured specimen. (b) Scanning electron micrograph at the region of fracture. (c) Photomicrograph of the sectioned specimen near the fracture.

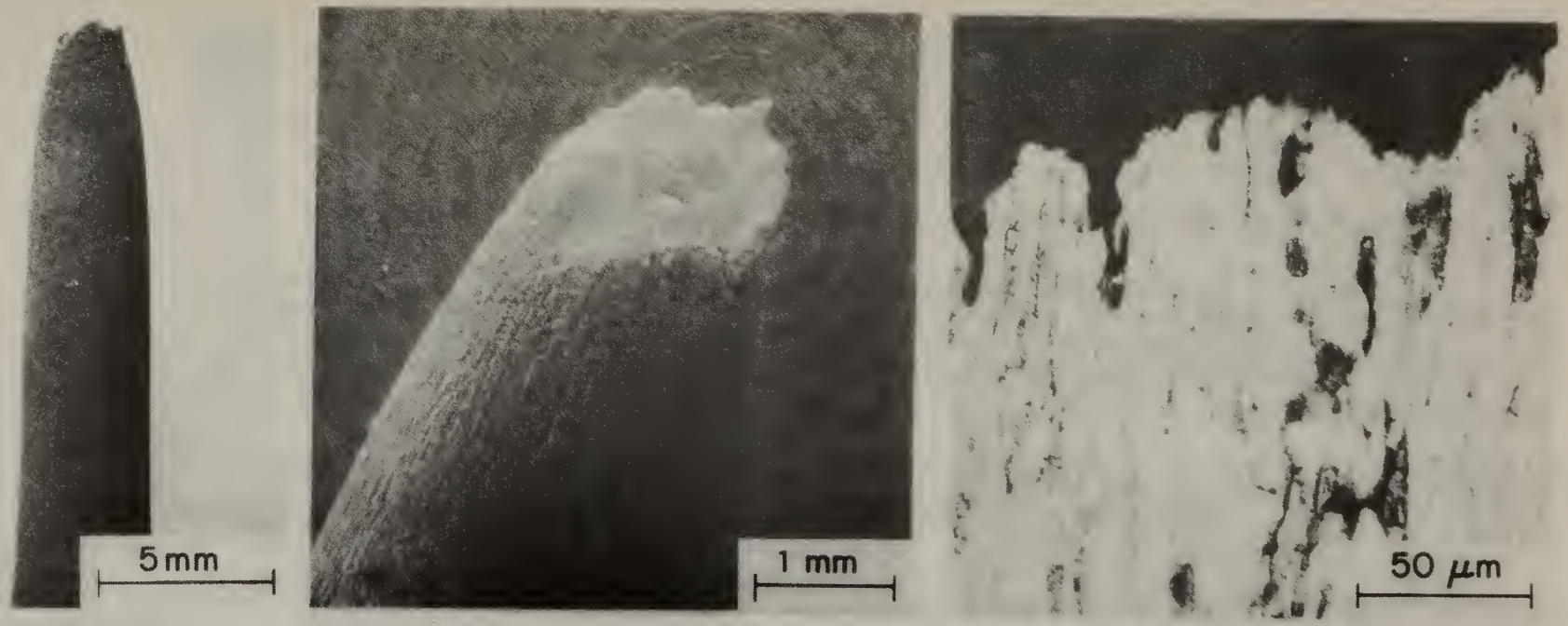

UTS — 152 MPa (22,000 psi)
Elongation — 62.0%
RA — 86.2%

Fig. 43. Type 446 stainless steel tested in He at 600 °C at a strain rate of 1×10^{-6}/s. (a) Photomicrograph of the fractured specimen. (b) Scanning electron micrograph at the region of fracture. (c) Photomicrograph of the sectioned specimen near the fracture.

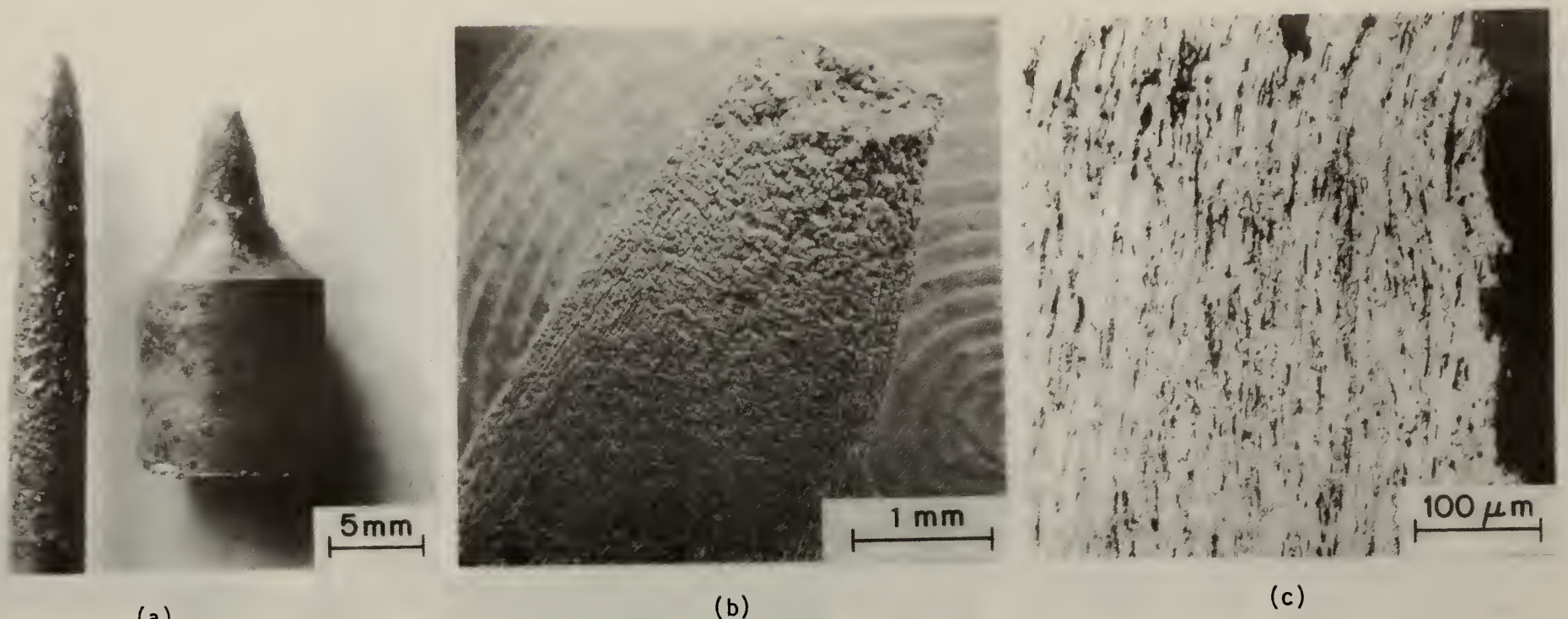

UTS — 109 MPa (15,800 psi)
Elongation — 34.7%
RA — 88.3 %

Fig. 44. Type 446 stainless steel tested in the oxidizing/sulfidizing environment at 600 °C at a strain rate of 1 X 10^{-6}/s. (a) Photomicrograph of the fractured specimen. (b) Scanning electron micrograph at the region of fracture. (c) Photomicrograph of the sectioned specimen near the fracture.

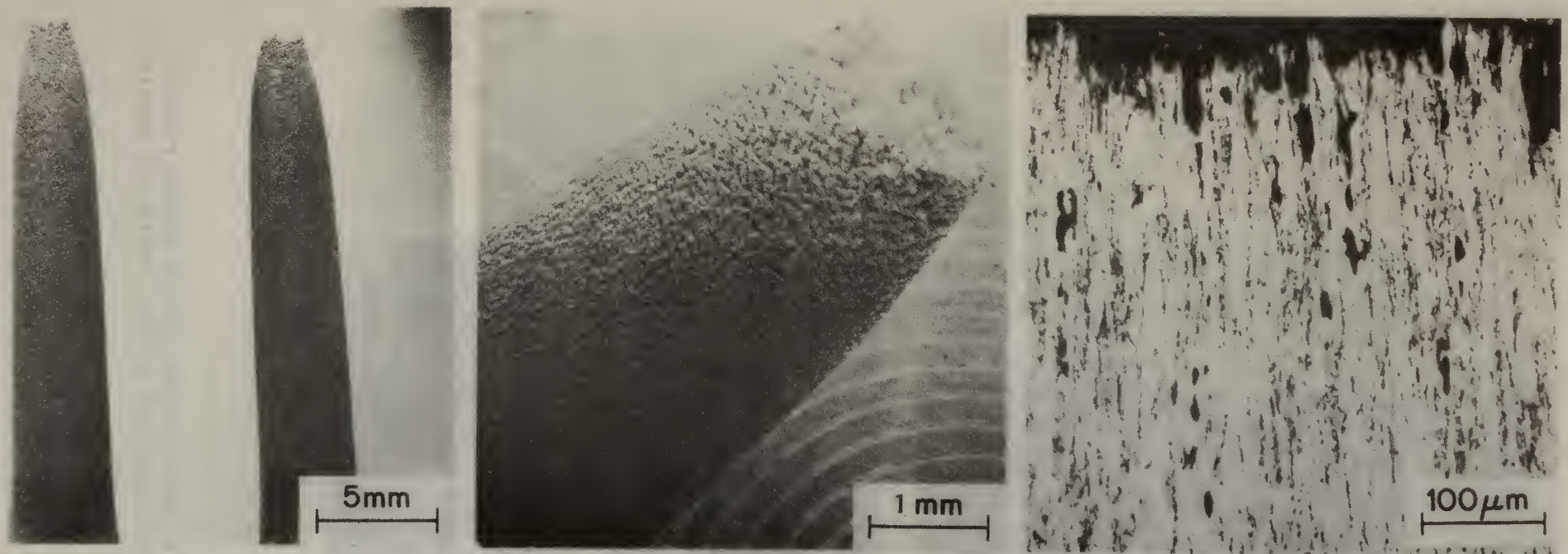

UTS — 160 MPa (23,200 psi)
Elongation — 49.5%
RA — 83.3%

Fig. 45. Type 446 stainless steel tested in the oxidizing/sulfidizing/carburizing environment at 600 °C at a strain rate of 1 X 10^{-6}/s. (a) Photomicrograph of the fractured specimen. (b) Scanning electron micrograph at the region of fracture. (c) Photomicrograph of the sectioned specimen near the fracture.

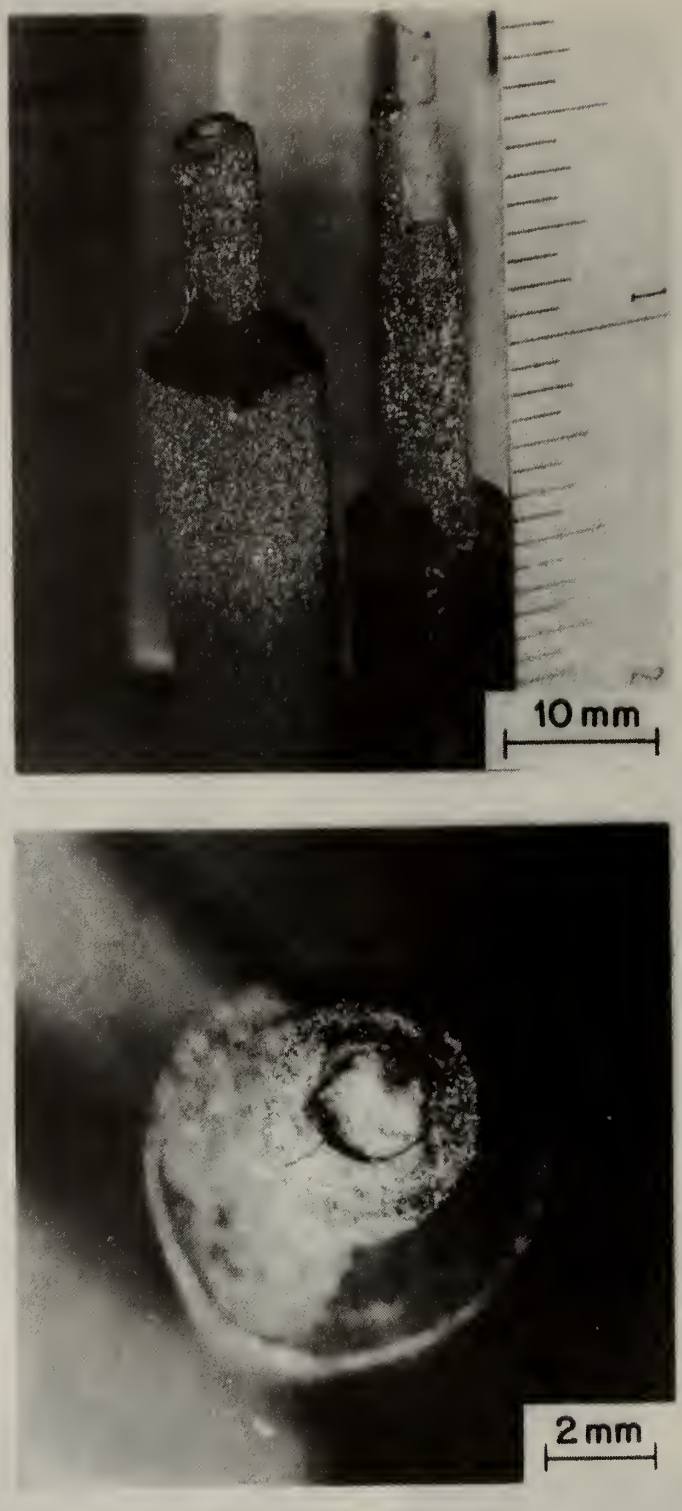

Fig. 46. In 800 specimen tested at 540 °C in wet H_2S at strain rate of 1.7×10^{-7}/s showing large amount of surface scale and remaining metal.

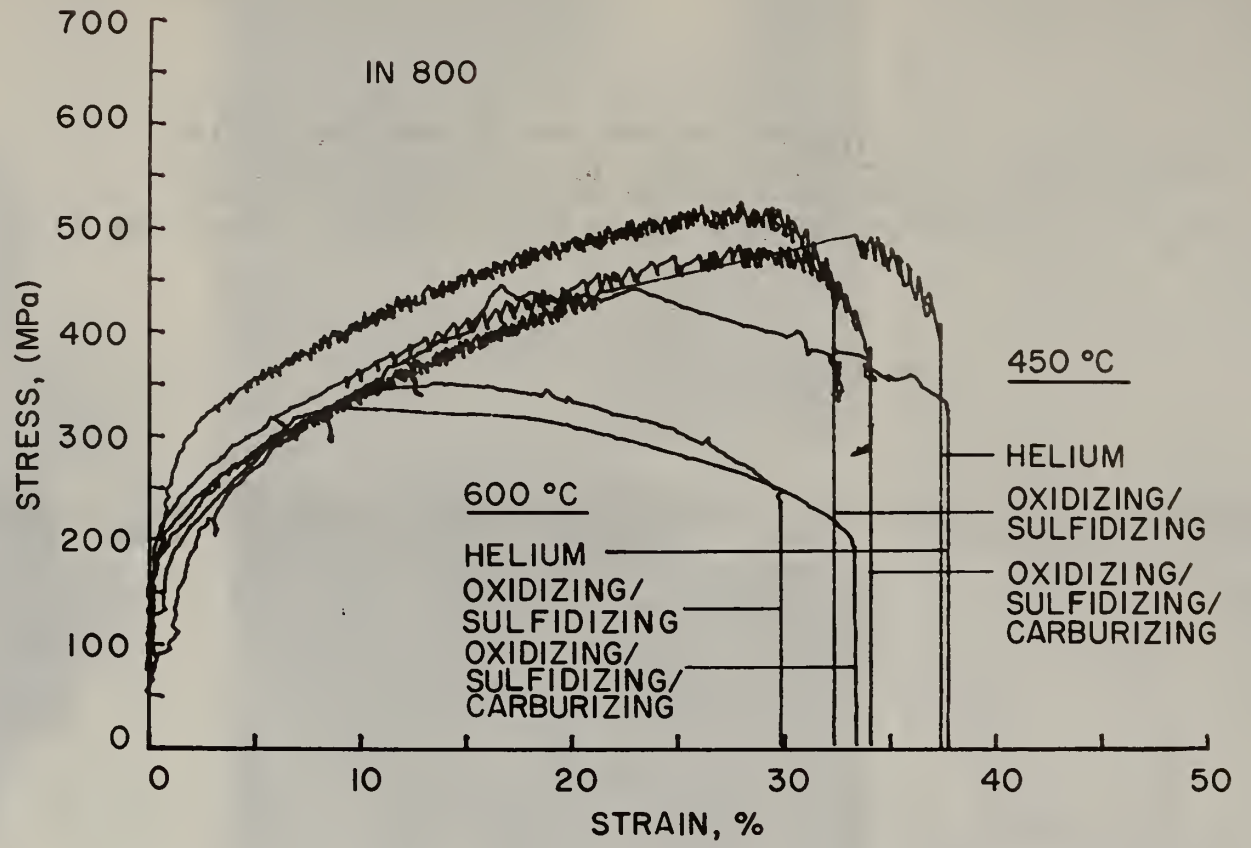

Fig. 47. Stress-strain curves for Incoloy 800 tested at 450 °C (840 °F) and 600 °C (1100 °F) in He and in oxidizing/sulfidizing and oxidizing/sulfidizing/carburizing coal gasification environments at a strain rate of 1 X 10^{-6}/s.

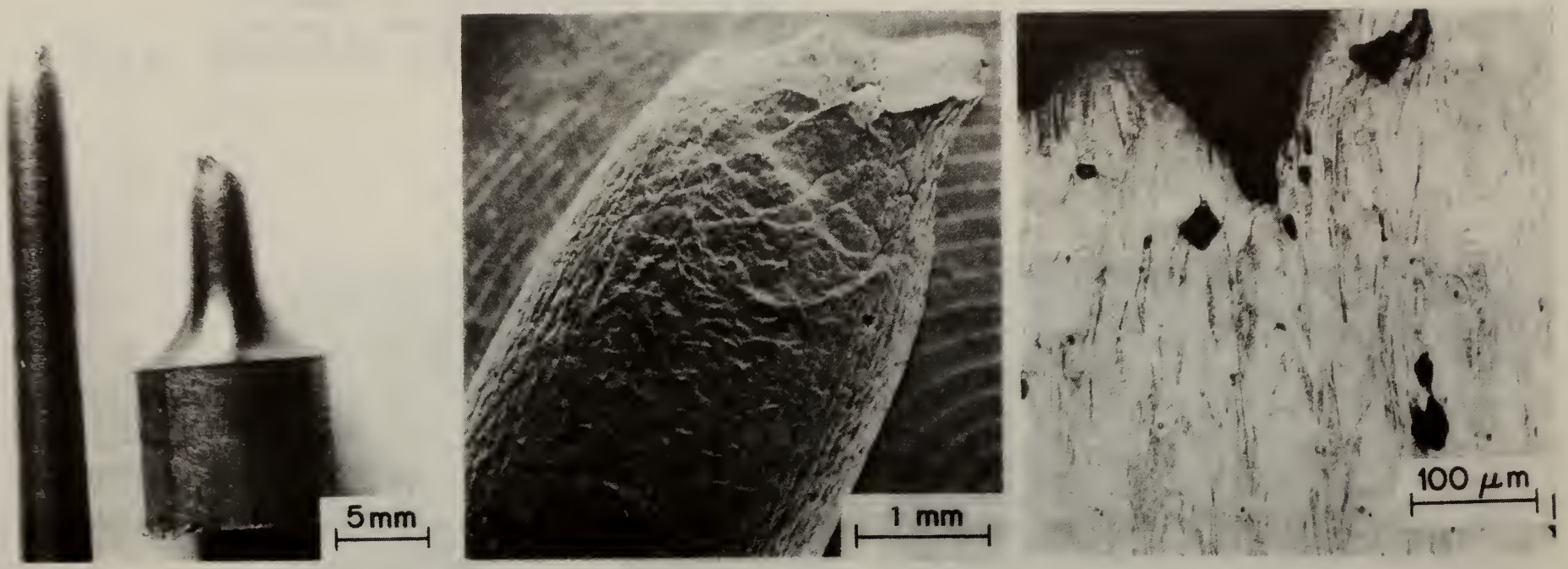

UTS — 526 MPa (76,200 psi)
Elongation — 37.3%
RA — 72.1%

Fig. 48. Incoloy 800 tested in He at 450 °C at a strain rate of 1 X 10^{-6}/s. (a) Photomicrograph of the fractured specimen. (b) Scanning electron micrograph at the region of fracture. (c) Photomicrograph of the sectioned specimen near the fracture.

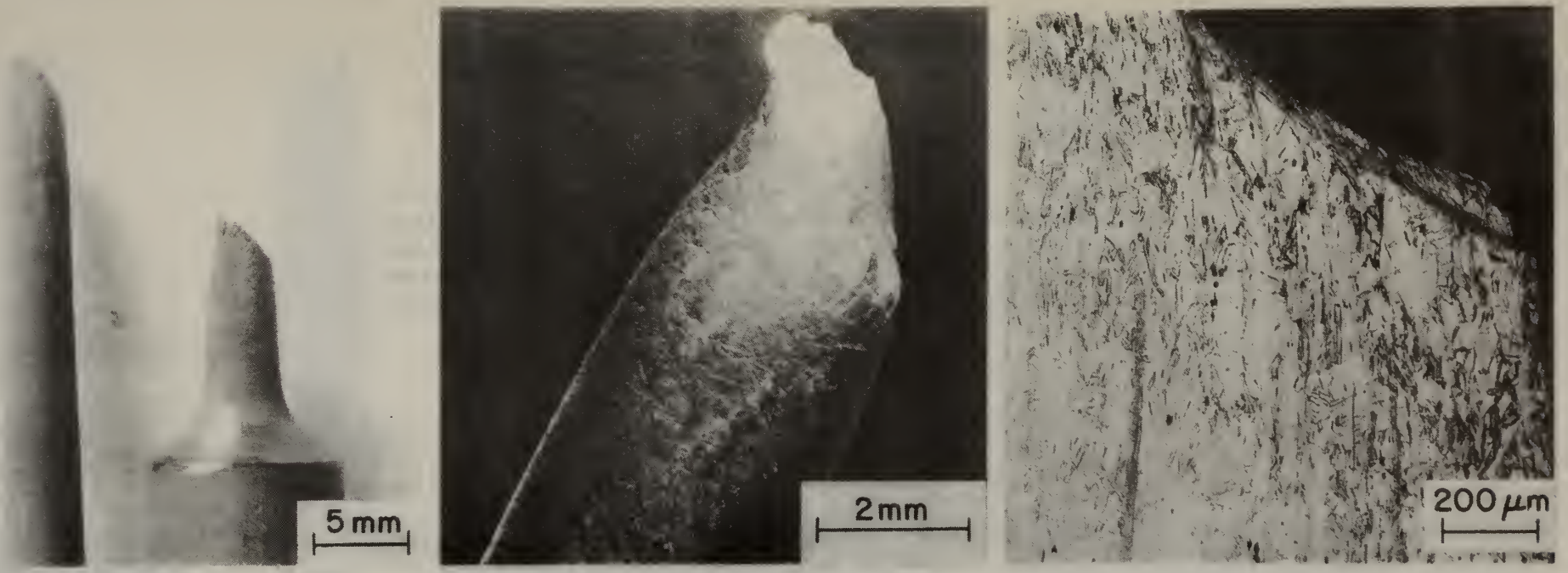

UTS — 544 MPa (78,900 psi)
Elongation — 32.6%
RA — 65.8%

Fig. 49. Incoloy 800 tested in the oxidizing/sulfidizing environment at 450 °C at a strain rate of 1 X 10^{-6}/s. (a) Photomicrograph of the fractured specimen. (b) Scanning electron micrograph at the region of fracture. (c) Photomicrograph of the sectioned specimen near the fracture.

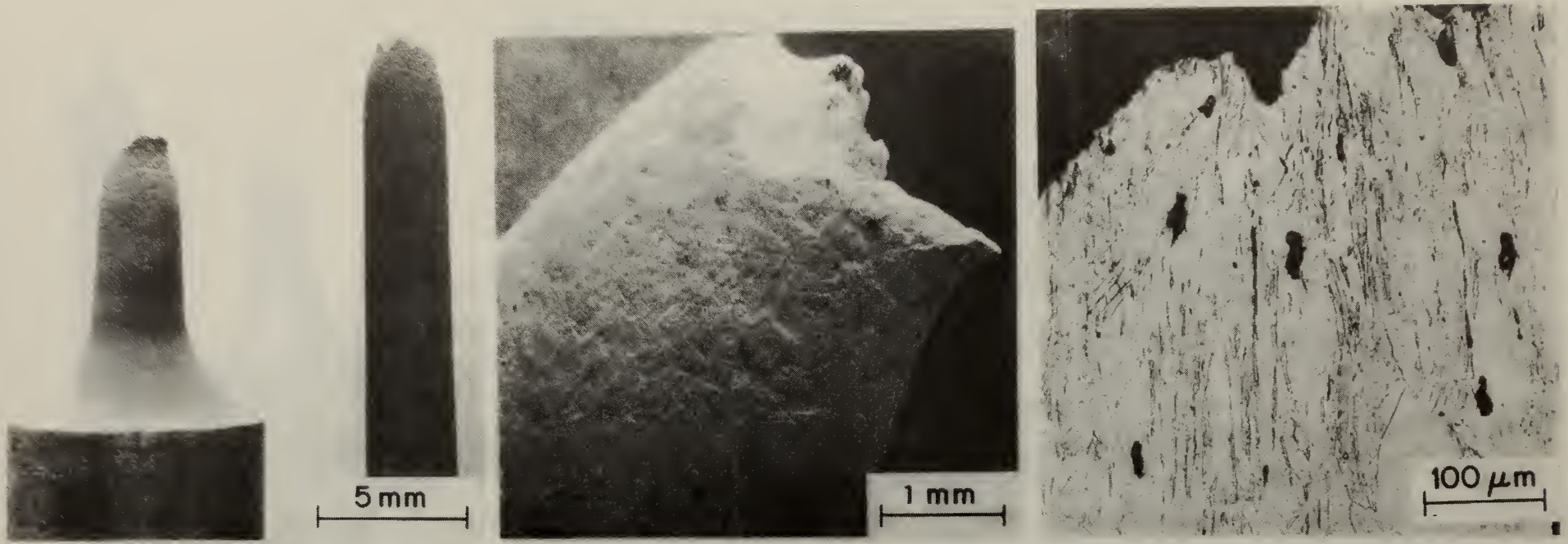

UTS — 551 MPa (79,800 psi)
Elongation — 34.3%
RA — 70.5%

Fig. 50. Incoloy 800 tested in the oxidizing/sulfidizing/carburizing environment at 450 °C at a strain rate of 1 X 10^{-6}/s. (a) Photomicrograph of the fractured specimen. (b) Scanning electron micrograph at the region of fracture. (c) Photomicrograph of the sectioned specimen near the fracture.

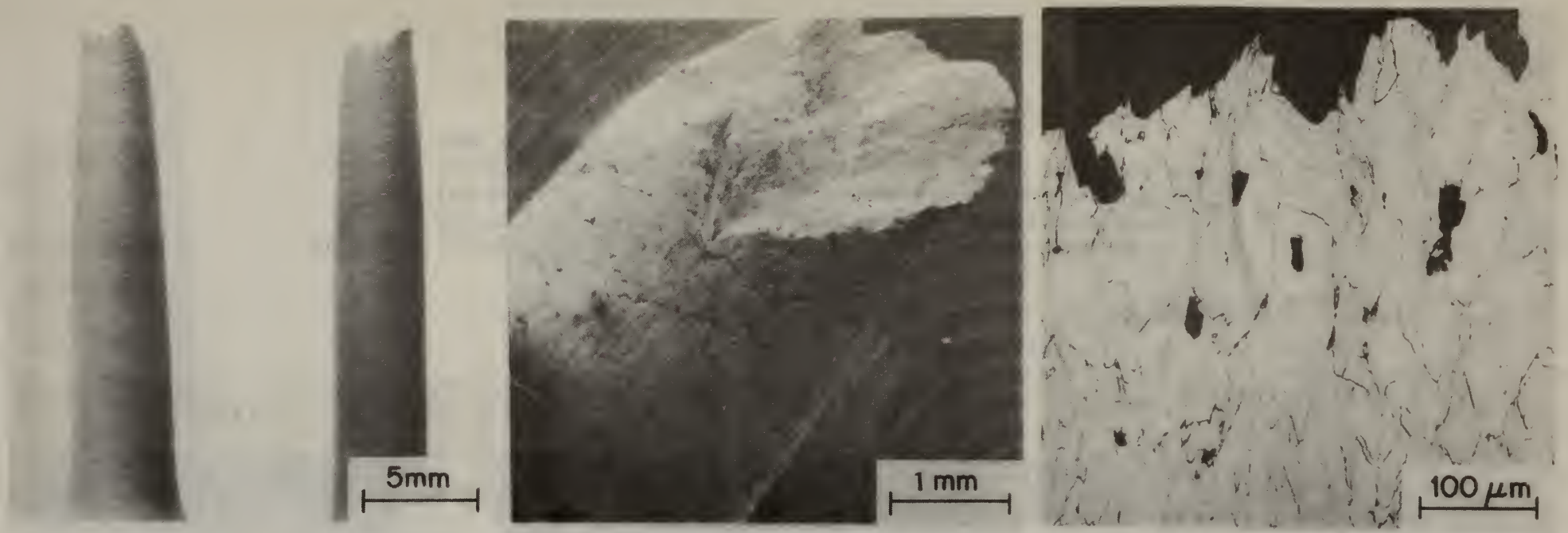

UTS — 467 MPa (67,700 psi)
Elongation — 37.1%
RA — 60.1%

Fig. 51. Incoloy 800 tested in He at 600 °C at a strain rate of 1×10^{-6}/s. (a) Photomicrograph of the fractured specimen. (b) Scanning electron micrograph at the region of fracture. (c) Photomicrograph of the sectioned specimen near the fracture.

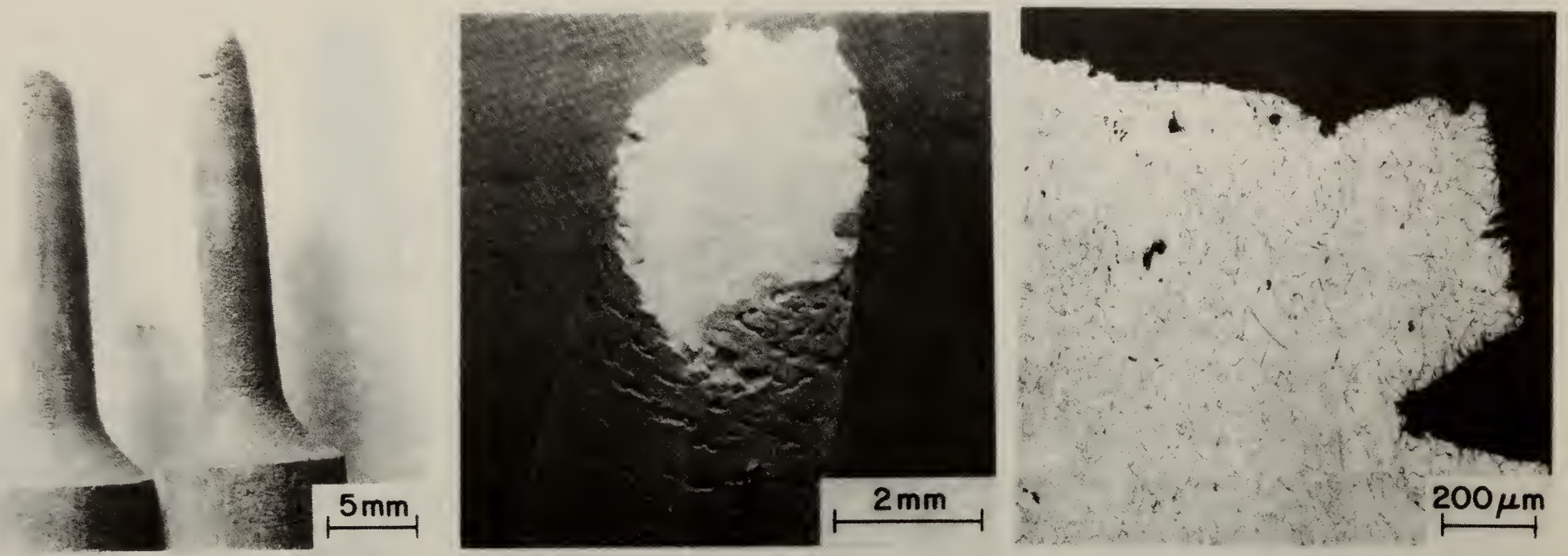

(a) (b) (c)

UTS — 368 MPa (53,400 psi)
Elongation — 29.4%
RA — 49.4%

Fig. 52. Incoloy 800 tested in the oxidizing/sulfidizing environment at 600 °C at a strain rate of 1 X 10^{-6}/s. (a) Photomicrograph of the fractured specimen. (b) Scanning electron micrograph at the region of fracture. (c) Photomicrograph of the sectioned specimen near the fracture.

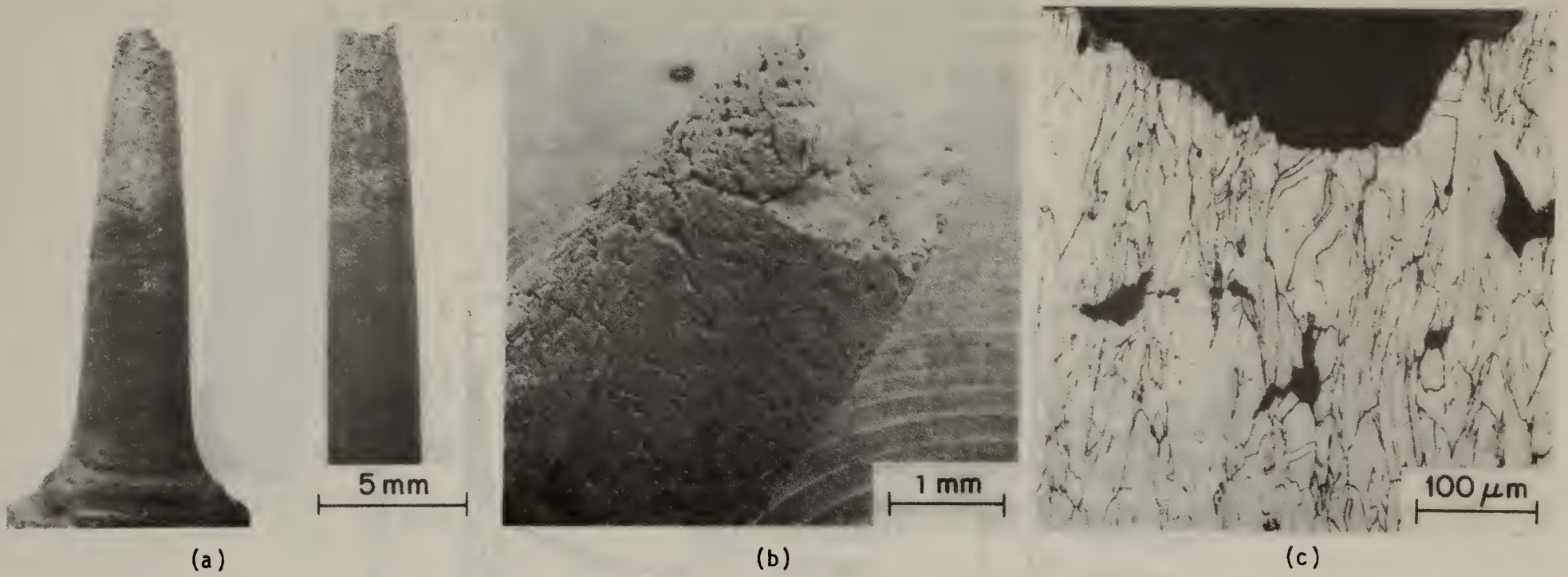

UTS — 353 MPa (51,100 psi)
Elongation — 32.7%
RA — 61.7%

Fig. 53. Incoloy 800 tested in the oxidizing/sulfidizing/carburizing environment at 600 °C at a strain rate of 1 X 10^{-6}/s. (a) Photomicrograph of the fractured specimen. (b) Scanning electron micrograph at the region of fracture. (c) Photomicrograph of the sectioned specimen near the fracture.

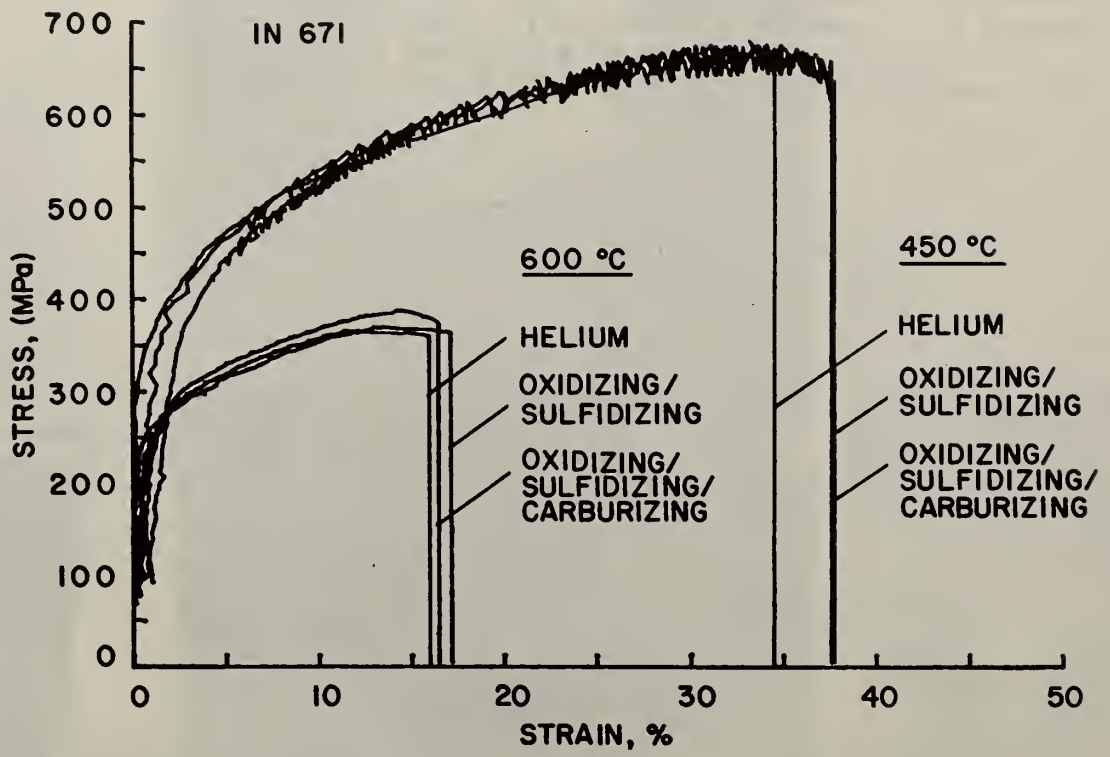

Fig. 54. Stress-strain curves for Inconel 671 tested at 450 °C (840 °F) and 600 °C (1100 °F) in He and in oxidizing/sulfidizing and oxidizing/sulfidizing/carburizing coal gasification environments at a strain rate of 1 X 10^{-6}/s.

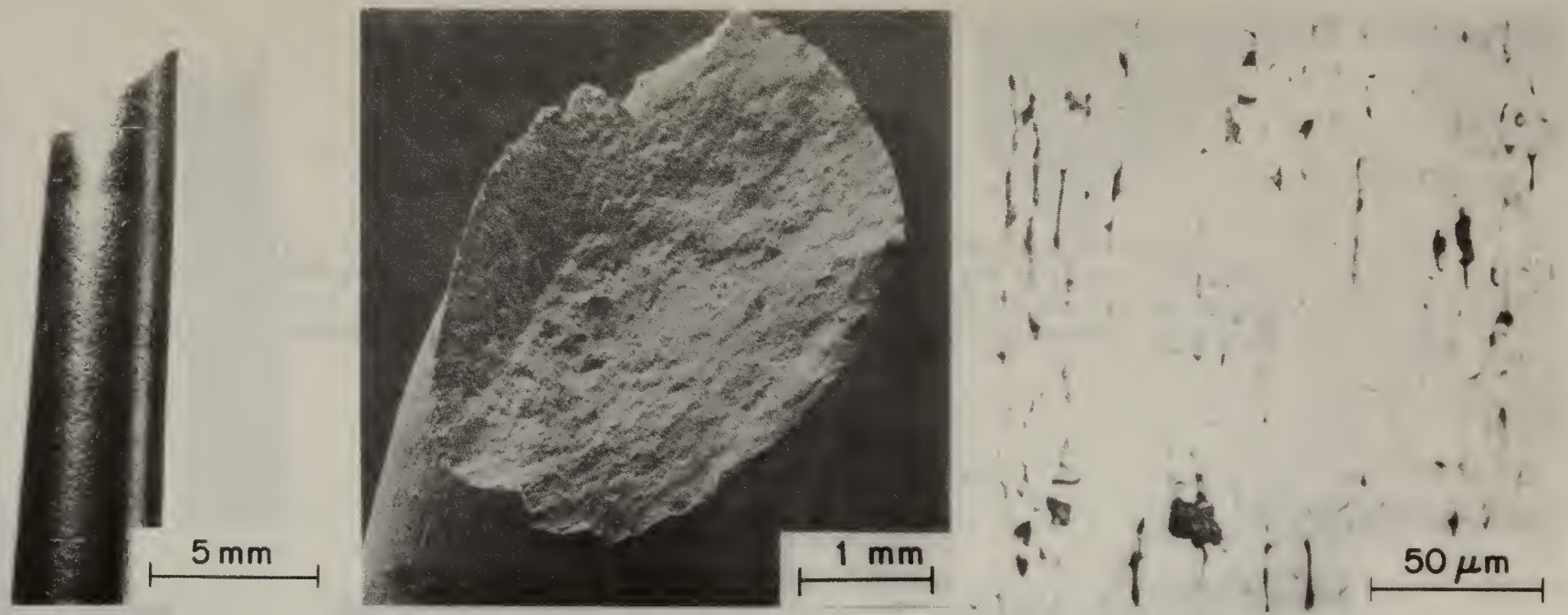

UTS	— 680 MPa (98,600 psi)
Elongation	— 32.8%
RA	— 37.7%

Fig. 55. Inconel 671 tested in He at 450 °C at a strain rate of 1 X 10^{-6}/s. (a) Photomicrograph of the fractured specimen. (b) Scanning electron micrograph at the region of fracture. (c) Photomicrograph of the sectioned specimen near the fracture.

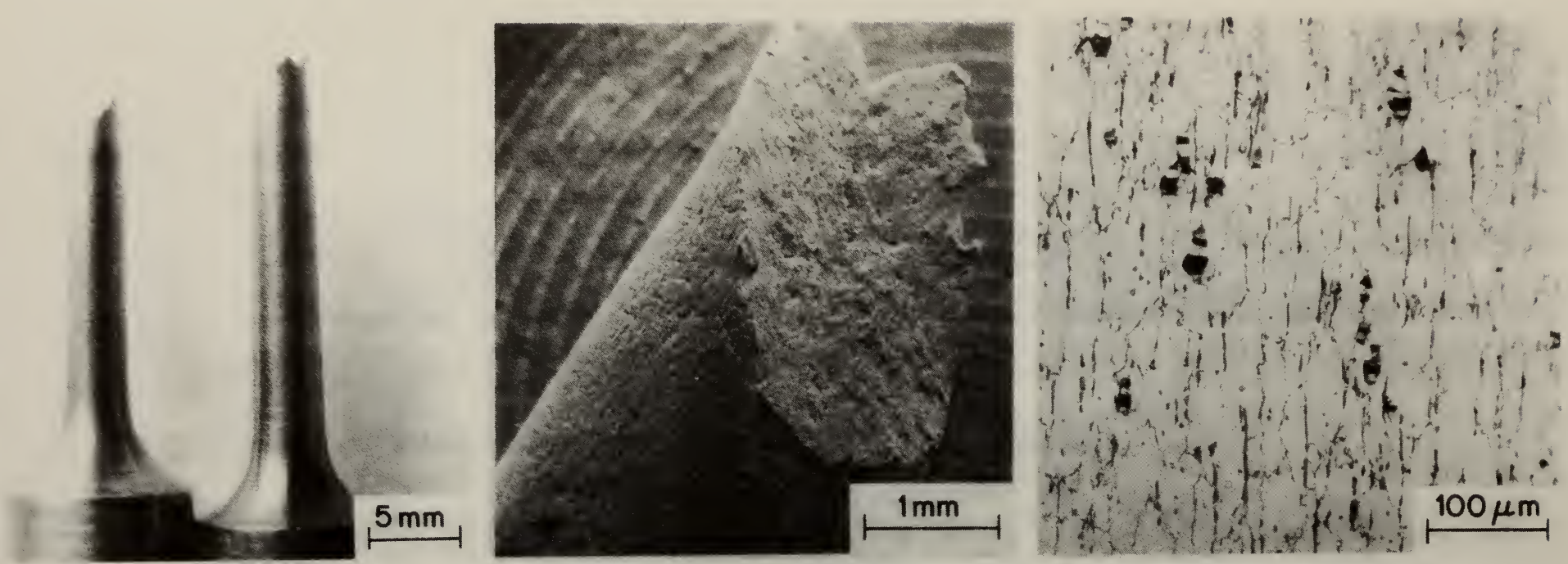

(a) (b) (c)

UTS	— 670 MPa (97,100 psi)
Elongation	— 38.6%
RA	— 45.3%

Fig. 56. Inconel 671 tested in the oxidizing/sulfidizing environment at 450 °C at a strain rate of 1 X 10^{-6}/s. (a) Photomicrograph of the fractured specimen. (b) Scanning electron micrograph at the region of fracture. (c) Photomicrograph of the sectioned specimen near the fracture.

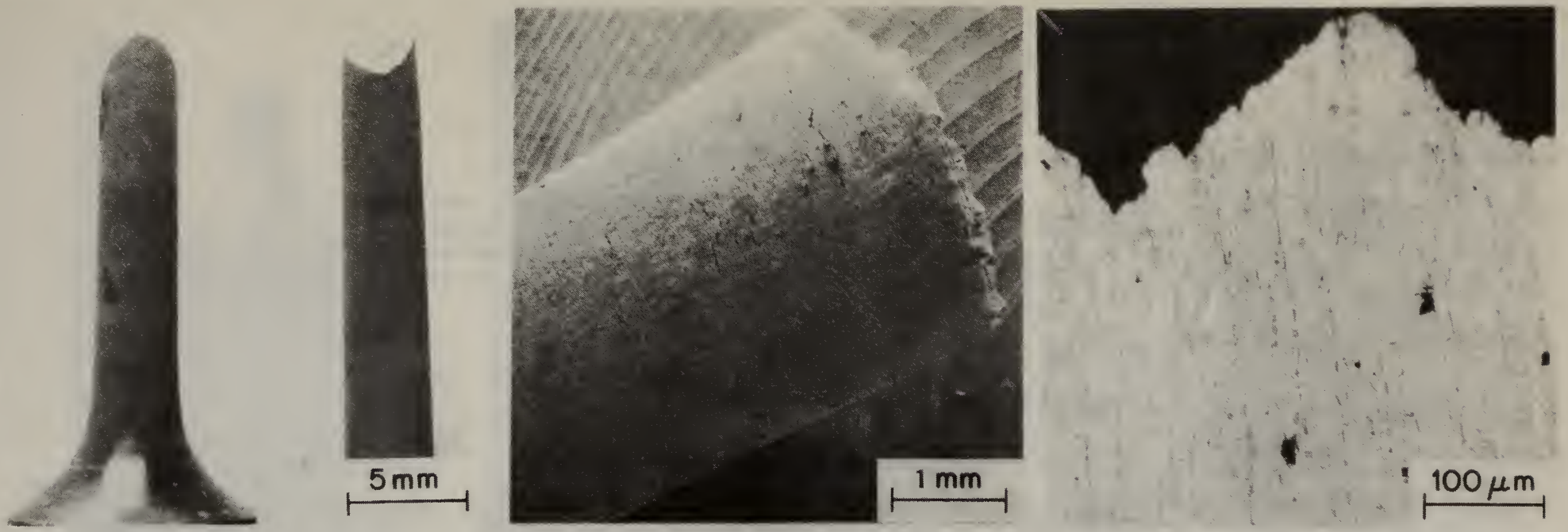

UTS — 676 MPa (97,900 psi)
Elongation — 38.0%
RA — 39.3%

Fig. 57. Inconel 671 tested in the oxidizing/sulfidizing/carburizing environment at 450 °C at a strain rate of 1 X 10^{-6}/s. (a) Photomicrograph of the fractured specimen. (b) Scanning electron micrograph at the region of fracture. (c) Photomicrograph of the sectioned specimen near the fracture.

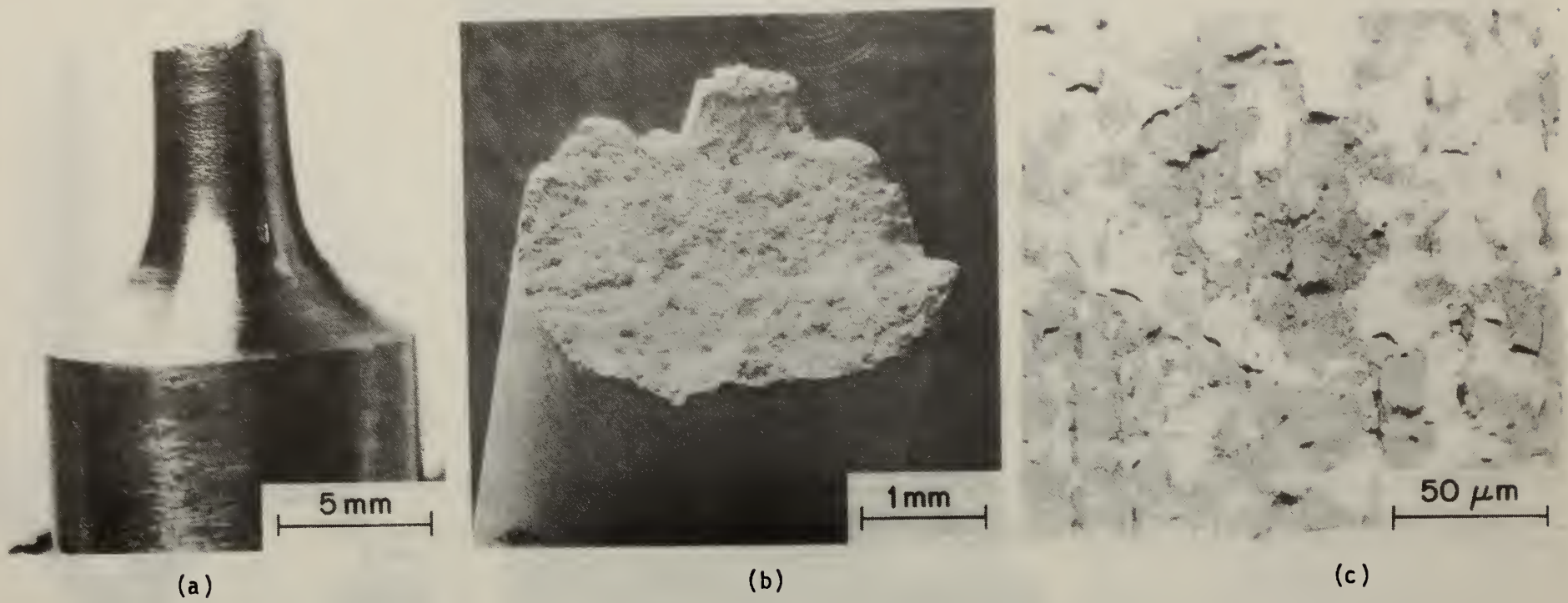

UTS — 416 MPa (60,300 psi)
Elongation — 16.1%
RA — 16.3%

Fig. 58. Inconel 671 tested in He at 600 °C at a strain rate of 1 X 10^{-6}/s. (a) Photomicrograph of the fractured specimen. (b) Scanning electron micrograph at the region of fracture. (c) Photomicrograph of the sectioned specimen near the fracture.

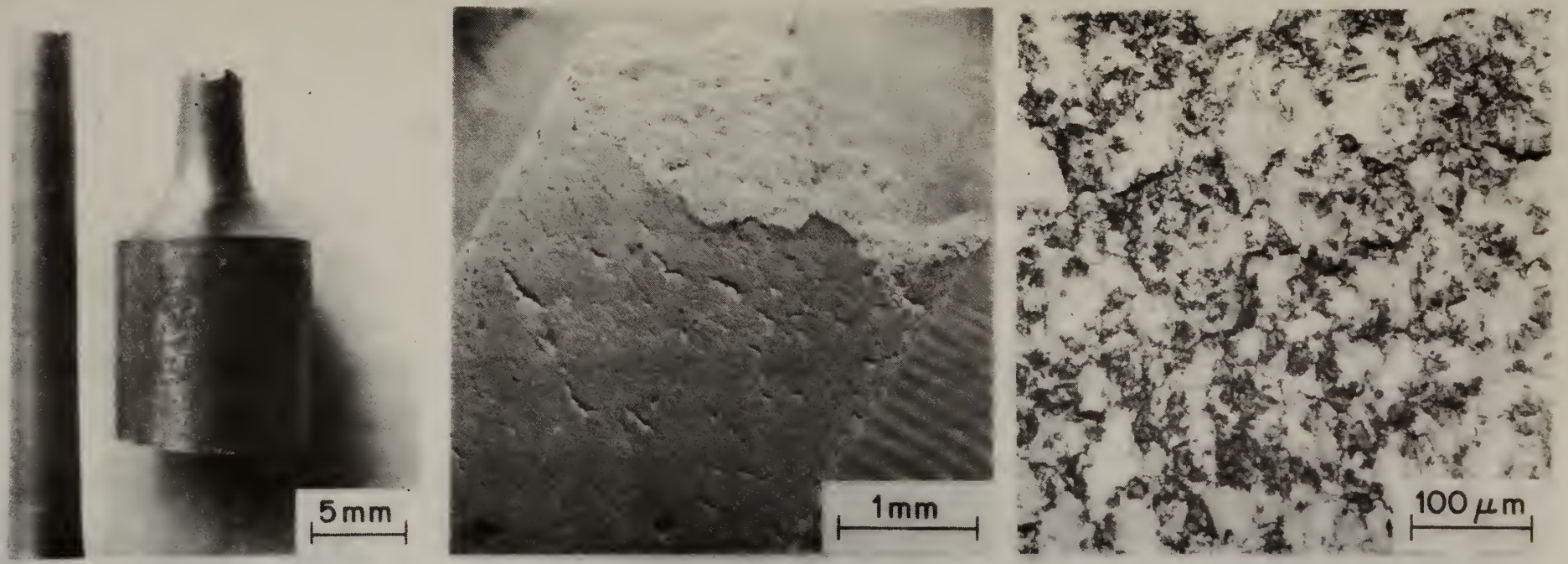

(a) (b) (c)

UTS — 397 MPa (57,600 psi)
Elongation — 17.5%
RA — 20.7%

Fig. 59. Inconel 671 tested in the oxidizing/sulfidizing environment at 600 °C at a strain rate of 1 X 10^{-6}/s. (a) Photomicrograph of the fractured specimen. (b) Scanning electron micrograph at the region of fracture. (c) Photomicrograph of the sectioned specimen near the fracture.

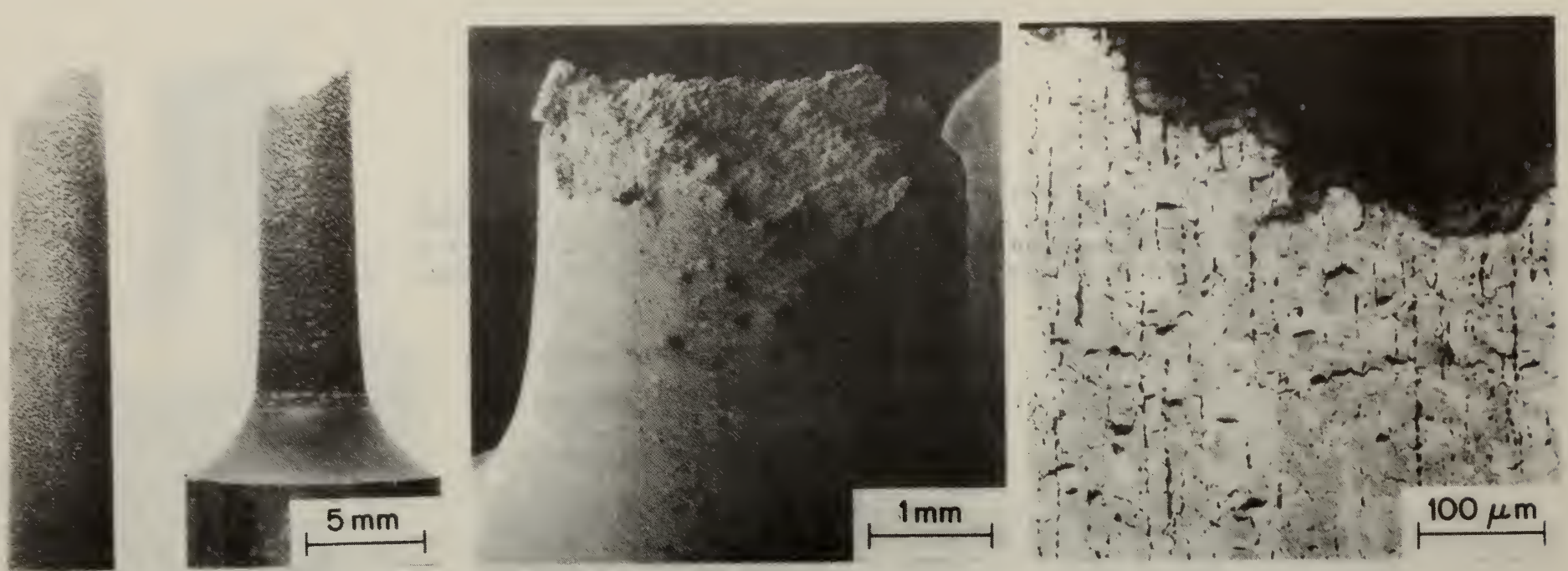

UTS — 448 MPa (64,900 psi)
Elongation — 16.3%
RA — 16.8%

Fig. 60. Inconel 671 tested in the oxidizing/sulfidizing/carburizing environment at 600 °C at a strain rate of 1 X 10^{-6}/s. (a) Photomicrograph of the fractured specimen. (b) Scanning electron micrograph at the region of fracture. (c) Photomicrograph of the sectioned specimen near the fracture.

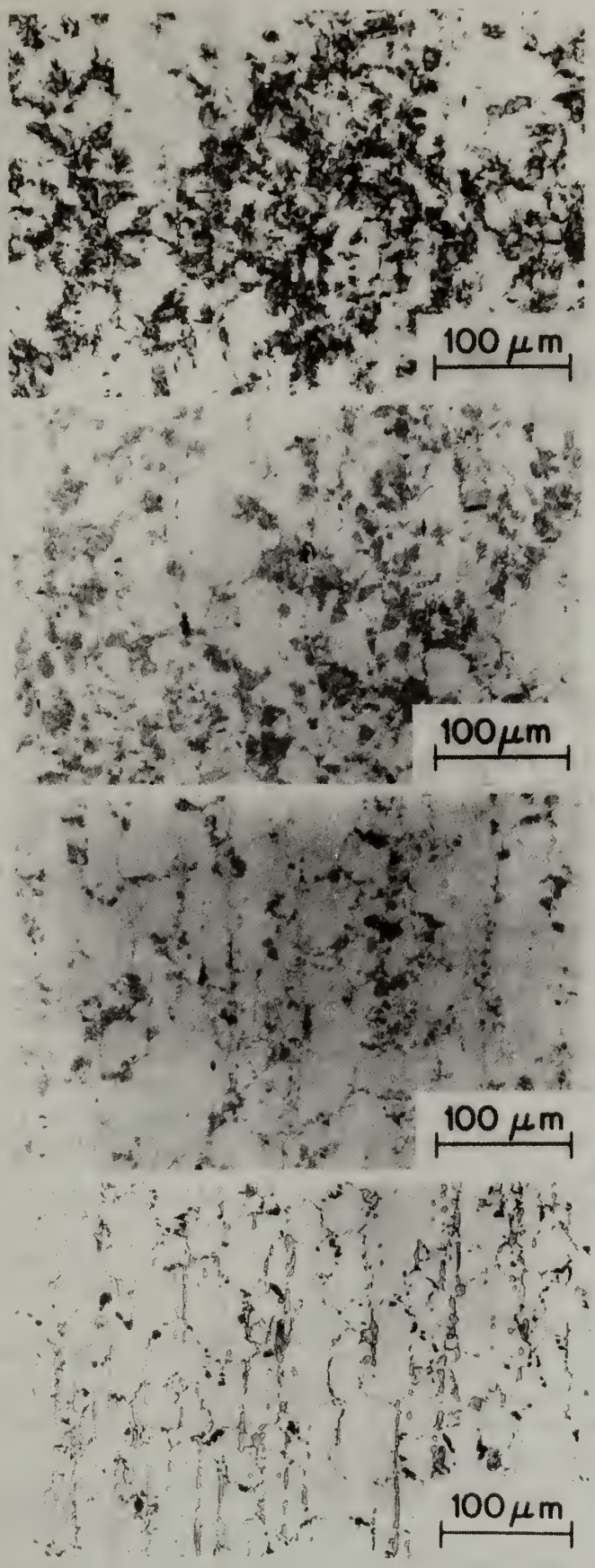

Fig. 61. Inconel 671 tested at 600 °C in oxidizing/sulfidizing/carburizing environment at 1 X 10^{-6}/s. (Top to Bottom) Alpha-chromium phase present in alloy due to combined effects of temperature and strain. Progressing from maximum strain (fracture surface) to a smaller strain (near shoulder area of reduced section). 200 X.

NBS-114A (REV. 9-78)

U.S. DEPT. OF COMM. BIBLIOGRAPHIC DATA SHEET	1. PUBLICATION OR REPORT NO. NBSIR 81-2191 (DoE)	2. Gov't. Accession No.	3. Recipient's Accession No.

4. TITLE AND SUBTITLE

The Use of the Slow Strain Rate Technique for the Evaluation of Structural Materials for Application in High-temperature Gaseous Environments

5. Publication Date

6. Performing Organization Code

561

7. AUTHOR(S)

G. M. Ugiansky and C. E. Johnson

8. Performing Organ. Report No.

9. PERFORMING ORGANIZATION NAME AND ADDRESS

NATIONAL BUREAU OF STANDARDS
DEPARTMENT OF COMMERCE
WASHINGTON, DC 20234

10. Project/Task/Work Unit No.

11. Contract/Grant No.

12. SPONSORING ORGANIZATION NAME AND COMPLETE ADDRESS *(Street, City, State, ZIP)*

Department of Energy
Division of Systems Engineering/Energy Technology
Mail Stop GTN C-155
Washington, DC 20545

13. Type of Report & Period Covered

Final

14. Sponsoring Agency Code

15. SUPPLEMENTARY NOTES

☐ Document describes a computer program; SF-185, FIPS Software Summary, is attached.

16. ABSTRACT *(A 200-word or less factual summary of most significant information. If document includes a significant bibliography or literature survey, mention it here.)*

The slow strain rate technique has been evaluated as an accelerated test for determining the performance of structural materials in simulated coal gasification environments. Seven alloys, namely Types 309, 310, 310S, 347 and 446 stainless steels; Incoloy 800; and Inconel 671, were tested at temperatures from 370 °C to 1040 °C at strain rates from 10^{-4} to 10^{-7}/s in H_2S plus water, gaseous mixtures of CO, CO_2, H_2, CH_4, H_2S, and H_2O, and in nominally inert environments of He and Ar. Type 310 steel, the most extensively studied material, showed a marked reduction in mechanical properties at low strain rates ($<10^{-5}$/s) in H_2S/H_2O at 540 °C, and this was associated with the occurrence of a large degree of secondary intergranular cracking in addition to the main ductile fracture mode. The occurrence of the secondary cracking was taken as the primary indication of embrittlement in subsequent tests. Of particular significance, it occurred to some degree in all alloys tested in the simulated coal-gasification environments at 600 °C. Consequently, the mechanism(s) of the embrittlement phenomena remain uncertain; a number of possible causes including creep and several environmentally-induced fracture processes are outlined. It is shown that the overall results of the test program are in good agreement with in-plan experience. It is concluded that the slow strain rate technique is an effective method for evaluating the performance of structural materials in the elevated-temperature gaseous environments.

17. KEY WORDS *(six to twelve entries; alphabetical order; capitalize only the first letter of the first key word unless a proper name; separated by semicolons)*

Austenitic stainless steels; coal gasification; elevated temperatures; ferritic stainless steel; gaseous environments; nickel alloy 671; nickel alloy 800; slow strain rate test; structural materials

18. AVAILABILITY ☒ Unlimited

☐ For Official Distribution. Do Not Release to NTIS

☐ Order From Sup. of Doc., U.S. Government Printing Office, Washington, DC 20402, SD Stock No. SN003-003-

☐ Order From National Technical Information Service (NTIS), Springfield, VA. 22161

19. SECURITY CLASS (THIS REPORT) UNCLASSIFIED

20. SECURITY CLASS (THIS PAGE) UNCLASSIFIED

21. NO. OF PRINTED PAGES

22. Price

USCOMM-DC